Issue 4 2014 | Volume 10

The Journal on Advanced Studies in Theoretical and Experimental Physics, including Related Themes from Mathematics

PROGRESS IN PHYSICS

"All scientists shall have the right to present their scientific research results, in whole or in part, at relevant scientific conferences, and to publish the same in printed scientific journals, electronic archives, and any other media." — Declaration of Academic Freedom, Article 8

ISSN 1555-5534

The Journal on Advanced Studies in Theoretical and Experimental Physics, including Related Themes from Mathematics

PROGRESS IN PHYSICS

A quarterly issue scientific journal, registered with the Library of Congress (DC, USA). This journal is peer reviewed and included in the abstracting and indexing coverage of: Mathematical Reviews and MathSciNet (AMS, USA), DOAJ of Lund University (Sweden), Zentralblatt MATH (Germany), Scientific Commons of the University of St. Gallen (Switzerland), Open-J-Gate (India), Referativnyi Zhurnal VINITI (Russia), etc.

Electronic version of this journal:
http://www.ptep-online.com

ISSN: 1555-5534 (print)
ISSN: 1555-5615 (online)

Standard Address Number: 297-5092
Printed in the United States of America

October 2014 **Vol. 10, Issue 4**

CONTENTS

Information for Authors and Subscribers

Progress in Physics has been created for publications on advanced studies in theoretical and experimental physics, including related themes from mathematics and astronomy. All submitted papers should be professional, in good English, containing a brief review of a problem and obtained results.

All submissions should be designed in LaTeX format using *Progress in Physics* template. This template can be downloaded from *Progress in Physics* home page http://www.ptep-online.com. Abstract and the necessary information about author(s) should be included into the papers. To submit a paper, mail the file(s) to the Editor-in-Chief.

All submitted papers should be as brief as possible. We accept brief papers, no larger than 8 typeset journal pages. Short articles are preferable. Large papers can be considered in exceptional cases to the section *Special Reports* intended for such publications in the journal. Letters related to the publications in the journal or to the events among the science community can be applied to the section *Letters to Progress in Physics*.

All that has been accepted for the online issue of *Progress in Physics* is printed in the paper version of the journal. To order printed issues, contact the Editors.

This journal is non-commercial, academic edition. It is printed from private donations. (Look for the current author fee in the online version of the journal.)

On Materiality and Dimensionality of the Space. Is There Some Unit of the Field?

Anatoly V. Belyakov

E-mail: belyakov.lih@gmail.com

The article presents arguments with a view to recognize that space is material and has possibly a fractal dimension in the range of from three to two. It is proposed that along to the unit of substance (atom) Some Unit of the field (vortex tubes) should be set. It is shown that the formation of the field structures being a kind "doubles" of atomic ones is possible. The existence of the three-zone electron structure is confirmed. It is indicated that this concept have already resulted in to the successful explanation of phenomena and to finding of their important parameters at different levels of the organization of matter.

1 Introduction

Some of the observed cosmological effects can not find a satisfactory explanation. These include, in particular, mismatch of the rotation velocity around the galactic center of the substance, located on the periphery of galaxies, to Kepler's laws.

In accordance with Kepler's laws, following the law of universal gravitation, the peripheral rotation velocity of galactic objects should, in accordance with their distancing from the galactic center to the periphery, decrease inversely proportional to the square of their distance from the center. Measurements also showed that this rotation velocity remains almost constant for many galaxies at a very significant distance from the center. The need to explain these facts has led to the conclusion that there is a dark matter filling up the galactic halo.

The other explanation was given by Israeli astrophysicist Mordechai Milgrom. His Modified Newtonian Dynamics (MOND) is an empirical correction of Newton's laws of gravity and inertia, proposed as an alternative to dark matter. The basic idea is that at accelerations below $a_0 \sim 10^{-8}$ cm/sec^2 effective gravitational attraction approaches the value $(g_N\, a_0)$, where g_N — usual Newtonian acceleration; that allows phenomenologically to reproduce the flat rotation curves of spiral galaxies [1].

It is possible that the reported anomalous acceleration detected by the Pioneer spacecrafts refers to the same type of phenomena, i.e. it is caused by not so rapid decrease in the force of attraction, as the Newton's law requires.

2 On the true dimensionality of the space and of its materiality

Is there a need to involve extra entities (dark matter) or to modify forcibly the fundamental Newton's law to explain of this and others cosmological effects? Could be more natural to accept reduction of the dimensionality of the space from three — in the region of cluster masses, to two — for the void intergalactic space?

Assume that wih distancing from the cluster masses at intergalactic distances the three-dimensional space gradually "flattens" in a two-dimensional surface. The force of gravity in the case of the three-dimensional space is inversely proportional to the square of the distance between gravitating masses. With decreasing the dimensionality of the space the natural modification of Newton's law occurs, and the force of gravitational attraction for the two-dimensional space becomes inversely proportional to the distance in the first degree, which leads to the constancy of the rotation velocity of objects at great distances from the galactic center.

Perhaps a slight dimension decreasing and therefore the modification of Newton's law manifests itself at a lower scale with the distance incresing from the Sun, which may explain the anomaly of the Pioneer spacecrafts.

Thus, a picture emerges of three-dimensional or nearly three-dimensional material galaxies islands floating in a two-dimensional or nearly two-dimensional void spatial sea. Obviously, need has ripened for recognizing of the existence of ***a unified material medium*** and for replacement by this concept of the whole variety entities like ether, physical vacuum, space, and matter.

Indeed, according to the concept of J. A. Wheeler's idea, the surface can be two-dimensional, but at the same time is fractalized, topologically non-unitary coherent and consists of linkages of "appendices" or "wormholes" of the first and subsequent orders forming as a whole the three-dimensional structure [2]. Thus matter itself can finally be organized with step-by-step complication of the initial cells and be a "woven cloth", which in its turn, is deformed into the objects (masses, substance) we observe. The objects therefore are the very fractalized (upto micro-world scales) *surfaces*, which have a fractional dimension of the value almost approaching three and presumably equal to the number e [3]. As a result, empty space is logically interpreted as a nondeformed surface and, accordingly, electromagnetic waves as surface waves thereon.

Note, it is the concept of a flat two-dimensional intergalactic space that agrees best with the point of view existing

today among the majority of cosmologists that the observable universe has zero curvature and is very close to spatially flat having local deformations at the location where there are massive objects (flat Universe).

There are also other facts pointing to the reasonableness of the foregoing. Recently in the paper [4] interesting effects have been given, namely —:

— the unusual nature of the distribution of "hot" and "cold" spots in the cosmic microwave radiation;

— the damping of a signal at large scales (there is absence of any clearly expressed "hot" or "cold" areas at the angles greater than about 60°);

— the form of small spots on the map, drawn WMAP, like an ellipse.

The authors consider that these effects can be explained by assuming that the Universe has the shape of a horn. Then its curvature explains these facts, because the whole surface of the horn is a continuous saddle. This negatively curved space acts like a distorting lens, turning spots in something like an ellipse.

It would be interesting to analyze, whether the same effects can be explained in accordance with the concept set forth above, i.e. be the result of observation out of the three-dimensional space of our galaxy of remote objects through a void two-dimensional space?

Finally, there is a known *photometric paradox* that is, in the framework of the proposed concept, explained naturally by decrease in the amount of luminous objects entering the target of the observer during the transition of a solid angle in a planar angle as far as these objects are moving away from the observer.

3 Field masses and their structurization

The idea about transitions between distant regions of space in the form of Wheeler's "appendices" or "wormholes" can be extended to the scale of macrocosm, and some contemporary astrophysical theories has already made use of it [5]. These "wormholes", obviously, should be interpreted as vortical current tubes or threads, or field lines of some kind.

It is considered that matter exists in the form of the substance and the field. A familiar element of our world is an atom, i.e. the *unit of the substance* is the structure that is, on Bohr' model, based (simplified, of course) on the balance between dynamic and electric forces. By analogy, one can imagine the *unit of the field* — the structure that is based (also simplified) on the balance between *dynamic and magnetic forces*.

In the paper [6] it is shown that the balance of dynamic and magnetic forces defines a family of unidirectional vortex threads of number n_i, of the length l_i, rotating about the longitudinal axis of the radius r_i with the rotary velocity v_{0i}; with the additional presence of the balance of *gravitational and magnetic forces* contra-directional closed vortex tubes form closed structures or contours. These structures can be attributed to some mass, but not in the ordinary sense of the word, but as having the sense of the measures of organization of the field.

It is given that the elementary unit of vortex tubes is the unit with the radius and mass close to those of a classical electron (r_e and m_e) [7, 8]. Then the linear density of the vortex tube for vacuum will be:

$$\varepsilon_0 = \frac{m_e}{r_e} = 3.231{\times}10^{-16}\ \text{kg/m}. \tag{1}$$

Accepted that for a medium other than vacuum the mass of a vortex tube or the mass of a conture, i.e. the mass per unit of the field, is proportional to the number of vortex threads in the tube. Then the total mass of the contour of the length l_i will be:

$$M_i = \varepsilon_0 n_i l_i\,. \tag{2}$$

Number of vortex threads shows how material medium differs from vacuum, and their greatest value corresponds to the ratio of electrical-to-gravitational forces, i.e. value:

$$f = \frac{c^2}{\varepsilon_0 \gamma} = 4.167{\times}10^{42}, \tag{3}$$

where c, γ are the light velocity and the gravitational constant.

The balance of *electrical and magnetic* forces gives a characteristic linear parameter that is independent of the direction of the vortex tubes and the number of charges:

$$R_c = \sqrt{2\pi}\, c \times [\text{sec}] = 7.515{\times}10^{8}\ \text{m}. \tag{4}$$

This quantity has a magnitude close to the Sun radius and the sizes of typical stars.

Further, this value corresponds to the characteristic gravitational mass, close to the *Jeans mass* during recombination:

$$M_m = R_c \frac{c^2}{\gamma} = f R_c \varepsilon_0 = 1.012{\times}10^{36}\ \text{kg}. \tag{5}$$

Let the field structure meets the above conditions and has a total mass $M_0 = z_i M_i$, i.e. consists of z_i vortex tubes which, in turn, consist of n_i of vortex threads. While atomic objects are complicated with increasing its mass, field objects are, on the contrary, complicated with decreasing its mass, forming the hierarchy of structures. These changes can be traced if some additional relations are set, for example:

$$z_i = \frac{R_c}{l_i}\,, \qquad a^j = \frac{R_c}{r_i}\,, \tag{6}$$

where a is the reciprocal fine structure constant and $j = 0, 1, 2\ldots$.

In the paper [6] the formulas are given, where all parameters of objects are expressed in the terms of a dimensionless mass $M = M_0/M_m$.

Parameters	Objects					
	Jeans mass	Typical star	Typical small planet	Biggest multicellular organism	Human individual	Most small multicellular organism
j	0	2	4	11	12	15
z_i	1	26.6	706	6.8×10^7	3.5×10^8	4.8×10^{10}
r_i, m	7.5×10^8	4.0×10^4	2.13	2.3×10^{-15}	1.7×10^{-17}	6.8×10^{-24}
l_i, m	7.5×10^8	2.8×10^7	1.1×10^6	11.0	2.13	0.016
v_{i0}, m/sec	3.0×10^8	1.1×10^7	4.2×10^5	4.4	0.85	0.0063
M_0, kg	1.0×10^{36}	2.0×10^{30}	4.1×10^{24}	4.6×10^4	65.5	1.9×10^{-7}
n_i	4.2×10^{42}	8.3×10^{36}	1.7×10^{31}	1.9×10^{11}	2.8×10^8	~1

Table that here shows the hierarchy of the parameters z_i, r_i, l_i, v_{0i}, M_0, n_i with decreasing the mass M_0 for some values of j. It is evident that the fine structure constan is the scale factor in the whole range of mass.

Calculations show that some parameters of objects are quite characteristic. For example, at $j = 2$ the mass of an object is exactly equal to the mass of the Sun, at $j = 4$ the mass of an object is equal to the mass of Earth-like planets. Apparently, the mass range for $j = 11 \ldots 15$ correspond to the masses of living multicellular organisms.

Indeed, for the minimum mass at $j = 15$ the parameter $n_i = 1$, and it limits the existence of the complex structures having masses below $1.9{\times}10^{-7}$ kg. For the maximum mass at $j > 11\, r_i < r_e$. In this case, there is a possibility of the formation within the vortex tubes of $p^+{-}e^-$ contours of general radius r_e (their parameters were previously determined from the condition of the charge constancy [7]) *of even more fine secondary structures* consisting of the vortex elements of radius r_i.

It would be reasonable to assume that the additional information filling of such structures, i.e. the ability to record and store information on a deeper level than the atomic-molecular level (DNA), just also is the condition of the formation of the most complex organisms (multicellular ones).

Provided $r_i = r_e$, the maximum mass of such organism is limited to 59 tons (with roughly at $j = 11$). The overwhelming diversity of living multicellular organisms fit into this mass range. This applies to both flora and fauna. The smallest animals endowed with a cerebrum and nervous system are rotifers (Rotatoria), and the most massive animals are whales (Cetacea), and among multicellular plants — from wolffia rootless (Wolffia arrhiza) to redwoods (Sequoia). Their mean masses are close to those specified in the table of minimum and maximum masses.

It is interesting to note that at $j = 12$ the mass of the object becomes equal to the average mass of a human individual, while the length of the vortex tube corresponds to the length of a stretched human DNA. Complexity of such a field structure containing $3.5{\times}10^8$ vortex tubes, each of which contains nearly the same amount by $2.8{\times}10^8$ vortex threads, *is comparable to the complexity of a human body*, which contains about 10^{14} cells.

Thus, the atomic structures are accompanied by their field "doubles"; this duality in general determines the total properties of objects. And possibly it is the "harmonic complexity" of the existing wave objects having masses close to that of human that defines the most highly organized biological life and the existence of mind.

One might ask why these vortex structures are not detected. But it is not quite so. There where there is a suitable material medium, plasma, for example, vortex structures manifest themselves at the different levels of organization of matter.

Undoubtedly, inside the Sun there is a gravimagnitodynamical structure that manifests itself in the form of paired dark spots in the equatorial zone of the Sun. These spots seem to be the outputs of the vortex force tubes undergoing magnetic reversal and changing their intensity and polarity. Their registered quantity (from several one to a hundred) does not contradict the calculated mean $z_i = 26.6$ [6].

On the Earth's surface the reflection of such structures are numerous geomagnetic anomalies, at least those that are not associated with the features of geological structure.

Regarding the scale of human, it can be assumed that the material essence of living in his field form is expressed through the form and structure of the corona discharge observed around living organisms (Kirlian effect).

4 About the three-zone electron structure and the divisibility of charge

In the microcosm the charge and spin of the electron are determined by momentum and angular momentum of the vortex $p^+{-}e^-$ contour, and these values are constant regardless of the size of the contour [7].

Let for some wave object, whose parameters are determined from the foregoing balances, the momentum of *one* vortex tube $M_i\, v_{0i}$ is also equal to the total momentum $p^+{-}e^-$ contour, i.e. the amount of charge (in the "coulombless" sys-

tem) corrected by the Weinberg angle cosine $e_x = e_0 \cos q_w$, where $q_w = 28.7^\circ$ [8]. Then using the formulas given in [6] *one* can find the number of vortex threads, *which one vortex tube* is composed of:

$$n_i = f\left(\frac{e_x}{c\,M_m}\right)^{2/3} = 2.973 \simeq 3. \qquad (7)$$

Thus, a unit contour or vortex tube having a momentum equivalent to the electron charge contains *three* unit vortex threads. This fact points to the three-zone electron structure and possible divisibility of the charge and confirms the conclusions reached in papers [8, 11].

5 Conclusion

The concept of the unified material medium and recognition of the existence the elementary vortex structures as material units of the field made it possible to reflect on and explain logically variety physical phenomena at the different scale levels of organization of matter using the single approach — J.Wheeler's geometrodynamic concept.

Someone might say that the author's constructions are too simplistic, mechanistic, even speculative and not supported by a properly mathematical apparatus, and some results could be occasional coincidences. However, the author has repeatedly stated that these works are not a formalized theory. These papers only have demonstrated by means of the illustrative mechanistic models the opportunities for understanding, interpretation, and, in some cases, for calculation of important physical parameters on the scale of from microcosm to cosmos.

This approach has proved successful. This proves the results, for example: the definition of the independent determination of the ultimate density of physical vacuum [3], the explanation of the nature of electron charge and finding its numerical value as well as numerical values of the constants of radiation [7, 9], the determination of the proton-electron mass ratio, the accounting of the forces of gravity in microcosm, the finding the neutron lifetime [8], the modeling the Hertzsprung-Russell diagram, the definition of model parameters of pulsars [6], the conclusion about the existence of two types of planetary systems [10], etc.

The obtained results totality, correct both qualitatively and quantitatively, is so great that this fact completely excludes the opportunity of occasional coincidences. Thus, the method of approach and proposed models can serve as a basis for the development of full physical theories based on the recognition of the existence of the unified material medium.

Submitted on June 28, 2014 / Accepted on July 02, 2014

References

1. Sanders R.H., McGaugh S.S. Modified Newtonian Dynamics as an alternative to Dark Matter. arXiv: astro-ph/0204521.
2. Dewitt B.S. Quantum gravity. *Scientific American*, v.249, December 1983, 112–129.
3. Belyakov A.V. On the independent determination of the ultimate density of physical vacuum. *Progress in Physics*, 2011, no.2, 27–29.
4. Aurich R., Lustig S., Steiner F., and Then H. Hyperbolic universes with a horned topology and the CMB anisotropy. arXiv: astro-ph/0403597.
5. Novikov I.D., Kardashev N.S., Shatskiy A.A. Multicomponent universe and astrophysic of the "wormhole". *Uspekhi-Physics*, 2007, v. 177(9), 1017–1023.
6. Belyakov A.V. Evolution of stellar objects according to J. Wheeler's geometrodynamic concept. *Progress in Physics*, 2013, v.9, no.1, 25–40.
7. Belyakov A.V. Charge of the electron, and the constants of radiation according to J. A. Wheeler's geometrodynamic model. *Progress in Physics*, 2010, v.6, no.4, 90–94.
8. Belyakov A.V. Macro-analogies and gravitation in the micro-world: further elaboration of Wheeler's model of geometrodynamics. *Progress in Physics*, 2012, v.8, no.2, 47–57.
9. Belyakov A.V. On the uniform dimension system. Is there necessity for Coulomb? *Progress in Physics*, 2013, v.9, no.3, 142–143.
10. Belyakov A.V. On some general regularities of formation of the planetary systems. *Progress in Physics*, 2014, v.10, no.1, 28–35.
11. *New Scientist*, 1998, No. 2119, 36.

LETTERS TO PROGRESS IN PHYSICS

On the Cosmophysical Origin of Random Processes

Open Letter to the Scientific Community on the Basis of Experimental Results Obtained During 1954–2014

Simon E. Shnoll

Institute of Theor. and Experim. Biophysics, Russian Academy of Sciences,
Pushino 142290, Russia. E-mail: shnoll@mail.ru

This is a summary of the presentations at the seminar headed by Yakov G. Sinai. Held in July 8, 2014, in Institute for Information Transmission Problems, Russian Academy of Sciences, in Moscow.

> "My lords! I came to you to tell most unpleasant news: random physical processes do not exist."

No one person, never, got random time series in the measurements of physical processes on the Earth. There is "non-vanishing scatter of results" which can be found in any physical measurements and observations. It remains existing in the registered data after vanishing all conceivable and inconceivable sources of errors. The "non-vanishing scatter of results" is not random. It is due to the following factors:

— the daily motion and the orbital motion of the planet Earth, where all the observers are located, through the non-isotropic and inhomogeneous cosmic space;

— the motion of the Solar System in the Galaxy;

— changes in the relative positions of the Earth, Moon, Sun and planets.

These conclusions are based on the transformation of the time series of physical measurement data into the series of "insolvent histograms" (such histograms, in which the number of bits and the number of measurements are comparable).

The evidence of non-randomness of the time series is the periodic change of shape of the insolvent histograms.

The non-randomness of shape of the insolvent histograms follows from the next experimental facts:

1. Significant similarity of the histograms obtained from the measurement any processes (from Brownian motion to the alpha-decay) that were recorded in the same moment of time, and in the same geographic location. We call this the "effect of absolute synchroneity";

2. Significant similarity of the histograms, obtained in different geographic locations, but in the same moments of local time;

3. Significantly higher probability of the similarity of the histograms created on the basis of the neighbour (near) non-overlapping segments of the time series, compared to the distant segments of the time series (the "near-zone effect");

4. The clear presence of the near-day, near 27-day, and yearly periods of the appearance of similar histograms;

5. The "space anisotropy effect". It means, in the measurement of nuclear decay fluctuations, that the histogram shape depends on the space direction of the collimators. Also, in light fluctuation measurements, the space anisotropy effect means that the histogram shape depends on the space direction of the light beam generated by LEDs or lasers;

6. The near-day periods of similar histograms were not registered when the light beam coming from a LED, or the alpha-particle beam coming through a collimator are directed to Polaris (this effect was registered in Puschino, Russia). Also, the near-day periods of similar histograms were not registered in the measurements done at the North Pole;

7. Splitting the near-day period into the "sidereal period" (1436 min) and the "solar period" (1440 min);

8. Splitting the yearly period of similar histograms into the "calendar period" (365 days), the "tropical period" (365 days, 5 hours, 48 min), and the "sidereal (stellar) period" (365 days, 6 hours, 9 min);

9. Appearance of similar histograms with the rotation periods of a source slowly rotating in a special device;

10. No near-day periods was registered on a source rotating with a speed of one revolution per day in the opposite direction than the Earth's rotation (thus compensating the daily rotation of the Earth);

11. The "palindrome effect". It is the periodic repetition of mirrored histograms in the moments of time when the daily, orbital, or artificial rotation change its sign (i.e. in the opposite locations on the rotation circle);

12. The algorithmic nature of shape of histograms. Discrete distributions of the number of cofactors. Fluctuations of the number system. Omnibus of the natural numbers.

* * *

Nature (physics) of the registered regularities that are discussed herein is as follows:

1. Because the very different scales of energies in the registered processes (Brownian motion, visible light, alpha-decay), the registered effects can not be explained by "external influences" on these processes. The effects can only be

explained due to the appearance of the observer in similar regions of space along the Earth's trajectory in the cosmos;

2. There exist an optimally small number of measurements used in the histogram creation, in which the accuracy of the similarity of histograms is maximally high. This optimally small number does not depend on the duration of the time interval of the histograms. A fractality is observed: from hours to milliseconds;

3. Similarity of "insolvent histograms" is not due to the statistical (random) regularities. Goodness criteria of hypotheses are inapplicable for histogram shape (the fine structure of insolvent histograms);

4. Beginning from some number of measurement, the fine structure of the distributions does not depend on this number. Remaining this fine structure unchanged with the increase of measurement number contradicts to the large number law. This leads to the "layered histograms phenomenon". It is unclear whether this phenomenon can be explained by the "statistical inertia" or not?

5. Could the characteristic structure of changes in the number of cofactors in the natural numbers, and the dependence of the number system on the "scale unit" to explain the regularities of insolvent histograms?

6. Is the amazing phenomenon of chirality of insolvent histograms also depending on the motion of the Earth in the anisotropic space?

7. Synchronous change of histograms in different geographic locations, with the collimators directed to some special directions in space does not depend on the distance between the locations. The measurements were done along the geographic latitude (the North Pole — Antarctic). Also, synchronous change of histograms is apparently not screened;

8. Nevertheless, when located at a fixed place on the Earth, but with the oppositely directed collimators (to the West and the East) the similarity of histograms appears with the half-day period. It was also registered in experiments with artificial rotation of the source;

9. The presence of clear daily and yearly periods of histograms means that the spatial structure (relievo) of the fractal "coastline" of the Universe remains stable (at least within the scale of our lifespan);

10. It is amazing and remains unexplained that the similarity of histogram series obtained from the measurements done in the equinox moments of time: the moments of transit of the Sun, Moon, Mars, Venus, Mercury through the "point-gap" in the plane of the celestial equator, from above or below the plane;

11. The equinox moments of time also manifested the palindrome effect — the periodic repetition of mirrored histograms.

Submitted on July 05, 2014 / Accepted on July 07, 2014

References

1. Shnoll S. E. Cosmophysical Factors in Stochastic Processes. American Research Press, Rehoboth (New Mexico, USA), 2012.
2. Shnoll S. E. Changes in the fine structure of stochastic distributions as a consequence of space-time fluctuations. *Progress in Physics*, 2006, vol. 2, issue 2, 39–45.

The Real/Virtual Exchange of Quantum Particles as a Basis for the Resolution of Wave-Particle Duality and Other Anomalies of the Quantum Phenomena

Abdul Malek

980 Rue Robert Brossard, Québec J4X 1C9, Canada. E-mail: abdulmalek@qc.aibn.com

A hypothesis based on the exchange and the inter-conversion of the "real" and the equivalent "virtual" particles of the quantum vacuum can resolve the contradiction of wave-particle duality, the "spookiness" and the other conflicting properties of the quantum particles. It can be shown using simple mathematics that the extent of the wave or the particle nature of a quantum particle depends on the rate of this "real/virtual" particle exchange, the velocity and the rest mass of the exchanging "real" particle.

The revolutionary quantum phenomena has posed both ontological and epistemological problems for natural science and philosophy; that remains unresolved even after more than a century of its discovery. The wave-particle duality, the characteristic non-locality, the prevalence of the interplay of chance and necessity among other things distinguish the quantum phenomena, from hitherto anything previous epistemology could even conceive of. The great intuition of Democritus that matter is composed of some elementary particles or atoms more or less holds true and has been vindicated even at the subatomic level; but the contrary nature of matter as a wave at quantum level has also now been well established.

This has given rise to conflicting and mutually exclusive philosophical claims of the objective reality, ranging from positivist and subjective idealism to the realist views of a deterministic, unchanging and a permanent objective reality, to a mechanistic measurement problem as expressed by the Heisenberg's uncertainty principle, But however much wildly differing interpretations of the quantum phenomena are, the rationalist notion of a certain, deterministic and inherently unchanging reality (knowable or not) as the basis of epistemology is widely accepted. At the quantum level this amounts to assuming that the stable quantum particles like protons, electrons, photons, etc., retain their unique and singular identity on a permanent basis; or at least since the creation of the universe, through a Big Bang or otherwise. The only recognized change of the stable and the everlasting fundamental particles is their fusion at the core of the stars to form higher elements.

Albert Einstein, who was a pioneer in the development of the quantum theory, rejected the "spooky" quantum phenomena for its lack of certainty and causality. He (and many others) also opposed the generally accepted but confusing and opportunistic interpretation of the Copenhagen consensus. Einstein tried to avoid the quantum conundrum by adopting a notion of physical reality based on a "continuous field" rather than material particles, particularly in his theory of general relativity (GR). In Einstein's own words, "Since the theory of general relativity (GR) implies the representation of physical reality by a continuous field, the concept of particles and material points cannot play a fundamental part and neither can the concept of motion. The particle can only appear as a limited region in space in which the field strength or energy density is particularly high" [1].

The popularity of "continuous field" based GR have been responsible for the undermining of the original particle based orientation of quantum electrodynamics (QED); as "field" based theories like quantum field theory (QFT) now dominate quantum mechanics and the related domains of cosmology. The fact that the quantum vacuum is seething with ghostly virtual particles that pop in and out of existence has been very well established after the discovery of the Lamb Shift [2], with a precision that is unmatched by any other physical measurements. The Casimir Force is also generally attributed to be due to the presence of virtual particles. These virtual particles can be made real using various well-known techniques [3]. Yet except for being a mere nuisance for creating infinities in the quantum mechanical equations, the virtual particles has so far received little attention from an ontological and epistemological point of view. A new theoretical and experimental re-evaluation of the intuitively derived uncertainty principle of Werner Heisenberg suggest that, the uncertainty does not always come from the disturbing influence of the measurement, but from the more fundamental quantum nature of the particle itself [4]. This points to a possible role of the virtual particles in the uncertainty relation.

All the experimental evidence and technological experience so far, suggest that the virtual particles of the quantum vacuum may play a significant role in determining the attributes of the quantum phenomena, namely the wave-particle duality, its non-locality, its uncertain nature and influence (based on chance and necessity) on the macroscopic biochemical and astrophysical processes etc., than hitherto appreciated.

In opposition to the view of a static objective reality, where the stable and fundamental quantum particles retain their permanent and unique identity; it is assumed in the present hypothesis that the objective reality is dynamic, where there is perpetual exchange of position and identity between the real quantum particles with their respective and reciprocal virtual counterparts; such that no permanent and unique iden-

tity of "real" quantum particles is possible. This exchange is mediated by Heisenberg's uncertainty relation:

$$\Delta E\,\Delta t \geqslant \frac{h}{4\pi}\,,$$

where ΔE is the energy gained by the virtual particle during the time interval Δt, that is equivalent to the mass/energy of the real particle that would exchange with it, and h is the Planck constant. It is clear that the time Δt required for this exchange is extremely small compared to the time of the change in position or the velocity of the real quantum particles that must be within the limit of the velocity of light (c) according to Einstein's theory of special relativity (SR).

If we consider a point source for a "real" quantum particle at the centre of a sphere, then the particle could be any where (during a specific time interval) within this sphere defined by a radius which is proportional to the velocity of the particle. The particle will then have the possibility to exchange position and identity with equivalent virtual particles within this sphere; assuming that the real/virtual exchange does not affect the velocity of the real particle under consideration. This rate (R) of exchange of "virtual" particles par "real" particle par unit time, then will be directly proportional to the volume of the sphere and inversely proportional to ΔE, the energy equivalent of the mass (m) of the real particle that is exchanged with a corresponding virtual particle, according to the following equation:

$$R = \frac{\frac{h}{4\pi}\frac{4}{3}\pi r^3}{\Delta E} = \frac{\frac{h}{3}r^3}{\Delta E} = \frac{\frac{h}{3}kv^3}{mc^2}\,,$$

where h is the Planck constant, r is the radius of the sphere that is proportional to the velocity v of the particle, and k is a proportionality constant. For a particle with the velocity of light (c), the rate is

$$R = \frac{\frac{h}{3}kc}{m}\,.$$

Now, it is obvious from the above equation that for particles with zero rest mass like photons, neutrinos, gravitons etc. the rate of exchange will be infinite, hence the particle or a group of particles will have a wave character spreading in all three dimensions and also can act as long range force carriers.

With massive and stable particles like electrons, positrons, protons, etc., this exchange rate will be finite but much smaller and hence will be restricted around the direction (from the source) of the motion of the particle as a cylindrical or a conical wave front and like an arc in two dimensions; over a tangible distance. The arc-length of the wave packet in two dimensions will depend on the mass and the velocity of the quantum particle. The heavier the mass and slower the velocity, the shorter will be the length of the arc and the wave-packet. The rapid slowing down of the quantum particle along the original direction of its motion is likely to taper down the cylindrical wave-front into a cone shape. More massive and slow moving objects will demonstrate no wave character at all and follow the laws of classical mechanics. It is because a slower velocity will cover less volume of space in specified time and the greater mass will have exorbitant energy requirement for the uncertainty principle and hence lower exchange rate with the potential virtual particles. These aspects of the wave-packet for different quantum particles can possibly be verified with adjustable two slit experiments. This approach to the problem of the propagation of quantum particles very superficially compares with the "Path Integral Formulation" of quantum mechanics by Richard Feynman, where the integration over an infinity of possible trajectories is used to compute a "quantum amplitude" [5].

This real/virtual (and vice versa) exchange of the quantum particles explains their "spookiness", the wave-particle dual character and their non-locality within the limit of the speed of light. Whether all the properties of the quantum particles aside from their charge, such as parity, spin etc. are also conserved or whether their entanglement is affected during these exchanges; needs to be worked out. This hypothesis will be contrary to the generally accepted notions of causality and formal logic, or what G. W. F. Hegel termed as "the view of understanding". But it will be in conformity with the law of "the unity of the opposites" and the other laws of dialectics.

The "view of understanding" abhors contradictions and posits a sharp distinction between the opposites, based on Aristotelian doctrine of "unity, opposition and an excluded middle in between". This view assumes the presence (at least from the time of the creation of the world) of an objective reality that is essentially permanent, certain, unchanging, deterministic and continuous etc. Any change, motion or development in this view can only come from an "impulse" from outside; following the law of cause and effect. There is little wonder that the conflicting and the uncertain nature of the quantum phenomena has given rise to confusion and to mutually exclusive philosophical claims of the objective reality, ranging from the positivist and subjective idealism to the realist views of the "guiding waves" of a continuous and permanent objective reality on the one hand and to a mechanistic and simplistic measurement problem as expressed by the Heisenberg's uncertainty principle, on the other.

An exactly opposite view of the objective reality mainly attributed to the Greek philosopher Heraclitus and later developed by G. W. F. Hegel, Karl Marx and Frederick Engels posits "eternal change due to inner strife" as the permanent feature of the objective reality and the world. Any stability or apparent permanence is only relative and conditional. The world in this view is infinite, eternal and ever changing. This view follows from Hegel's elaboration of dialectics as the "Absolute Identity of identity and non-identity" — "the unity of the opposites" i.e., a simultaneous unity and conflict of the opposites residing together at the very element of a thing or a process in a logical contradiction. Any material existence is a

contradiction of the opposites and must eternally be resolved to a new "becoming" through a dialectical "negation of the negation", in a chain of processes in triads that give rise to the phenomenology of the world. At fundamental quantum level, the objective reality is a contradiction of "being" and "nothing", giving rise to "becoming" or existence. The QED established fact that the quantum vacuum seethes with virtual particles, the notion of an eternal real/virtual exchange and a dynamic equilibrium as the basis of the objective reality is in conformity with a dialectical view of the universe.

From a dialectical point of view, "being" and "nothing" must always exist together in contradiction, as a part of the objective reality of the universe. One cannot supersede or exhaust the other, so there can be no question of a beginning or an end of the universe. For dialectics, there is also no mega-leap (like Big Bang) in nature; precisely because nature is made entirely of infinite leaps of the "negation of the negation", mediated by chance and an iron necessity that is inherent in chance! In addition to real/virtual particle exchange, inter-conversion of real and virtual particles through quantum tunnelling and through yet other still unknown processes is possible. The energetic core of the galaxies are likely to be the favourable sites for the generation of new matter and anti-matter from the virtual particles This author had previously attempted to use these ideas to explain some cosmic phenomena [6], the origin, evolution and the structure of the galaxies [7] and other aspects of modern cosmology [8].

Submitted on July 15, 2014 / Accepted on July 17, 2014

References

1. Einstein A. On the General Theory of Relativity. In: *The Scientific American Book of the Cosmos*, David Levy (Ed.), N.Y., 2000, 18–19.
2. Lamb W.E. and Retherford R.C. Fine structure of the hydrogen atom by a microwave method. *Phys. Rev.*, 1947, v.72, 241.
3. Ruffini R., Verreshchagin G., and Xue S. Electron-positron pairs in physics and astrophysics: from heavy nuclei to black holes. arXiv: 0910.0974.
4. Erhart J. et al. Experimental demonstration of a universally valid error-disturbance uncertainty relation in spin measurements. *Nature Physics Volume*, 2012, v.8, 185–189.
5. Feynman R.P., Hibbs A.R., and Styer D.F. Quantum Mechanics and Path Integrals. Dover Publications, Mineola, N.Y., pp. 29–31.
6. Malek A. The cosmic gamma-ray halo — new imperative for a dialectical perspective of the Universe. *Apeiron*, 2003, v. 10, no. 2, 165.
7. Malek A. Ambartsumian, Arp and the breeding galaxies. Apeiron, 2005, v. 12, no. 2, 256.
8. Malek A. The Dialectical Universe — Some Reflections on Cosmology. Agamee Prakashani Publishers, Dhaka, 2012.

LETTERS TO PROGRESS IN PHYSICS

The Infinite as a Hegelian Philosophical Category and Its Implication for Modern Theoretical Natural Science

Abdul Malek

980 Rue Robert Brossard, Québec J4X 1C9, Canada. E-mail: abdulmalek@qc.aibn.com

The concept of the infinite as a mathematical, a scientific and as a philosophical category is differentiated. A distinction between Hegel's dialectical concept of the infinite as opposed to his idealist-philosophical "system" of the "Absolute Idea" as the "True Infinite" is emphasized.

1 The infinite as a mathematical category

The concept of the infinite as a mathematical category arose naturally enough with the invention of the numerical system by the Sumerians around 3000 B.C. and the subsequent developments of the concepts of geometry, the measure of time, mathematical operations (arithmetic, algebraic, exponentials etc.), One could always add or subtract a unit of number, length or time to get a new one ad infinitum without an end. This infinite is undetermined, has no characterization and was termed the "spurious" or the "false" infinite (*bad infinity*) by G. W. F. Hegel (1770–1831 A.D.), as opposed to the "True Infinite" (to be discussed later).

"The spurious infinite" according to Hegel [1],

> "...seems to superficial reflection something very grand, the greatest possible. ... When time and space for example are spoken of as infinite, it is in the first place the infinite progression on which our thoughts fasten ... the infinity of which has formed the theme of barren declamation to astronomers with a talent for edification. In an attempt to contemplate such an infinite our thought, we are commonly informed, must sink exhausted. It is true indeed that we must abandon the unending contemplation, not however because the occupation is too sublime, but because it is too tedious ... the same thing is constantly recurring. We lay down a limit: then pass it: next we have a limit once more, and so for ever."

The infinite as a mathematical category took a mystical form once Pythagoras of Samoa (580?–520 B.C.), and later Plato (429–347 B.C.) idealized the numbers, their relations and geometry into their philosophical system, where the infinite along with the numbers and the forms were universals that exists in a realm beyond space and time for all eternity, a realm that sense perception cannot reach; it is only given to thought and intuition.

As Frederick Engels [2, p. 46] wrote,

> "Like all other sciences, mathematics arose out of the *need* of man; from measurement of land and of the content of vessels, from computation of time and mechanics. But, as in every department of thought, at a certain stage of development, the laws abstracted from the real world become divorced from the real world and are set over against it as something independent, as laws coming from outside to which the world has to conform. This took place in society and in the state, and in this way, and not otherwise, *pure* mathematics is subsequently *applied* to the world, although it is borrowed from this same world and only represents one section of its forms of interconnection — and it is only just precisely because of this that it can be applied at all".

The mathematical pursuit of the infinite therefore, of necessity became a spiritual endeavor. In his attempt to know the infinite and to prove his continuum hypothesis, Georg Cantor (1845–1914 A.D.) for example, was eventually compelled to make a distinction between *consistent* and *inconsistent* collections; for him only the former were *sets*. Cantor called the *inconsistent* collections the *absolute infinite* that God alone could know. His idea of an "actual infinite" attracted theological interest because of its implication for an all-encompassing God; but at the same time it inspired scorn of the contemporary mathematicians. What Cantor, other mathematicians and natural science pursued in reality is the "spurious infinite" of Hegel. An infinite series starting with a first term is also undefined, because there is no end to the other side, and one cannot come back to the first term starting from the other end. Cantor's pursuit of the infinite led him to the ridiculous idea of the *infinity* of infinities, and no other mathematicians followed his steps. If there is more than one infinite then by definition they become mere finites. Mathematicians of all ages had no clue as to the nature of the infinite; some denied its existence all together; while others maintained (following Plato) that mathematical entities can-

not be reduced to logical propositions, originating instead in the intuitions of the mind.

2 The infinite as a scientific category

Historically, natural science took a rather pragmatic and an opportunistic approach towards infinity, i.e., *reductio ad absurdum* argument which avoids the use of the infinite. It truncates infinity by putting an arbitrary limit as Georg Cantor did, and calls the rest the "absolute infinite" that is known only to infinite God. It deals with infinity with some arbitrary mathematical tricks, for example, a circle is the limit of regular polygons as the number of sides goes to infinity; an infinite series starts with a first term; in renormalization, one set of infinite is cancelled by invoking another set of infinite to get a finite result that was desired in the first place and so on.

Isaac Newton (1642–1727 A.D.) and Albert Einstein (1879–1955 A.D.) faced the same conceptual problems of the infinite universe in formulating their theories of gravity. Einstein declared, "Only the closed ness of the universe can get rid of this dilemma" [3]. He then set himself to develop a theory of gravity based on geometry, because geometry deals with closed space!

But an attempt to truncate infinity this way can only lead us back to medieval geocentric cosmology. The unpleasant fact is that, by definition a truncated infinite is also infinity and any mathematical operation on infinity leaves it unchanged as Galileo asserted in his famous 1638 pronouncement on infinity that, "Equal", "greater", and "less" cannot apply to infinite quantities [4]. The arbitrary renormalization process and *reductio ad absurdum* practiced by natural science cannot resolve the contradiction of the infinite; it only leads to more and more contradictions and a dependence on ever more mysteries and theology, as we observe in modern theoretical natural science. The reason why Albert Einstein chose a finite and closed universe as opposed to the open ones was not only to make his equations meaningful and/or because of his love for *simplicity* and *aesthetics*, as reductionist ideologues and worshipers of symmetry would have us believe, but also because of his sober realization that his Machean-philosophy based cosmology collapses in an infinite universe. If Mach's principle is followed, then an infinite universe means that the inertia and the mass of atoms etc. also become infinite. To keep the world as we see it now (inertia, mass, etc.); all Mach based cosmologies must have the universe started at a finite past and also must have a finite extension. So this way the contradiction of infinity is not solved.

The notion of the infinite in natural science became ever more clouded after Albert Einstein established the primary role of mathematics in natural science. Natural science became seduced to the idea that where experimental evidence and empirical data is difficult and/or impossible to obtain "logical consistency of mathematics" will lead the way. The stunning success of the theories of relativity in early 20th century, led Einstein to revive Pythagoras's notion of mathematics. "How can it be" he wondered, "that mathematics being a *product of human thought* which is *independent of experience*, is so admirably appropriate to the objects of reality?" [5].

The theory of general relativity is a classic example where the power of mathematics, pure thought and aesthetics devoid of any empirical content is purported to have conceived the ultimate reality of the universe. "Our experience hitherto justifies us in believing that nature is the realization of the simplest conceivable mathematical ideas. I am convinced that we can discover by means of purely mathematical constructions the concepts and the laws connecting them with each other, which furnish the key to the understanding of natural phenomena. ... In a certain sense, therefore, I hold it true that pure thought can grasp reality, as the ancients dreamed", declares Albert Einstein [6].

With his mathematical idealism Einstein erased the difference between the *pure* mathematics, whose program is the *exact* deduction of consequences from logically independent postulates, and the *applied* mathematics of *approximation* needed for science. Natural science uses approximate empirical data, which are fitted on in various ways to *analytic functions* of *pure* mathematics that helps in the systematization, generalization, and the formulation of tentative theories. But the results and the inferences are only valid in a narrow range of the data values for the argument for which approximate empirical information is available.

A convenient property of the analytic functions (such as the field equations) is that, such functions are known for all values of their argument when their values in any small range of the argument values are known and thereby allowing an unlimited extension of this procedure from the macrocosm to the microcosm. Thus, the *a priori* assumption that the laws of Nature involve *analytic functions* leads to a complete mechanistic determination of the world based on their experimentally determined value in a narrow range only. But the validity of such a procedure of unlimited extension of mathematical functions for the real world, were questioned both by mathematician/philosophers such as Bridgman [7] and scientists like Klein [8] at the advent of quantum mechanics; based as they argued (on different grounds) on the unavoidable inaccuracies of empirical knowledge. And as quantum mechanics clearly shows, there is uncertainty in the ontological nature of reality itself at micro level. So, our epistemological knowledge must always be defective, tentative and approximate, increasing in scope from one generation of humanity to the next; like an infinite mathematical series, without ever coming to a termination or without ever reaching one final and ultimate truth.

The quantum phenomena and the failure so far [9]; (in spite of over a century-long intense efforts by some of

the most brilliant mathematicians including Einstein) to unify "ALL" the particles and "ALL" the forces of Nature into a simple and reductionistic "theory of everything" demonstrate the folly of this kind of naïve and over- simplified extrapolation of idealized mathematics to the real world at the two opposite directions of infinity, i.e., macrocosm and microcosm.

3 The infinite as a philosophical category

The concept of the infinite was implicit in the early philosophical developments especially among the early Greek thinkers that centered around the basic questions of the primacy of spirit or nature, unity or multipliticity, stasis or motion. This debate divided the philosophers into two great camps. Those who asserted the primacy of spirit, unity and stasis formed the camp of idealism; the contrary camp formed the various schools of materialism.

The earliest idealist Greek philosophers (the Eleatics) denied the reality of becoming, multiplicity or motion; these characteristics they maintained, are of the sense-world or physical Nature. These they argued are not *real* but only *appearances* and hence these are illusions. For Parmenides (515–450 B.C.) for example the sole reality is Being, Being is One, only the One is; the Many not. This Being cannot be perceived by senses, it is given only to thought or mind. This line of thinking permeates the range of idealist philosophers like Plato, Aristotle, Berkeley, Hume, Hegel and all monotheistic religions. The Unity of Being in this view means that the infinite must be contained in this one Being. The Being meaning God in theological terms, the infinite, then became associated with abstract God. The idealist view of infinity was later incorporated into mathematics and theoretical natural science.

But the dialectically opposite and the materialist view of reality — i.e. the validity of the sense perception of change, multiplicity and motion in material Nature also arose simultaneously in early Greek philosophy. The founder of the dialectical view, Heraclitus (544–483 B.C.) on the contrary saw the world as a process — as changing eternally. For him Unity is not a homogenous unity, but is a "unity of the opposites or of opposite tendencies". The Unity is a complex entity that contains at least two dominant opposite fragments that are in constant conflict with each other and renders this unity susceptible to diversity, change and movement. The concept of the infinite in this view is therefore, open ended. Epicurus (341~270 B.C.) following the tradition of Heraclitus was the first to assert that the universe is infinite in its extension in all directions and that multiplicity, time and motion are endless.

Benedict Spinoza (1632–1677 A.D.) made an important advance on the concept of infinity along the dialectical tradition which helped Hegel (himself an idealist) to formulate in a comprehensive way the dialectical view of the infinite in particular and his dialectical method in general. Spinoza formulated the profound idea that to define something is to set boundaries for it; i.e., to determine is to limit. The infinite then is something that is undetermined or that has no limit or boundary. In other words the Infinite is limited only by itself and like God is "self-determined".

In popular concept, God is supposed to be infinite. Spinoza's idea of the infinite led to an insurmountable difficulty for conventional philosophy and theology which regarded the infinite and the finite as mutually exclusive opposites; absolutely cut off from each other. How then the infinite can be conceived; how infinite God can have contact with finite man, since it will limit His infiniteness. Finiteness of the world became a primary requirement for medieval theology. The inquisition did not hesitate to spill blood and torture victims to defend its doctrine. Hegel, following Spinoza called the "Absolute Idea" of his philosophy the "True Infinite" which is self-determined. For him the material world or Nature is a crude replica — an alienated form of the "Absolute Idea".

The fundamental difference between these two worldviews and hence their implication for the concept of infinity gets its concrete expression in the question of *matter* and *motion*. While Newton recognized matter as a *real entity*, for Einstein matter is a particular representation of an all pervading (space-time) reality ("Being" of Parmenides?). Einstein expressed this point of view in an unambiguous way, "Since the theory of general relativity (GR) implies the representation of physical reality by a continuous field, the concept of particles and material points cannot play a fundamental part and neither can the concept of motion. The particle can only appear as a limited region in space in which the field strength or energy density is particularly high" [10]. Motion in the view of both Newton and Einstein could only arise from an *impulse* from without — from God — the "unmoved mover". And why energy density at particular points must arbitrarily be high to form material points must also depend on intervention by Providence. For dialectics (and quantum mechanics) on the contrary, matter and motion are the fundamental elements and the primary conditions of all physical reality; *motion is the mode of existence of matter. Matter without motion is as inconceivable as motion without matter*.

The only way the conceptual problem of infinity can be resolved is through the dialectics of Hegel — the law of the unity of the opposites. The notion that the finite and the infinite reside together in a contradiction; that they are united as well as are in opposition to each other. That, the finite **is** the infinite and vice versa. That this contradiction resolves itself continuously in the never-ending development in time and extension in space of the universe, in the same way as for example intellectual advance find its resolution in the progressive evolution of humanity from one particular generation to the next. Just as Nature or the universe (ontologically) is incapable of reaching a final, ever lasting, unchanging or an ideal state so is thought (which is only a reflection of Nature in the mind of man) epistemologically is incapable of comprehending a completed, exhaustive or immutable knowledge

— the so-called absolute truth of the world. For dialectics, "eternal change" (with temporary stages of infinite number of leaps) is the only thing that is permanent and the only absolute. Hegel's dialectics therefore, is a condemnation of all claims to absolute truth by all idealism including the mathematical idealism of modern official natural science, which is but a reincarnation or rather restoration of the old idealism. In human history, as well as in the history of natural science, hitherto all claims to the "final truth" are but the partial masquerading as the complete.

The continuous resolution of the contradiction of the finite and the infinite like the other evolutionary processes are not only dialectical but they also develop historically following the three general laws i.e. i) transformation of quantity into quality and vice versa, ii) interpenetration of the opposites and iii) the negation of the negation. Engels [11] summarized these three laws from Hegel's *Logic*, where the first law comprises the *Doctrine of Being*, the second, the *Doctrine of Essence*, while the third constitutes the fundamental law for the construction of the whole system. Hegel deduced his philosophy from the history of Nature, of society and of thought. The infinite universe is not a mere abstract, quality less, boring, endless extension of uniformity (spurious or *bad infinity*), it includes a variety of qualitative contents with different forms of movements passing one into the other and developing historically. The infinite space is adorned with the drama of things "coming into being" and "passing out of existence" in each of the innumerable island universes; each island universe with innumerable galaxies and each galaxy in turn with innumerable stars and planets. Under favorable conditions, galaxies propagate [12, 13]; the stars produce the higher elements; the planets give rise to the evolution of molecules, to organic life and finally to the thinking brain through which infinite Nature (for a brief period of time) *becomes conscious of itself* ! Self-consciousness is therefore, the property of the highest developed form of matter, which like everything else comes into being and passes out of existence as temporary bubbles in the eternal and infinite universe.

The knowledge of the infinite is therefore proportional to the knowledge of the finite. This knowledge is necessarily a historical and an iterative process progressing through successive generations of mankind without ever terminating in one final or absolute truth a quest of which was the aim of all idealism — mathematical, scientific or philosophical. A progressively better understanding of the infinite universe can only come about by studying the finite around us guided by the general laws of dialectics.

There are innumerable number of water and other molecules and atoms on earth and yet we understand (in a limited sense) and live at ease with these! The properties of matter and its structure under the various conditions in terrestrial nature must be the same that exists under similar conditions billions of light years away. In fact, one sun with its planets and its life supporting earth and one Milky Way galaxy with its surrounding family group form the essential basis for an understanding of the universe. Beyond 15 billion light years there is no wonderland or lurking monsters to be seen. What we will see there is more or less the same we now see within a few million light years around us! The same applies to the micro-world. There is no limit of space, time or length in any direction; up-down, left-right; back-front, at least up to the level beyond which the terms mass, time or length lose their meaning (in the usual sense of the term) because of quantum uncertainty and due to other yet unknown effects. The limits from quasars (at the ultimate boundary of the universe?) to the quarks at the lowest end, set by Official Science must therefore be false; because this represents an arbitrary limitation of infinity, conditioned by the limitation of the empirical knowledge of our time.

4 The "Absolute Idea" of Hegel as the "True Infinite"

As Engels pointed out [14], the dialectical view of the infinite as discussed above, are necessary logical conclusions from the dialectical method of Hegel; but conclusions he himself never expressed so explicitly. Hegel was an idealist and above all he was the official philosopher of the Royal Prussian court of Frederick William III. His task was to make a system of philosophy that must specify one absolute truth or a "first cause" of the world, as tradition demanded it. Therefore, even though Hegel, especially in his *Logic* emphasized that this absolute truth is nothing but the logical. i.e., historical *process* itself, he nevertheless found it necessary to bring his dialectical process to a termination in the "Absolute Idea". For his philosophical "system" his dialectical "method" had to be untrue. Hegel also turned his philosophy upside down, where the "Absolute Idea" (like all idealism) became primary and nature only a crude reflection of the "Idea", even though (through unprecedented detail and encyclopedic work) he extracted the laws of dialectics from the history of the material and the human world.

But nevertheless, the dialectical method of Hegel helped him to overcome the impossible contradiction of the infinite and the finite faced by Spinoza, theology and all previous idealist philosophies. For Hegel, the finite and the infinite are no independent entities separated from each other by an unbridgeable gap in between, as old philosophy asserted; but these are the integral components of a single unity within which the two opposites reside together in active unity and opposition, and hence in a logical contradiction. A resolution of this contradiction to an ever new "unity of the opposites" and so on — *the negation of the negation* is what gives rise to motion, change, development, and historical evolution of the universe as a never ending process.

Idealist Hegel can terminate the infinite process of change by making his "Absolute Idea" (the self-determined, the True Infinite") as the ultimate end result of all change, motion, development or history, and making it the beginning again, i.e.

the end as the true beginning. For Hegel, the finite Nature or man IS the infinite "Absolute Idea" itself! The "Absolute Idea" alienates and disguises itself into Nature, evolves historically through all the usual twists and turns following the laws of dialectics and comes back to itself again through the consciousness of man and particularly through the philosophy of Hegel himself, who for the first time in the history of mankind perceived in thought the ultimate truth of this dialectical movement, in absolute profoundness. For Hegel the "Absolute Idea" which is the end result of all change, development, motion, history etc. — the static reality of Parmenides, the abstract God of theology, the self-determined entity of Spinoza, is the "True Infinite" and the absolute truth of the world.

But this "Absolute Idea" or the "True Infinite" of Hegel like the mathematical "Absolute Infinite" of Cantor; are only absolutes in the sense that they have absolutely nothing to say about it! Thus in spite of his prodigious intellect and in spite of the logical implication of his profound dialectical "method" to the contrary, Hegel unfortunately pursued the illusion of an absolute truth, like all the other idealist philosophers and all theological prophets of all times. The mathematical idealism and reductionism of modern official theoretical natural science inherited this illusion — i.e., the empty shell of all idealism but not the kernel — the dialectical "method" of this great idealist thinker.

5 Conclusion

During the last few centuries especially since Copernicus (1473–1543), natural science accumulated impressive empirical evidence and gained variable degrees of understanding of the terrestrial nature; that collectively vindicate Hegel's assertion that *change* is the only absolute truth and that the dialectical laws are the only eternal laws that govern the development and the transformation of matter and life. But ironically, natural science claims its own invariable truth exactly in the areas where it possesses the least empirical evidence! As intoxicated modern official natural science celebrates its achievement of a definitive knowledge of one single event i.e., the "Big Bang" origin of the universe and the triumph of its mathematical idealism; with the award of Nobel Prizes, and as the world awaits in breathless anticipation the imminent discovery of a "theory of everything" that will bring an "End of Physics" and possibly the end of all knowledge (by "knowing the mind of God", according to one of the leading physicists Stephen Hawking [15]); it would be instructive for us to remember the sober dialectical assessment of Frederick Engels [2, pp. 43–44] — one of the greatest inheritors of Hegel's philosophy:

> "The perception that all the phenomena of Nature are systematically interconnected drives science to prove this interconnection throughout, both in general and in detail. But an adequate, exhaustive scientific statement of this interconnection, the formulation in thought of an exact picture of the world system in which we live, is impossible for us, and will always remain impossible. If at any time in the evolution of mankind such a final, conclusive system of the interconnections within the world — physical as well as mental and historical — were brought to completion, this would mean that human knowledge had reached its limit, and, from the moment when society had been brought into accord with that system, further historical evolution would be cut short — which would be an absurd idea, pure nonsense. Mankind therefore finds itself faced with a contradiction; on the one hand, it has to gain an exhaustive knowledge of the world system in all in its interrelations; and on the other hand, because of the nature both of man and of the world system, this task can never be completely fulfilled. But this contradiction lies not only in the nature of the two factors — the world, and man — it is also the main lever of all intellectual advance, and finds its solution continuously, day by day, in the endless progressive evolution of humanity. . . ".

Submitted on July 15, 2014 / Accepted on July 18, 2014

References

1. Wallace W. "The Logic of Hegel". Oxford, Clarendon Press, 1892, §94. Cited from: Stace W.T. The Philosophy of Hegel. Dover, N.Y., 1955, §198.
2. Engels F. Anti-Dühring. International Publishers, N.Y., 1939.
3. Kragh H. Cosmology & Controversy. Princeton Univ. Press, 1996, p. 7.
4. Kaplan R. and Kaplan E. The Art of the Infinite. Oxford Univ. Press, Oxford, 2003, p. 228.
5. Einstein A. Sidelights on Relativity. Dover, N.Y., 1983, p. 28.
6. Einstein A. Essays in Science. Transl. by Alan Harris from: Mein Weltbild. Quedro Verlag, Amsterdam, 1933, pp. 16–17.
7. Bridgman P.W. The logic of Modern Physics. Macmillan, N.Y., 1927.
8. Klein F. Elementarmathematik von Höheren Standpunkt aus. Bd. 3, Springer, Berlin, 1924. Cited from: Condon E.U. and Morse P.M. Quantum Mechanics. McGraw-Hill, N.Y., 1929, p. 11.
9. Smolin L. The Trouble with Physics. Houghton Miffin Co., Boston–N.Y., 2006.
10. Einstein A. On the General Theory of Relativity. In: *The Scientific American Book of the Cosmos*, N.Y., 2000, p. 13.
11. Engels F. Dialectics of Nature. International Publishers, N.Y., 1940, p. 26.
12. Malek A. Ambartsumian, Arp and the breeding galaxies. *Apeiron*, 2005, v. 12, no. 2, 2005, 256–271.
13. Arp H.C. Seeing Red: Redshifts, Cosmology and Academic Science. Apeiron Publishers, Montreal, 1998.
14. Engels F. Ludwig Feuerbach and Outcome of Classical German Philosophy. International Publishers, N.Y., 1941, pp. 12–13.
15. Hawking S. A Brief History of Time. Bantam Books, N.Y., 1990, p. 175.

A Monte Carlo Simulation Framework for Testing Cosmological Models

Yuri Heymann

3 rue Chandieu, 1202 Geneva, Switzerland. E-mail: y.heymann@yahoo.com

We tested alternative cosmologies using Monte Carlo simulations based on the sampling method of the zCosmos galactic survey. The survey encompasses a collection of observable galaxies with respective redshifts that have been obtained for a given spectroscopic area of the sky. Using a cosmological model, we can convert the redshifts into light-travel times and, by slicing the survey into small redshift buckets, compute a curve of galactic density over time. Because foreground galaxies obstruct the images of more distant galaxies, we simulated the theoretical galactic density curve using an average galactic radius. By comparing the galactic density curves of the simulations with that of the survey, we could assess the cosmologies. We applied the test to the expanding-universe cosmology of de Sitter and to a dichotomous cosmology.

1 Introduction

We tested cosmological models using relatively small simulations that can be run on a home computer. Simulation is a promising and powerful tool for the field of cosmology. For example, the Millennium Simulation project at the Max Planck Institute for Astrophysics, the largest N-body simulation carried out so far, simulated the formation of large structures in the universe using a cluster of 512 processors. Our rationale was to slice a galactic survey into small redshift buckets. We then used cosmological models to compute the volume of each bucket and derived the galactic density curve versus the redshift, or light-travel time. We used the simulation to generate a uniform distribution of galaxies for each redshift bucket. We then computed the number of visible galaxies (i.e. those that were not covered by foreground galaxies) to derive a simulated galactic density curve. Our method requires only a cosmological model, a behavior for the galactic density, and the average galactic radius versus the redshift.

We are interested in a special class of cosmological models: cosmologies with a Hubble constant that does not vary over time to conform to the linear relationship between the luminosity distance and the redshift observed for Type Ia supernovae [1]. This choice was motivated by the idea that the laws of nature follow simple principles. There are two distinct cosmologies that satisfy this condition: the de Sitter flat-universe cosmology and the dichotomous cosmology introduced in [2].

The de Sitter cosmology is a solution to the Friedmann equation for an empty universe, without matter, dominated by a repulsive cosmological constant Λ corresponding to a positive vacuum energy density, which sets the expansion rate $H = \sqrt{\frac{1}{3}\Lambda}$. The dichotomous cosmology consists of a static material world and an expanding luminous world. It is not difficult to envision a mechanism whereby light expands and matter is static. For example, consider that the light wavelength is stretched via a tired-light process when photons lose energy. The number of light wave cycles is constant, resulting in an expanding luminous world and static material world. In order to maintain a constant speed of light, we would still have to introduce a time-dilation effect [2].

The same equation relates light-travel time to redshifts for both the dichotomous and the de Sitter cosmologies, making it easy to compare both models using our testing framework.

2 Method

2.1 The cosmological model

Consider an expanding luminous world, or an expanding universe, with a constant expansion rate H_0. Because of the expansion, the distance between two points is stretched. Let us introduce the Euclidean distance y, which is the equivalent distance measured if there were no expansion. The Euclidean distance is also the proper distance at the time light was emitted, which is the comoving distance times the scale factor at the time of emission. Now, consider a photon at a Euclidean distance y from the observer, moving towards the observer. Hence, y must satisfy the following differential equation:

$$\frac{dy}{dt} = -c + H_0 y\,, \tag{1}$$

where c is the speed of light.

By setting time zero at a reference T_b in the past, we get $t = T_b - T$; therefore, $dt = -dT$. Hence, (1) becomes:

$$\frac{dy}{dT} = c - H_0 y\,, \tag{2}$$

with boundary condition $y(T = 0) = 0$. Integrating (2) between 0 and T, we get:

$$y = \frac{c}{H_0}\left(1 - \exp(-H_0 T)\right)\,. \tag{3}$$

Because $dt = \frac{da}{H\,a}$, where a is the scale factor, the proper light-travel time versus redshift is:

$$T = \int_{1/(1+z)}^{1} \frac{da}{H_0\,a} = \frac{1}{H_0}\ln(1+z)\,. \tag{4}$$

By substitution of (4) into (3), we get:

$$y = \frac{c}{H_0}\frac{z}{(1+z)}\,. \tag{5}$$

As $T_0 = \frac{y}{c}$, we finally get:

$$T_0 = \frac{1}{H_0}\frac{z}{(1+z)}\,, \tag{6}$$

where T_0 is the light-travel time in the temporal reference frame of the observer, H_0 the Hubble constant, and z the redshift. Eq. (6) is our cosmological model relating light-travel time to redshifts.

2.2 The sampling method

The zCosmos-deep galactic survey [3] consists of a collection of visible galaxies with respective redshifts obtained for a given spectroscopic area in the sky. Here we used Data Release DR1, which contains galactic observations up to a redshift of 5.2. We sliced the collection of galaxies into small redshift buckets and counted the number of galaxies in each bucket. Using our cosmological model, we converted the redshifts into light-travel times. The volume of each bucket is equal to the volume of the slice for the whole sphere contained between the lower and upper radius boundaries of the bucket multiplied by the ratio of the spectroscopic area of the survey divided by the solid angle of the sphere.

For an observer at the center of a sphere, the volume of a slice of the sphere is:

$$V_i = \frac{4\pi}{3}\left(r_i^3 - r_{i-1}^3\right)\,, \tag{7}$$

where r_{i-1} and r_i are the lower and upper radius boundaries of the bucket, respectively.

The spectroscopic area of the zCosmos galactic survey was determined to be 0.075 square degrees [4]. Hence, the ratio of the survey spectroscopic area divided by the solid angle of the sphere is as follows:

$$\eta_{surv} = \frac{0.075}{4\pi(180/\pi)^2} = 1.81806\times 10^{-6}\,. \tag{8}$$

Thus, the volume of the i^{th} bucket of the survey is $\eta_{surv}V_i$. The galactic density of the bucket is the number of galaxies contained within the redshift boundaries of the bucket divided by the bucket volume. By computing the galactic density for each bucket, we get the galactic density curve of the survey versus the redshift or light-travel time.

2.3 The simulation method

To simulate the galactic density curve, we need in addition to a cosmological model, two other behaviors: the galactic density versus redshift and the relationship between the average galactic radius and redshifts. For the sake of convenience, we used the same redshift slicing that we used to compute the survey galactic-density curve, say $z \in \{0, z_1, z_2, ..., z_n\}$, where $z_{i+1} = z_i + \delta z$. By iteration from redshifts z_1 to z_n, we generated N_i galaxies with a uniform distribution in an isotropic universe and then determined whether each galaxy is visible amongst the foreground galaxies. We determined the position of each galaxy using the astronomical spherical coordinates (r, θ, φ), where r is the radial distance, $\theta \in [-\frac{\pi}{2}, \frac{\pi}{2}]$ is the declination, and $\varphi \in [0, 2\pi]$ is the right ascension. Each galaxy also has an associated radius.

First, we fixed the spectroscopic area of the simulation by taking boundaries for the declination and right ascension, say $\varphi \in [\varphi_{min}, \varphi_{max}]$ and $\theta \in [\theta_{min}, \theta_{max}]$. The spectroscopic area of the simulation is:

$$\begin{aligned}\text{specArea} = \left(\frac{180}{\pi}\right)^2 (\sin\theta_{max} - \sin\theta_{min}) \times \\ \times\, (\varphi_{max} - \varphi_{min})\end{aligned} \tag{9}$$

and the spectroscopic area of the simulation to solid angle of the sphere is:

$$\eta_{sim} = \frac{\text{specArea}}{4\pi(180/\pi)^2}\,. \tag{10}$$

To determine the number of galaxies to generate for a redshift bucket $[z_{i-1}, z_i]$, we computed the volume V_i of the spherical shell using (7) and then multiplied the galactic density by $\eta_{sim}V_i$, hence:

$$N_i = \rho_i\,\eta_{sim}V_i\,, \tag{11}$$

where N_i is the number of galaxies generated, ρ_i is the galactic density at redshift z_i, and η_{sim} and V_i are as defined previously.

To generate a galaxy, we drew two independent, uniform random variables, say X and Y, on the interval [0, 1] and computed the declination and right ascension of the galaxy as follows:

$$\begin{aligned}\theta &= \theta_{min} + X(\theta_{max} - \theta_{min}) \\ \varphi &= \varphi_{min} + Y(\varphi_{max} - \varphi_{min})\,.\end{aligned} \tag{12}$$

The newly generated galaxy was attributed the radial distance corresponding to the light-travel time at redshift z_i.

Next, we determined whether each generated galaxy was hidden by foreground galaxies. As an example, consider the calculations for galaxy B with galaxy A in the foreground. We compute the distance between the projection of galaxy A on the plan of galaxy B and galaxy B itself, which we call the "projected distance" projectedDist. If the projected distance is smaller than or equal to the critical distance, then galaxy B is determined to be not visible. The projected distance is calculated as:

$$\text{projectedDist} = \sqrt{\text{squareDist}}\,, \tag{13}$$

where the square distance is:

$$\text{squareDist} = (x_A - x_B)^2 + (y_A - y_B)^2 + (z_A - z_B)^2\,, \tag{14}$$

and (x, y, z) are the Cartesian coordinates of both galaxies projected in the plan of galaxy B, and subscripts A and B designate the coordinates of galaxies A and B, respectively.

The spherical coordinates are converted to Cartesian coordinates as follows:

$$\begin{aligned} x &= r_B \cos\theta \sin\varphi\,, \\ y &= r_B \cos\theta \cos\varphi\,, \\ z &= r_B \sin\theta\,, \end{aligned} \tag{15}$$

where r_B is the radial distance of galaxy B required to project galaxy A into the plan of galaxy B. The critical distance is calculated as:

$$\text{criticalDist} = \frac{r_B}{r_A} R_A + R_B\,, \tag{16}$$

where R_A and R_B are the respective radii of galaxies A and B. The ratio of radial distances, r_B/r_A, applied to the radius of galaxy A represents the projection of galaxy A into the plan of galaxy B according to Thales' theorem.

For the special case when the foreground galaxy A lies over galaxy B but covers it only partially (see Fig. 1), we consider galaxy B to be not visible. The zCosmos galactic survey was obtained using an automated device, and an algorithm cannot identify a galaxy that is not isolated from other sources of light. Still, galaxy B could hide more distant galaxies.

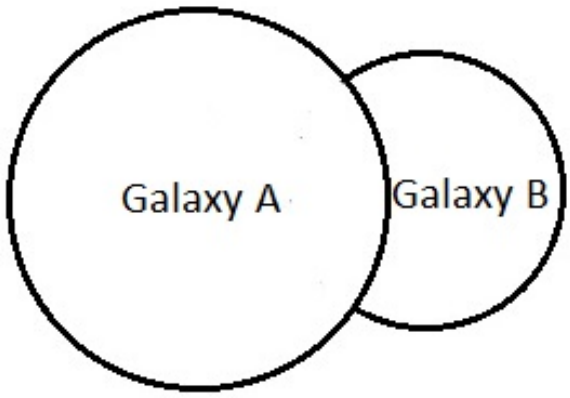

Fig. 1: A foreground galaxy partially covering a more distant galaxy.

Finally, we count the visible galaxies in each redshift bucket and multiply the counts by the ratio of the survey area to the simulated spectroscopic area in order to have numbers that are comparable between the survey and the simulation.

To generate the declination and right ascension angles of a galaxy, we used the Mersenne Twister algorithm [5], which is a pseudo-random number generator based on the Mersenne prime $2^{19937} - 1$. The algorithm has a very long period of $2^{19937} - 1$ and passes numerous tests for statistical randomness.

2.4 Galactic density and radius function of redshifts

In the dichotomous cosmology, where the material world is static and the luminous world is expanding, the galactic density is constant over time, but the image of galaxies is dilated by a factor of $(1 + z)$, because the expanding luminous world acts like a magnifying glass. Because light is stretched, the apparent size of galaxies is also stretched by the same factor, resulting in a lensing effect across the whole sky. In contrast, in the expanding universe theory, the galactic density increases by a factor $(1 + z)^3$ as we look back in time.

The radius of a galaxy in an expanding universe can be tackled in two different ways. If we consider that the whole space expands, then the galactic radius expands over time and is divided by the factor $(1 + z)$. Because the expanding universe has the same magnifying effect as the expanding luminous world, the galactic radius is also multiplied by a factor of $(1 + z)$. The net effect is that the galactic radius is constant over time, as in Expanding Cosmology A in Table 1. The other approach is to consider that galaxies do not expand in size, but because of the magnifying effect of the expansion, the image of the galaxies is dilated by a factor $(1 + z)$, as in Expanding Cosmology B in Table 1.

In Table 1, ρ_0 is the present galactic density, and R_0 is the present average galactic radius. Because of the cluster of galaxies around the Milky Way, the number of galaxies in the bucket with redshift 0.1 was generated to match the galactic density of the survey. For buckets with redshifts above 0.1, we used the functions in Table 1.

3 Results and discussion

3.1 Galactic density curves

For both the survey and simulated galactic density curves, we used redshift buckets of size $\delta z = 0.1$. We used 0.082 square degrees as the spectroscopic area for the dichotomous cosmology simulation. We used a smaller value of 0.025 square degrees for the expanding universe theory because of the large number of galaxies generated. For the Hubble constant employed in the cosmological model (6), we used a value of $H_0 = 67.3\,\text{km}\,\text{s}^{-1}\,\text{Mpc}^{-1}$, or $2.16 \times 10^{-18}\,\text{sec}^{-1}$ [1].

Figure 2 shows the simulated galactic density curve for the dichotomous cosmology versus the galactic density curve obtained from the survey. For this simulation, we used a constant galactic density of $\rho = 3 \times 10^6$ galactic counts per cubic Glyr (billion light years) and an average galactic radius of $R = 40,000\,(1 + z)$ light years. The factor $(1 + z)$ accounts for the magnifying effect of the expanding luminous world in the dichotomous cosmology (see section 2.4).

The present average galactic radius of 40,000 light years is within the range of dwarf galaxies and large galaxies. In

Table 1: Galactic density and radius functions of redshifts for the dichotomous cosmology and expanding universe theory.

	Galactic density	Galactic radius
Dichotomous Cosmology	ρ_0	$R_0(1+z)$
Expanding Cosmology A	$\rho_0(1+z)^3$	R_0
Expanding Cosmology B	$\rho_0(1+z)^3$	$R_0(1+z)$

[6], the galaxies were divided into two groups based on their respective mass: a group with $M_* \approx 10^{11} M_\odot$, corresponding to dwarf galaxies, and a group with $M_* > 10^{11.5} M_\odot$, corresponding to large galaxies. According to that study, the present average radius of dwarf galaxies is 20, 200 light years, whereas that of large galaxies is 65, 200 light years. Because dwarf galaxies are much more numerous than large galaxies, we would expect the overall average galactic radius to be smaller than 40, 000 light years. The gravitational lensing effect that creates a halo around galaxies, and some blurring effect from the luminosity of galaxies, can be accounted for by the fact that foreground galaxies obstruct the images of distant galaxies over a larger area than that of the circle defined by the intrinsic radius of the foreground galaxies. Furthermore, a minimum distance must be observed between galaxies for the selection algorithm of the telescope to be able to identify the galaxies as being distinct from one another.

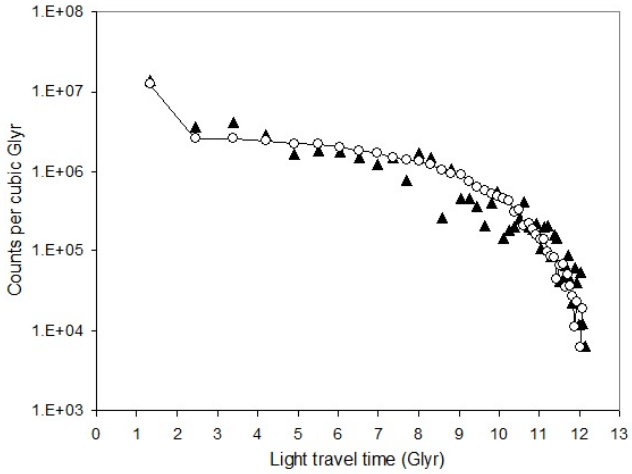

Fig. 2: Galactic density curve for the dichotomous cosmology. Glyr are billion light years. The solid triangles indicate densities based on the zCosmos survey. The open dots indicate densities obtained by Monte Carlo simulation for the dichotomous cosmology with a galactic radius of 40,000 light years.

Figure 3 shows the simulated galactic density curve for Expanding Cosmology A versus the galactic density curve obtained from the survey. The galactic density used for this simulation was $\rho = 3 \times 10^6 (1+z)^3$ counts per cubic Glyr. Two curves were simulated with an average galactic radius of 48, 000 and 78, 000 light years, respectively. The grounds for using a constant galactic radius in Expanding Cosmology A are explained in Section 2.4. In this cosmology, we can vary ρ_0 and R_0, and there is no solution such that the simulated galactic density curve matches the galactic density curve of the survey.

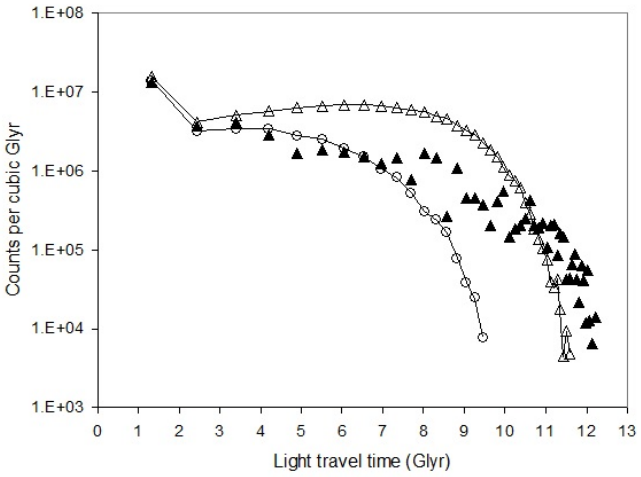

Fig. 3: Galactic density curve for Expanding Cosmology A, where Glyr are billion light years. The solid triangles indicate densities based on the zCosmos survey. The open dots indicate densities obtained by Monte Carlo simulation with a galactic radius of 78,000 light years. The open triangles are the simulated densities obtained with a galactic radius of 48,000 light years.

Figure 4 shows the simulated galactic density curve for Expanding Cosmology B versus the galactic density curve obtained from the survey. We again used a galactic density $\rho = 3 \times 10^6 (1+z)^3$ counts per cubic Glyr. The two curves simulated for this cosmology have an average galactic radius of $R = 40,000(1+z)$ light years and $R = 13,000(1+z)$ light years, respectively. There is no solution for Expanding Cosmology B such that the simulated galactic density curve matches the galactic density curve of the survey.

3.2 Size-biased selection in galactic surveys

As the redshift increases, the number of foreground galaxies increases, leaving only small areas where more distant galaxies can be observed. This effect of increasing redshifts decreases the likelihood of selecting large galaxies and smaller galaxies are preferentially selected. This size-biased selection

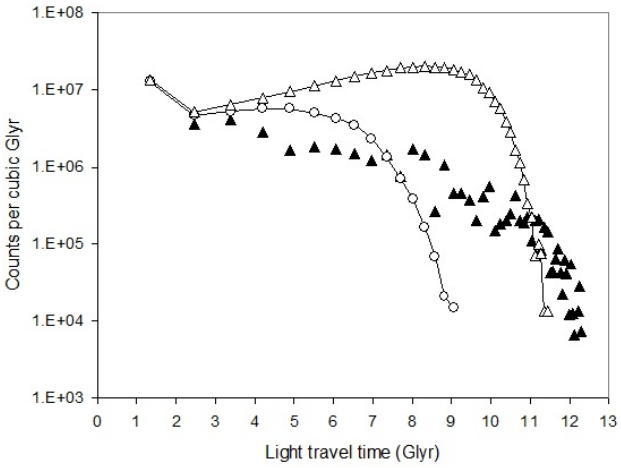

Fig. 4: Galactic density curve for Expanding Cosmology B. Glyr are billion light years. The solid triangles indicate densities based on the zCosmos survey. The open dots indicate densities obtained by Monte Carlo simulation with a galactic radius of 40,000 light years. The open triangles are the simulated densities obtained with a galactic radius of 13,000 light years.

could have a significant impact on studies of the morphological evolution of galaxies. The effect of size-biased selection can be quantified by using a Monte Carlo simulation to generate galactic radii with a size distribution obtained from galactic surveys at low redshifts.

4 Conclusion

We developed a Monte Carlo simulation framework to test cosmologies. The framework is based on the sampling method of the zCosmos galactic survey. We used simulations to generate a theoretical galactic density curve for a given cosmology. The theoretical density curve was then compared with the galactic density curve obtained from the galactic survey. We applied the test to the flat-universe de Sitter cosmology and to a dichotomous cosmology.

The simulated galactic density curve of the dichotomous cosmology matched the survey galactic density curve remarkably well. For the expanding universe classes that we considered, there was no solution such that the simulated galactic density curve matched the galactic density curve of the survey. On the basis of this test, we conclude that the dichotomous cosmology provides an accurate description of the physics underlying cosmological redshifts.

5 Acknowledgements

This work is based on zCOSMOS observations carried out using the Very Large Telescope at the ESO Paranal Observatory under Programme ID: LP175.A-0839. I would also like to thank Prof. Arto Annila for insightful comments and our inspiring discussion.

Submitted on July 20, 2014 / Accepted on July 28, 2014

References

1. Heymann Y. On the Luminosity Distance and the Hubble Constant. *Progress in Physics*, 2013, v. 3, 5–6.
2. Heymann Y. The Dichotomous Cosmology with a Static Material World and Expanding Luminous World. *Progress in Physics*, 2014, v. 10, 178–181.
3. Lilly S. J., Le Fevre O., Renzini A., Zamorani G., Scodeggio M., Contini T., Carollo C. M., Hasinger G., Kneib J.-P., Lovino A., Le Brun V., Mainieri V., Mignoli M., Silverman J., Tasca L. A. M., Bolzonella M., Bongiorno A., Bottini D., Capak P., Caputi K., Cimatti A., Cucciati O., Daddi E., Feldmann R., Franzetti P., Garilli B., Guzzo L., Ilbert O., Kampczyk P., Kovak K., Lamareille F., Leauthaud A., Le Borgne J.-F., McCracken H. J., Marinoni C., Pello R., Ricciardelli E., Scarlata C., Vergani D., Sanders D. B., Schinnerer E., Scoville N., Taniguchi Y., Arnouts S., Aussel H., Bardelli S., Brusa M., Cappi A., Ciliegi P., Finoguenov A., Foucaud S., Franceshini R., Halliday C., Impey C., Knobel C., Koekemoer A., Kurk J., Maccagni D., Maddox S., Marano B., Marconi G., Meneux B., Mobasher B., Moreau C., Peacock J. A., Porciani C., Pozzetti L., Scaramella R., Schiminovich D., Shopbell P., Smail I., Thompson D., Tresse L., Vettolani G., Zanichelli A., and Zucca E. zCosmos: A Large VLT/VIMOS Redshift Survey Covering $0 < z < 3$ in the COSMOS Field. *The Astrophysical Journal Supplement Series*, 2007, v. 172, 70–85.
4. Heymann Y. Building galactic density profiles. *Progress in Physics*, 2011, v. 4, 63–67.
5. Matsumoto M., and Nishimura T. Mersenne Twister: a 623-dimensionally equidistributed uniform pseudo-random number generator. *ACM Transactions on Modeling and Computer Simulation - Special issue on uniform random number generation*, 1998, v. 8, 3–30.
6. Stringer M. J., Shankar F., Novak G. S., Huertas-Company M., Combes F., and Moster B. P. Galaxy size trends as a consequence of cosmology. arxiv: abs/1310.3823.

Climate Change Resulting from Lunar Impact in the Year 1178 AD

David W. Chapman

Gold Mountain Technology, PO Box 1240, Palo Alto, CA 94302. E-mail: dave@goldmountain.com

In June of the year 1178, an impact was observed on the Moon. Within a few years, Europe experienced a climatic event known as the Little Ice Age. Calculations of the reduction in sunlight due to dust in high earth orbit are consistent with the historical temperature decrease. Other past temperature reductions may have resulted from similar impacts on the Moon.

1 Historical events

Shortly after sunset on June 25, 1178 AD, a large explosion occurred on the surface of the Moon. This event was observed by several people in Canterbury, England and recorded in the Chronicles of Gervase. The Julian calendar date was June 18, or June 25 Gregorian.

> In this year on the Sunday before the feast of St John the Baptist, after sunset when the Moon had first become visible, a marvellouse phenomenon was witnessed by some five or more men ...and suddenly the upper horn slit in two. From the midpoint of this division a flaming torch sprang up, spewing out over a considerable distance fire, hot coals and sparks. Meanwhile the body of the Moon which was below, writhed, as it were in anxiety... and throbbed like a wounded snake. Afterwards it resumed its proper state. This phenomenon was repeated a dozen times or more, the flames assuming various twisting shapes at random and then returning to normal. Then after these transformations the Moon from horn to horn, that is along its whole length took on a blackish appearance. [4]

2 The crater Giordano Bruno

This event was caused by the impact of a comet or asteroid onto the surface of the Moon, in the approximate area 45 degrees North latitude, 90 degrees East longitude. The crater named Giordano Bruno is believed to have been formed by this impact [6]. Giordano Bruno is a crater which is 20 kilometres in diameter, having unusually sharp rims and an extremely large system of rays. Sharp rims are indicative of recent formation, since micro-meteorites cause erosion which gradually softens land features on the surface of the Moon. Rays, which are believed to be powered material ejected during the crater's formation, do not last very long and are also regarded as evidence of very recent formation. The physical features and location of this crater are consistent with its having been formed by the event of 1178.

3 Energy of crater formation

When an object, such as a comet or asteroid, impacts the surface of the Moon, it penetrates a relatively short distance before being slowed to sub-sonic velocity. Once this has happened, vaporized material from the impact site expands up and out, forming a fireball and a crater. Factors such as the density of the impactor, the density of the target, and the angle of impact affect the size of the final crater. The most important factor is the total energy of the impacting projectile. In general, calculations involving the crater size will provide only a minimum energy of crater formation. Various formulae have been published which relate the size of a crater to the impact parameters. These formulae show a high sensitivity to the exponent used for the energy, and produce results which rarely have more than one digit of accuracy.

The first method of estimating the energy of formation of the crater is to calculate the energy using a formula which was calibrated with actual data from nuclear bomb tests and multi-ton conventional explosions.

The relationship between crater size and explosion size for an optimal crater forming explosion is the Glasstone formula [5]:

$$\text{Yield} = \left(\frac{\text{Crater Radius at Lip}}{62.5 \text{ meters}} \right)^{3.33} .$$

Yield is quoted in kilotons of TNT, which are defined in this context as 4.184×10^{12} Joules. In standard format:

$$D = 2.03 \times 10^{-2} \, E^{0.3003},$$

where D is crater diameter in meters, E is energy in Joules.

The crater Giordano Bruno has a radius of 10 km, or 10,000 meters. Using the Glasstone formula gives an explosion energy of 21,800,000 kilotons, or $9.1 \times E^{19}$ Joules. This is approximately the energy required to vaporize 21 Gigatons of rock.

A second formula has been published, based on similar data sets, the Dence formula [3]. This formula is for a crater produced by an explosion (sphere or hemisphere) on a flat surface):

$$D = 1.96 \times 10^{-2} \, E^{0.294},$$

where D is crater diameter in meters, E in energy in Joules.

Using the Dence formula gives 2.74×10^{20} Joules, or 65.5 Gigatons. This is larger than the Glasstone number by a factor of 3, which shows the difference between an optimal depth crater-forming explosion and a surface explosion.

The third method of estimating the energy of formation of the crater relies on laboratory data and computer simulations. The de Pater formula is [2]:

$$D = 1.8\rho_i^{0.11}\rho_t^{-0.33}g_t^{-0.22}\ (\sin\theta)^{0.333}\ (2r)^{0.13}\ E^{0.22}.$$

These parameters are as follows:

$D = 20,000$	crater diameter	meters,
$\rho_i = 2$	density of impactor	gram/cm^3,
$\rho_t = 3.333$	density of the Moon	gram/cm^3,
$g_t = 1.625$	gravity of the Moon	meters/sec^2,
$\theta = 45$	impact angle	degrees,
$r = 300$	radius	meters,
$v = 28,000$	velocity of impact	meters/sec,
E	energy	Joules.

This formula requires us to either make an assumption about the velocity of the incoming object, or about its mass (radius). Because of the date of the impact, the object which caused Giordano Bruno is believed to be part of the Taurid meteor complex, which would imply an impact velocity of 28000 meters/sec and a density of 2. Based on these numbers, the radius of the impactor is calculated to be 300 meters, which gives an energy of impact formula of

$$20000 = 1.8 \times 1.08 \times 0.67 \times 0.90 \times 0.89 \times 2.3 \times E^{0.22},$$

which resolves to 6.6×10^{17} Joules (158 Megatons). This is less than 1% of the Glasstone number.

The fourth method is to measure the volume of the crater in cubic meters, estimate the weight of the material which was removed, and estimate how much energy was required to remove the material. The way it works is to model the crater as a hemi-spheroid, then find the mass of the ejecta, and then to calculate the energy required to lift the ejecta to an altitude equal to the crater radius. This method produces a minimalistic number, and is intended as a sanity check on the other methods:

$$\begin{aligned}
\text{volume} &= \tfrac{2}{3}\pi \times \text{radius}^2 \times \text{depth} \\
&= \tfrac{2}{3}\pi \times 10000^2 \times 1000 \\
&= 2.09 \times 10^{11} && \text{m}^3, \\
\text{mass} &= \text{volume} \times 1000 \times \text{density} \\
&= (2.09 \times 10^{11}) \times 1000 \times 3.333 \\
&= 7.0 \times 10^{14} && \text{kg}, \\
E &= \text{mass} \times \text{g} \times \text{altitude} \\
&= (7 \times 10^{14}) \times 1.625 \times 10000 \\
&= 1.1 \times 10^{19} && \text{Joules}, \\
&= 2.7 && \text{Gigatons}.
\end{aligned}$$

In standard form, this is:

$$D = 1.9 \times 10^{-1} \times E^{0.25}.$$

Note that this formula produces a number which is proportional to the crater radius to the one-fourth power. This is consistent with the simplest formula published [2].

The four methods of estimating the energy of formation of the crater are as follows:

Glasstone	9.1×10^{19}	Joules,
Dence	2.7×10^{20}	Joules,
de Pater	6.2×10^{17}	Joules,
volume method	1.1×10^{19}	Joules.

What is interesting is how much effect the exponent in the formula has:

Glasstone	$E^{0.30}$,
Dence	$E^{0.29}$,
de Pater	$E^{0.22}$,
volume method	$E^{0.25}$.

A relatively small change in the exponent between Glasstone and Dence produced a relatively large change between those two results, and the de Pater result is far away from the others. Given that the Glasstone formula is described as calculating an explosion *at optimal cratering depth*, I suspect that the true number is somewhere between Glasstone and Dence. The best estimate for the energy of crater formation is therefore 1×10^{20} Joules.

4 Historical temperature decrease

Various historical records indicate a global temperature decrease starting in approximately the year 1190 AD [7]. The grape crop in England, which was moderately large in the year 1100, had dwindled to almost nothing by the year 1300. The records of harbour freezing in Reykjavik, Iceland, indicate that the weather became sharply colder around the year 1200. At the same time, the growing season in Greenland became so short that the Viking colonies there were abandoned. Poland and Russia experienced a major famine in the year 1215 AD, which was attributed to the cold weather causing large-scale crop failures:

> ...in AD 1215, when early frosts destroyed the harvest throughout the district around Novgorod, people ate pine bark and sold their children into slavery for bread, "many common graves were filled with corpses, but they could not bury them all. ...those who remained alive hastened to the sea".
>
> Other bad years came in 1229 and 1230, and in the latter there were many incidents of cannibalism "over the whole district of Russia with the sole exception of Kiev". [8]

Outside of Europe, tree ring data from around the world suggests that the planet became colder starting in the late 1100's [1, 7]. This temperature drop amounted to approximately 1 degree Kelvin.

5 Reduction in sunlight arriving on the planet

These recorded temperature declines are consistent with a reduction in the amount of sunlight arriving on the planet. To reduce the global temperature from 283 to 282 degrees Kelvin using a gray-body model would require that incident radiation be reduced by a factor $1-(282/283)^4$, or 1.4%. Using a more realistic model which includes positive feedback, only half of the temperature reduction needs to be caused by a decrease in sunlight. With a positive feedback model, we find that radiation needs to be reduced by a factor of $1-(282.5/283)^4$, which equals 0.7%. Such a temperature reduction would be caused by lunar dust orbiting the Earth.

The most efficient reduction in sunlight per unit mass results from dust particles approximately 1 micron in diameter. Dust particles smaller than this do not absorb light efficiently; they scatter it. Dust particles larger than 1 micron have a reduced surface area relative to their mass, and are less efficient at blocking sunlight.

Given that the required area density of dust particles is 0.7%, we find that 7×10^9 particles are needed per square meter of the Earth's surface. Assuming a dust cloud as high as the Moon, this equals an average particle density of 17.5 particles per cubic meter, or a total of 5.8×10^{26} particles:

$$\begin{aligned}\text{area shadow} &= 0.007/1\times10^{-12}\\ &= 7\times10^9 \text{ particles/m}^3,\\ \text{density of particles} &= 7\times10^9/4\times10^8\\ &= 17.5 \text{ particles/m}^3.\end{aligned}$$

An orbiting dust cloud can be modelled as a solid sphere which contains uniformly distributed particles. The cloud's radius is assumed to be at the altitude of the Moon (400,000 km). The volume is therefore:

$$\text{volume cloud} = \tfrac{4}{3}\,\pi\,(4\times10^8)^3 = 2.7\times10^{26}\text{ m}^3.$$

Assuming a mass density of 2, each particle would have a mass of 2×10^{-15} kilograms, which gives a mass for the total cloud of 9.5×10^{12} kilograms, or approximately 9.5 Gigatons:

$$\begin{aligned}\text{mass}_{\text{particle}} &= 2\times(1\times10^{-5})^3 = 2\times10^{-15}\text{ kg},\\ \text{mass}_{\text{total}} &= 2\times10^{-15}\times17.5\times2.7\times10^{26} = 9.5\times10^{12}\text{ kg}.\end{aligned}$$

The escape velocity of the Moon is 2373 m/sec, or 2.8×10^6 Joules per kilogram of mass removed from the Moon's gravity well. This gives a total energy required to lift the dust cloud of 2.6×10^{19} Joules, which is less than the calculated energy of the event:

$$E_{\text{orbital}} = 0.5\times(9.5\times10^{12})\times2373^2 = 2.6\times10^{19}\text{ Joules}.$$

Since not all of the energy went into placing matter into high earth orbit, and since not all of the orbiting matter is in the form of optimal light-blocking dust, we could expect an efficiency of perhaps 5% in converting the original explosion into an orbiting dust cloud. The indicated efficiency, given that the explosion was 1×10^{20} Joules, is 26%. This suggests that the actual energy of the crater-forming explosion was closer to the Dence number, above.

6 Orbital characteristics of a dust cloud

An orbiting dust cloud such as the one described above would not be stable. Individual particles would experience perturbations in their orbit due to the Moon's gravity, and would also be subject to orbital change due to solar wind, atmospheric drag, and collision with other particles.

In the intermediate term, particles colliding with each other would cause the cloud to assume the shape of a ring. In the long term, the particles would be removed from orbit.

The orbital velocity of the Moon is approximately 1000 meters/sec. For a dust particle moving through the dust cloud described above, the mean distance between collisions would be approximately 1.4×10^{10} meters, which is 1.4×10^7 seconds, or 6 months:

$$\begin{aligned}\text{cross section collision} &= 4\times(1\times10^{-6})^2\times17.5\\ &= 7\times10^{-11}\text{ m}^3,\\ \text{mean free path} &= 1/(7\times10^{-11})\\ &= 1.4\times10^{10}\text{ m},\\ \text{mean collision interval} &= \text{mean free path/velocity}\\ &= 1.4\times10^{10}/1000\\ &= 1.4\times10^7\text{ sec}.\end{aligned}$$

How long the cloud would remain in orbit depends on various assumptions regarding its initial orbital characteristics and the level of solar wind activity. An orbital half-life of a few decades seems reasonable.

7 Evidence of Lunar impacts in marine sediments

Much of the mass placed into earth orbit would be recaptured by the Moon, and some would escape to solar orbit, but some large fraction would be deposited on the surface of the Earth. Assuming that some large fraction of the dust eventually was deposited on the surface of the Earth, it should be possible to locate the characteristic Titanium Oxide from the Moon rock in marine sediment or polar ice core samples. If half of the total orbiting dust cloud was deposited on the Earth's surface, there would be approximately 5 grams/square meter. Of this, perhaps 10% (0.5 grams) would be Titanium.

$$\begin{aligned}\text{dust density} &= 50\%\times\text{mass}_{\text{total}}/\text{Earth surface area}\\ &= 0.5\times(9.5\times10^{12})/(4\pi\times(6.3\times10^6)^2)\\ &= 0.00475\text{ kg/m}^2,\\ \text{titanium density} &= 0.10\times\text{dust density}\\ &= 0.000475\text{ kg/m}^2.\end{aligned}$$

It must also be considered that many of the major ice ages were caused by orbiting dust from the Moon, and that they will also have left traces in the marine sediments. An examination of the sediment samples would show whether the Ice Age which began 15,000 years ago was also caused by an object impacting on the Moon.

8 Objections to this idea

It has been suggested that, after an impact on the Moon similar to the one described in this paper, a large amount of debris would impact the Earth a few days later. It has also been suggested that these impacts would create a spectacular meteor storm, and that the absence of such a meteor storm in the historical record suggests that there was no such impact in the year 1178.

Analysis shows that most of the debris would not create dramatic effects, and that the amount of light emitted by the impacts would be diffuse.

Objects falling from the altitude of the Moon will have an impact velocity approximately equal to the escape velocity of the Earth (11200 meters/sec). The energy released by a 1 micro-gram particle (the size of a grain of sand) impacting at this speed is 62.7 Joules. When this enters the Earth's atmosphere, it will look like a 60-Watt light bulb shining for one second, which is probably not going to create a big psychological impact. Dust particles will produce an even less dramatic effect. Even if 10 Megatons of lunar regolith and dust particles were to hit the Earth in the first month after the impact, it would only add up to 6×10^{14} Joules, or 240 Megawatts. More to the point, this is 4 micro-watts per square meter of the Earth's surface, which is less than 1% of the light from a full Moon.

This amount of light concentrated into a small number of fireballs might be noticed, but spread into billions of individual particles, the energy released would not be spectacular.

Submitted on August 08, 2014 / Accepted on August 12, 2014

References

1. Cook E. et al. Tree ring climate data. *Science*, Science, v. 253, 1266–1268.
2. De Pater I. and Lissauer J.J. Planetary Sciences. Cambridge University Press, 2005, page 165.
3. Dence M.C., Grieve R.A.F., and Robertson P.B. Terrestrial impact structures: Principal characteristics and energy consideration. In: *Impact and explosion cratering*, Pergamon Press, Oxford, 1977.
4. Gervase of Canterbury 1178: Chronicles Trinity College. Cambridge, UK.
5. Glasstone S. The Effects of Nuclear Weapons. US Department of Defence, 1977.
6. Hughes D.W. Giordano Bruno, the Moon's Latest Large Crater. *Nature*, 1976, v. 264, 212–213.
7. Lamb H.H. Climate: Past, Present, and Future, Volume I. Methuen, London, 1977.
8. Lamb H.H. Climate: Past, Present, and Future, Volume II. Methuen, London, 1977.

Dimension of Physical Space

Gunn Quznetsov

E-mail: gunn@mail.ru, quznets@yahoo.com

Each vector of state has its own corresponing element of the CayleyDickson algebra. Properties of a state vector require that this algebra was a normalized division algebra. By the Hurwitz and Frobenius theorems maximal dimension of such algebra is 8. Consequently, a dimension of corresponding complex state vectors is 4, and a dimension of the Clifford set elements is 4×4. Such set contains 5 matrices — among them — 3-diagonal. Hence, a dimension of the dot events space is equal to 3+1.

Further I use CayleyDickson algebras [1, 2]:

Let

$$1, \mathrm{i}, \mathrm{j}, \mathrm{k}, \mathrm{E}, \mathrm{I}, \mathrm{J}, \mathrm{K}$$

be basis elements of a 8-dimensional algebra Cayley (*the octavians algebra*) [1, 2]. A product of this algebra is defined the following way [1]:

1) For every basic element e:

$$\mathrm{ee} = -1;$$

2) If u_1, u_2, v_1, v_2 are real number then

$$(u_1 + u_2\mathrm{i})\,(v_1 + v_2\mathrm{i}) = (u_1v_1 - v_2u_2) + (v_2u_1 + u_2v_1)\,\mathrm{i}.$$

3) If u_1, u_2, v_1, v_2 are numbers of shape $w = w_1 + w_2\mathrm{i}$ (w_s, and $s \in \{1, 2\}$ are real numbers, and $\overline{w} = w_1 - w_2\mathrm{i}$) then

$$(u_1 + u_2\mathrm{j})\,(v_1 + v_2\mathrm{j}) = (u_1v_1 - \overline{v}_2u_2) + (v_2u_1 + u_2\overline{v}_1)\,\mathrm{j} \quad (1)$$

and $\mathrm{ij} = \mathrm{k}$.

4) If u_1, u_2, v_1, v_2 are number of shape $w = w_1 + w_2\mathrm{i} + w_3\mathrm{j} + w_4\mathrm{k}$ (w_s, and $s \in \{1, 2, 3, 4\}$ are real numbers, and $\overline{w} = w_1 - w_2\mathrm{i} - w_3\mathrm{j} - w_4\mathrm{k}$) then

$$(u_1 + u_2\mathrm{E})\,(v_1 + v_2\mathrm{E}) = (u_1v_1 - \overline{v}_2u_2) + (v_2u_1 + u_2\overline{v}_1)\,\mathrm{E} \quad (2)$$

and

$$\mathrm{iE} = \mathrm{I},$$
$$\mathrm{jE} = \mathrm{J},$$
$$\mathrm{kE} = \mathrm{K}.$$

Therefore, in accordance with point 2) the real numbers field (**R**) is extended to the complex numbers field (**R**), and in accordance with point 3) the complex numbers field is expanded to the quaternions field (**K**), and point 4) expands the quaternions fields to the octavians field (**O**). This method of expanding of fields is called *a Dickson doubling procedure* [1].

If

$$u = a + b\mathrm{i} + c\mathrm{j} + d\mathrm{k} + A\mathrm{E} + B\mathrm{I} + C\mathrm{J} + \mathrm{K}$$

with real a, b, c, d, A, B, C, D then a real number

$$\|u\| := \sqrt{u\overline{u}} = \left(a^2 + b^2 + c^2 + d^2 + A^2 + B^2 + C^2 + D^2\right)^{0.5}$$

is called *a norm* of octavian u [1].

For each octavians u and v:

$$\|uv\| = \|u\|\,\|v\|\,. \quad (3)$$

Algebras with this conditions are called *normalized algebras* [1, 2].

Any 3+1-vector of a probability density can be represented by the following equations in matrix form [4, 5]

$$\rho = \varphi^\dagger\varphi\,,$$
$$j_k = \varphi^\dagger\beta^{[k]}\varphi$$

with $k \in \{1, 2, 3\}$.

There $\beta^{[k]}$ are complex 2-diagonal 4×4-matrices of Clifford's set of rank 4, and φ is matrix columns with four complex components. The light and colored pentads of Clifford's set of such rank contain in threes 2-diagonal matrices, corresponding to 3 space coordinates in accordance with Dirac's equation. Hence, a space of these events is 3-dimensional.

Let $\rho(t, \mathbf{x})$ be a probability density of event $A\,(t, \mathbf{x})$, and

$$\rho_c(t, \mathbf{x}|t_0, \mathbf{x}_0)$$

be a probability density of event $A\,(t, \mathbf{x})$ on condition that event $B\,(t_0, \mathbf{x}_0)$.

In that case if function $q(t, \mathbf{x}|t_0, \mathbf{x}_0)$ is fulfilled to condition:

$$\rho_c(t, \mathbf{x}|t_0, \mathbf{x}_0) = q(t, \mathbf{x}|t_0, \mathbf{x}_0)\rho(t, \mathbf{x}), \quad (4)$$

then one is called *a disturbance function* B to A.

If $q = 1$ then B does not disturbance to A.

A conditional probability density of event $A\,(t, \mathbf{x})$ on condition that event $B\,(t_0, \mathbf{x}_0)$ is presented as:

$$\rho_c = \varphi_c^\dagger\varphi_c$$

like to a probability density of event $A\,(t, \mathbf{x})$.

Let

$$\varphi = \begin{bmatrix} \varphi_{1,1} + \mathrm{i}\varphi_{1,2} \\ \varphi_{2,1} + \mathrm{i}\varphi_{2,2} \\ \varphi_{3,1} + \mathrm{i}\varphi_{3,2} \\ \varphi_{4,1} + \mathrm{i}\varphi_{4,2} \end{bmatrix}$$

and

$$\varphi_c = \begin{bmatrix} \varphi_{c,1,1} + \mathrm{i}\varphi_{c,1,2} \\ \varphi_{c,2,1} + \mathrm{i}\varphi_{c,2,2} \\ \varphi_{c,3,1} + \mathrm{i}\varphi_{c,3,2} \\ \varphi_{c,4,1} + \mathrm{i}\varphi_{c,4,2} \end{bmatrix}$$

(all $\varphi_{r,s}$ and $\varphi_{c,r,s}$ are real numbers).

In that case octavian

$$u = \varphi_{1,1} + \varphi_{1,2}\mathrm{i} + \varphi_{2,1}\mathrm{j} + \varphi_{2,2}\mathrm{k} + \varphi_{3,1}\mathrm{E} + \\ + \varphi_{3,2}\mathrm{I} + \varphi_{4,1}\mathrm{J} + \varphi_{4,2}\mathrm{K}$$

is called *a Caylean* of φ. Therefore, octavian

$$u_c = \varphi_{c,1,1} + \varphi_{c,1,2}\mathrm{i} + \varphi_{c,2,1}\mathrm{j} + \varphi_{c,2,2}\mathrm{k} + \varphi_{c,3,1}\mathrm{E} + \\ + \varphi_{c,3,2}\mathrm{I} + \varphi_{c,4,1}\mathrm{J} + \varphi_{c,4,2}\mathrm{K}$$

is Caylean of φ_c.

In accordance with the octavian norm definition:

$$\begin{aligned} \|u_c\|^2 &= \rho_c\,, \\ \|u\|^2 &= \rho\,. \end{aligned} \tag{5}$$

Because the octavian algebra is a division algebra [1, 2] then for each octavians u and u_c there exists an octavian w such that

$$u_c = wu.$$

Because the octavians algebra is normalized then

$$\|u_c\|^2 = \|w\|^2 \|u\|^2\,.$$

Hence, from (4) and (5):

$$q = \|w\|^2\,.$$

Therefore, in a 3+1-dimensional space-time there exists an octavian-Caylean for a disturbance function of any event to any event.

In order to increase a space dimensionality the octavian algebra can be expanded by a Dickson doubling procedure:

Another 8 elements should be added to basic octavians:

$$\mathrm{z}_1,\ \mathrm{z}_2, \mathrm{z}_3,\ \mathrm{z}_4,\ \mathrm{z}_5,\ \mathrm{z}_6,\ \mathrm{z}_7,\ \mathrm{z}_8$$

such that:

$$\begin{aligned} \mathrm{z}_2 &= \mathrm{i}\mathrm{z}_1, \\ \mathrm{z}_3 &= \mathrm{j}\mathrm{z}_1, \\ \mathrm{z}_4 &= \mathrm{k}\mathrm{z}_1, \\ \mathrm{z}_5 &= \mathrm{E}\mathrm{z}_1, \\ \mathrm{z}_6 &= \mathrm{I}\mathrm{z}_1, \\ \mathrm{z}_7 &= \mathrm{J}\mathrm{z}_1, \\ \mathrm{z}_8 &= \mathrm{K}\mathrm{z}_1, \end{aligned}$$

and for every octavians u_1, u_2, v_1, v_2:

$$(u_1 + u_2\mathrm{z}_1)(v_1 + v_2\mathrm{z}_1) = (u_1v_1 - \overline{v}_2u_2) + (v_2u_1 + u_2\overline{v}_1)\,\mathrm{z}_1$$

(here: if $w = w_1 + w_2\mathrm{i} + w_3\mathrm{j} + w_4\mathrm{k} + w_5\mathrm{E} + w_6\mathrm{I} + w_7\mathrm{J} + w_8\mathrm{K}$ with real w_s then $\overline{w} = w_1 - w_2\mathrm{i} - w_3\mathrm{j} - w_4\mathrm{k} - w_5\mathrm{E} - w_6\mathrm{I} - w_7\mathrm{J} - w_8\mathrm{K}$).

It is a 16-dimensional Cayley-Dickson algebra.

In accordance with [3], for any natural number z there exists a Clifford set of rank 2^z. In considering case for $z = 3$ there is Clifford's seven:

$$\underline{\beta}^{[1]} = \begin{bmatrix} \beta^{[1]} & 0_4 \\ 0_4 & -\beta^{[1]} \end{bmatrix},\ \underline{\beta}^{[2]} = \begin{bmatrix} \beta^{[2]} & 0_4 \\ 0_4 & -\beta^{[2]} \end{bmatrix}, \tag{6}$$

$$\underline{\beta}^{[3]} = \begin{bmatrix} \beta^{[3]} & 0_4 \\ 0_4 & -\beta^{[3]} \end{bmatrix},\ \underline{\beta}^{[4]} = \begin{bmatrix} \beta^{[4]} & 0_4 \\ 0_4 & -\beta^{[4]} \end{bmatrix}, \tag{7}$$

$$\underline{\beta}^{[5]} = \begin{bmatrix} \gamma^{[0]} & 0_4 \\ 0_4 & -\gamma^{[0]} \end{bmatrix}, \tag{8}$$

$$\underline{\beta}^{[6]} = \begin{bmatrix} 0_4 & 1_4 \\ 1_4 & 0_4 \end{bmatrix},\ \underline{\beta}^{[7]} = \mathrm{i}\begin{bmatrix} 0_4 & -1_4 \\ 1_4 & 0_4 \end{bmatrix}. \tag{9}$$

Therefore, in this seven five 4-diagonal matrices (7) define a 5-dimensional space of events, and two 4-antidiagonal matrices (9) defined a 2-dimensional space for the electroweak transformations.

It is evident that such procedure of dimensions building up can be continued endlessly. But in accordance with the Hurwitz theorem* and with the generalized Frobenius theorem† a more than 8-dimensional Cayley-Dickson algebra does not a division algebra. Hence, there in a more than 3-dimensional space exist events such that a disturbance function between these events does not hold a Caylean. I call such disturbance *supernatural*.

Therefore, supernatural disturbance do not exist in a 3-dimensional space, but in a more than 3-dimensional space such supernatural disturbance act.

Submitted on August 15, 2014 / Accepted on August 17, 2014

References

1. Kantor I.L.; Solodownikow A.S. Hipercomplex Numbers, Nauka, Moscow, 1973, p. 99; Kantor I.L.; Solodownikow A.S. Hyperkomplexe Zahlen. B. G. Teubner, Leipzig, 1978.
2. Mel'nikov O.V., Remeslennikov V.N. et al. General Algebra. Nauka, Moscow, 1990, p. 396.
3. Zhelnorovich V.A. Theory of Spinors. Application to Mathematics and Physics. Nauka, Moscow, 1982, p. 21.
4. Abers E. Quantum Mechanics. Addison Wesley, 2004, p. 423.
5. Quznetsov G. Final Book on Fundamental Theoretical Physics. American Research Press, American Research Press, Rehoboth (NM), 2011, pp. 60–62.

*Every normalized algebra with unit is isomorphous to one of the following: the real numbers algebra **R**, the complex numbers algebra **C**, the quaternions algebra **K**, the octavians algebra **O** [1].

†A division algebra can be only either 1 or 2 or 4 or 8-dimensional [2].

Informational Time

Gunn Quznetsov

E-mail: gunn@mail.ru, quznets@yahoo.com

I call any subjects, connected with an information the informational objects. It is clear that information received from such informational object can be expressed by a text which is made of sentences. I call a set of sentences expressing information about some informational object recorder of this object. Some recorders systems form structures similar to clocks. The following results are obtained from the logical properties of a set of recorders: First, all such clocks have the same direction, i.e. if an event expressed by sentence A precedes an event expressed by sentence B according to one of such clocks then it is true according to the others. Secondly, time is irreversible according to these clocks, i.e. there's no recorder which can receive information about an event that has happened until this event really happens Thirdly, a set of recorders is naturally embedded into metrical space. Fourthly, if this metrical space is Euclidean, then the corresponding "space and time" of recorders obeys to transformations of the complete Poincare group. If this metric space is not Euclidean then suitable non-linear geometry may be built in this space.

Here I use numbering of definitions and theorems from book [1] which contains detailed proofs of all these theorems.

1 Recorders

Any information, received from physical devices, can be expressed by a text, made of sentences.

Let $\widehat{\mathbf{a}}$ be some object which is able to receive, save, and/or transmit an information. *A* set $\mathbf{a}$ of sentences, expressing an information of an object $\widehat{\mathbf{a}}$, is called *a recorder* of this object. Thus, statement: "Sentence $\ll A\gg$ is an element of the set $\mathbf{a}$" denotes: "$\widehat{\mathbf{a}}$ has information that the event, expressed by sentence $\ll A\gg$, took place". In short: "$\widehat{\mathbf{a}}$ knows that *A*". Or by designation: "$\mathbf{a}^\bullet \ll A\gg$".

Obviously, the following conditions are satisfied:

I. For any $\mathbf{a}$ and for every *A*: false is that $\mathbf{a}^\bullet (A\& (\neg A))$, thus, any recorder doesn't contain a logical contradiction;

II. For every $\mathbf{a}$, every *B*, and all *A*: if *B* is a logical consequence from *A*, and $\mathbf{a}^\bullet A$, then $\mathbf{a}^\bullet B$;

*III. For all $\mathbf{a}$, $\mathbf{b}$ and for every *A*: if $\mathbf{a}^\bullet \ll \mathbf{b}^\bullet A\gg$ then $\mathbf{a}^\bullet A$.

2 Time

Let's consider finite (probably empty) path of symbols of form $\mathbf{q}^\bullet$.

Def. 1.3.1: A path α is *a subpath* of a path β (design.: $\alpha \prec \beta$) if α can be got from β by deletion of some (probably all) elements.

Designation: $(\alpha)^1$ is α, and $(\alpha)^{k+1}$ is $\alpha\,(\alpha)^k$.

Therefore, if $k \leqslant l$ then $(\alpha)^k \prec (\alpha)^l$.

Def. 1.3.2: A path α is *equivalent* to a path β (design.: $\alpha \sim \beta$) if α can be got from β by substitution of a subpath of form $(\mathbf{a}^\bullet)^k$ by a path of the same form $(\mathbf{a}^\bullet)^s$.

In this case:

III. If $\beta \prec \alpha$ or $\beta \sim \alpha$ then for any *K*: if $\mathbf{a}^\bullet K$ then $\mathbf{a}^\bullet (K\& (\alpha A \Rightarrow \beta A))$.

Obviously, III is a refinement of condition *III.

Def. 1.3.3: A natural number *q* is *instant*, at which a registrates *B* according to *κ-clock* $\{\mathbf{g}_0, A, \mathbf{b}_0\}$ (design.: *q* is $[\mathbf{a}^\bullet B \uparrow \mathbf{a}, \{\mathbf{g}_0, A, \mathbf{b}_0\}]$) if:

1. for any *K*: if $\mathbf{a}^\bullet K$ then

$$\mathbf{a}^\bullet \left(K\& \left(\mathbf{a}^\bullet B \Rightarrow \mathbf{a}^\bullet \left(\mathbf{g}_0^\bullet \mathbf{b}_0^\bullet\right)^q \mathbf{g}_0^\bullet A\right)\right)$$

and

$$\mathbf{a}^\bullet \left(K\& \left(\mathbf{a}^\bullet \left(\mathbf{g}_0^\bullet \mathbf{b}_0^\bullet\right)^{q+1} \mathbf{g}_0^\bullet A \Rightarrow \mathbf{a}^\bullet B\right)\right).$$

2. $\mathbf{a}^\bullet \left(\mathbf{a}^\bullet B\& \left(\neg \mathbf{a}^\bullet \left(\mathbf{g}_0^\bullet \mathbf{b}_0^\bullet\right)^{q+1} \mathbf{g}_0^\bullet A\right)\right)$.

Def. 1.3.4: *κ*-clocks $\{\mathbf{g}_1, B, \mathbf{b}_1\}$ and $\{\mathbf{g}_2, B, \mathbf{b}_2\}$ have *the same direction* for $\mathbf{a}$ if the following condition is satisfied:

If

$$r = \left[\mathbf{a}^\bullet \left(\mathbf{g}_1^\bullet \mathbf{b}_1^\bullet\right)^q \mathbf{g}_1^\bullet B \uparrow \mathbf{a}, \{\mathbf{g}_2, B, \mathbf{b}_2\}\right],$$

$$s = \left[\mathbf{a}^\bullet \left(\mathbf{g}_1^\bullet \mathbf{b}_1^\bullet\right)^p \mathbf{g}_1^\bullet B \uparrow \mathbf{a}, \{\mathbf{g}_2, B, \mathbf{b}_2\}\right],$$

$$q < p,$$

then

$$r \leqslant s\,.$$

Th. 1.3.1: All *κ*-clocks have the same direction. Consequently, a recorder orders its sentences with respect to instants. Moreover, this order is linear and it doesn't matter according to which *κ*-clock it is established.

Def. 1.3.5: *κ*-clock $\{\mathbf{g}_2, B, \mathbf{b}_2\}$ is *k* times more precise than *κ*-clock $\{\mathbf{g}_1, B, \mathbf{b}_1\}$ for recorder $\mathbf{a}$ if for every *C* the following condition is satisfied: if

$$q_1 = [\mathbf{a}^\bullet C \uparrow \mathbf{a}, \{\mathbf{g}_1, B, \mathbf{b}_1\}],$$
$$q_2 = [\mathbf{a}^\bullet C \uparrow \mathbf{a}, \{\mathbf{g}_2, B, \mathbf{b}_2\}],$$

then

$$q_1 < \tfrac{q_2}{k} < q_1 + 1.$$

Def. 1.3.6: A sequence $\widetilde{H}$ of κ-clocks:

$$\left\langle \{\mathbf{g}_0, A, \mathbf{b}_0\},\ \{\mathbf{g}_1, A, \mathbf{b}_2\}, \ldots, \left\{\mathbf{g}_j, A, \mathbf{b}_j\right\},\ \ldots \right\rangle$$

is called *an absolutely precise* κ-clock of a recorder $\mathbf{a}$ if for every j exists a natural number k_j so that κ-clock$\left\{\mathbf{g}_j, A, \mathbf{b}_j\right\}$ is k_j times more precise than κ-clock$\left\{\mathbf{g}_{j-1}, A, \mathbf{b}_{j-1}\right\}$.

In this case if

$$q_j = \left[\mathbf{a}^\bullet C \uparrow \mathbf{a}, \left\{\mathbf{g}_j, A, \mathbf{b}_j\right\}\right]$$

and

$$t = q_0 + \sum_{j=1}^{\infty} \frac{q_j - q_{j-1} \cdot k_j}{k_1 \cdot k_2 \cdot \ldots \cdot k_j},$$

then

$$t \text{ is } \left[\mathbf{a}^\bullet C \uparrow \mathbf{a}, \widetilde{H}\right].$$

3 Space

Def. 1.4.1: A number t is called *a time, measured by a recorder* $\mathbf{a}$ *according to a* κ*-clock* $\widetilde{H}$*, during which a signal* C *did a path* $\mathbf{a}^\bullet\alpha\mathbf{a}^\bullet$, design.:

$$t := \mathfrak{m}\left(\mathbf{a}\widetilde{H}\right)(\mathbf{a}^\bullet\alpha\mathbf{a}^\bullet C),$$

if

$$t = \left[\mathbf{a}^\bullet\alpha\mathbf{a}^\bullet C \uparrow \mathbf{a}, \widetilde{H}\right] - \left[\mathbf{a}^\bullet C \uparrow \mathbf{a}, \widetilde{H}\right].$$

Th. 1.4.1:

$$\mathfrak{m}\left(\mathbf{a}\widetilde{H}\right)(\mathbf{a}^\bullet\alpha\mathbf{a}^\bullet C) \geqslant 0.$$

Def. 1.4.2:

1) for every recorder $\mathbf{a}$: $(\mathbf{a}^\bullet)^\dagger = (\mathbf{a}^\bullet)$;
2) for all paths α and β: $(\alpha\beta)^\dagger = (\beta)^\dagger(\alpha)^\dagger$.

Def. 1.4.3: A set $\mathfrak{R}$ of recorders is *an internally stationary system* for a recorder $\mathbf{a}$ with a κ-clock $\widetilde{H}$ (design.: $\mathfrak{R}$ is $ISS\left(\mathbf{a}, \widetilde{H}\right)$) if for all sentences B and C, for all elements $\mathbf{a}_1$ and $\mathbf{a}_2$ of set $\mathfrak{R}$, and for all paths α, made of elements of set $\mathfrak{R}$, the following conditions are satisfied:

1) $\left[\mathbf{a}^\bullet\mathbf{a}_2^\bullet\mathbf{a}_1^\bullet C \uparrow \mathbf{a}, \widetilde{H}\right] - \left[\mathbf{a}^\bullet\mathbf{a}_1^\bullet C \uparrow \mathbf{a}, \widetilde{H}\right] =$
$= \left[\mathbf{a}^\bullet\mathbf{a}_2^\bullet\mathbf{a}_1^\bullet B \uparrow \mathbf{a}, \widetilde{H}\right] - \left[\mathbf{a}^\bullet\mathbf{a}_1^\bullet B \uparrow \mathbf{a}, \widetilde{H}\right]$;
2) $\mathfrak{m}\left(\mathbf{a}\widetilde{H}\right)(\mathbf{a}^\bullet\alpha\mathbf{a}^\bullet C) = \mathfrak{m}\left(\mathbf{a}\widetilde{H}\right)\left(\mathbf{a}^\bullet\alpha^\dagger\mathbf{a}^\bullet C\right)$.

Th. 1.4.2:

$$\{\mathbf{a}\} - ISS\left(\mathbf{a}, \widetilde{H}\right).$$

Def. 1.4.4: A number l is called *an* $\mathbf{a}\widetilde{H}(B)$*-measure* of recorders $\mathbf{a}_1$ and $\mathbf{a}_2$, design.:

$$l = \ell\left(\mathbf{a}, \widetilde{H}, B\right)(\mathbf{a}_1, \mathbf{a}_2)$$

if

$$l = 0.5 \cdot \left(\left[\mathbf{a}^\bullet\mathbf{a}_1^\bullet\mathbf{a}_2^\bullet\mathbf{a}_1^\bullet B \uparrow \mathbf{a}, \widetilde{H}\right] - \left[\mathbf{a}^\bullet\mathbf{a}_1^\bullet B \uparrow \mathbf{a}, \widetilde{H}\right]\right).$$

Th. 1.4.3: If $\{\mathbf{a}, \mathbf{a}_1, \mathbf{a}_2, \mathbf{a}_3\}$ is $ISS\left(\mathbf{a}, \widetilde{H}\right)$ then

1) $\ell\left(\mathbf{a}, \widetilde{H}\right)(\mathbf{a}_1, \mathbf{a}_2) \geqslant 0$;
2) $\ell\left(\mathbf{a}, \widetilde{H}\right)(\mathbf{a}_1, \mathbf{a}_1) = 0$;
3) $\ell\left(\mathbf{a}, \widetilde{H}\right)(\mathbf{a}_1, \mathbf{a}_2) = \ell\left(\mathbf{a}, \widetilde{H}\right)(\mathbf{a}_2, \mathbf{a}_1)$;
4) $\ell\left(\mathbf{a}, \widetilde{H}\right)(\mathbf{a}_1, \mathbf{a}_2) + \ell\left(\mathbf{a}, \widetilde{H}\right)(\mathbf{a}_2, \mathbf{a}_3) \geqslant \ell\left(\mathbf{a}, \widetilde{H}\right)(\mathbf{a}_1, \mathbf{a}_3)$.

Thus, all four axioms of the metrical space are accomplished for $\ell\left(\mathbf{a}, \widetilde{H}\right)$ in an internally stationary systeminternally stationary system of recorders.

Consequently, $\ell\left(\mathbf{a}, \widetilde{H}\right)$ is a distance length similitude in this space.

Def. 1.4.6: B took place *in the same place as* $\mathbf{a}_1$ *for* $\mathbf{a}$ (design.: $\natural(\mathbf{a})(\mathbf{a}_1, B)$) if for every sequence α and for any sentence K the following condition is satisfied: if $\mathbf{a}^\bullet K$ then $\mathbf{a}^\bullet\left(K\&(\alpha B \Rightarrow \alpha\mathbf{a}_1^\bullet B)\right)$.

Th. 1.4.4:

$$\natural(\mathbf{a})\left(\mathbf{a}_1, \mathbf{a}_1^\bullet B\right).$$

Th. 1.4.5: If

$$\natural(\mathbf{a})(\mathbf{a}_1, B), \tag{1}$$
$$\natural(\mathbf{a})(\mathbf{a}_2, B), \tag{2}$$

then

$$\natural(\mathbf{a})(\mathbf{a}_2, \mathbf{a}_1^\bullet B).$$

Th. 1.4.6: If $\{\mathbf{a}, \mathbf{a}_1, \mathbf{a}_2\}$ is $ISS\left(\mathbf{a}, \widetilde{H}\right)$,

$$\natural(\mathbf{a})(\mathbf{a}_1, B), \tag{3}$$
$$\natural(\mathbf{a})(\mathbf{a}_2, B), \tag{4}$$

then

$$\ell\left(\mathbf{a}, \widetilde{H}\right)(\mathbf{a}_1, \mathbf{a}_2) = 0.$$

Th. 1.4.7: If $\{\mathbf{a}_1, \mathbf{a}_2, \mathbf{a}_3\}$ is $ISS\left(\mathbf{a}, \widetilde{H}\right)$ and there exists sentence B such that

$$\natural(\mathbf{a})(\mathbf{a}_1, B), \tag{5}$$
$$\natural(\mathbf{a})(\mathbf{a}_2, B), \tag{6}$$

then

$$\ell\left(\mathbf{a}, \widetilde{H}\right)(\mathbf{a}_3, \mathbf{a}_2) = \ell\left(\mathbf{a}, \widetilde{H}\right)(\mathbf{a}_3, \mathbf{a}_1).$$

Def. 1.4.7: A real number t is an instant of a sentence B in *frame of reference* $\left(\mathfrak{R}\mathbf{a}\widetilde{H}\right)$, design.:

$$t = \left[B \mid \mathfrak{R}\mathbf{a}\widetilde{H}\right],$$

if

1) $\mathfrak{R}$ is $ISS\left(\mathbf{a},\widetilde{H}\right)$,
2) there exists a recorder $\mathbf{b}$ so that $\mathbf{b}\in\mathfrak{R}$ and $\natural(\mathbf{a})(\mathbf{b},B)$,
3) $t=\left[\mathbf{a}^{\bullet}B\uparrow\mathbf{a},\widetilde{H}\right]-\ell\left(\mathbf{a},\widetilde{H}\right)(\mathbf{a},\mathbf{b})$.

Def. 1.4.8: A real number z is *a distance length* between B and C in a frame of reference $\left(\mathfrak{R}\mathbf{a}\widetilde{H}\right)$, design.:

$$z=\ell\left(\mathfrak{R}\mathbf{a}\widetilde{H}\right)(B,C),$$

if

1) $\mathfrak{R}$ is $ISS\left(\mathbf{a},\widetilde{H}\right)$,
2) there exist recorders $\mathbf{a}_1$ and $\mathbf{a}_2$ so that $\mathbf{a}_1\in\mathfrak{R}$, $\mathbf{a}_2\in\mathfrak{R}$, $\natural(\mathbf{a})(\mathbf{a}_1,B))$ and $\natural(\mathbf{a})(\mathbf{a}_2,C))$,
3) $z=\ell\left(\mathbf{a},\widetilde{H}\right)(\mathbf{a}_2,\mathbf{a}_1)$.

According to Theorem 1.4.3 such distance length satisfies conditions of all axioms of a metric space.

4 Relativity

Def. 1.5.1: Recorders $\mathbf{a}_1$ and $\mathbf{a}_2$ *equally receive a signal* about B for a recorder $\mathbf{a}$ if

$$\ll\natural(\mathbf{a})\left(\mathbf{a}_2,\mathbf{a}_1^{\bullet}B\right)\gg=\ll\natural(\mathbf{a})\left(\mathbf{a}_1,\mathbf{a}_2^{\bullet}B\right)\gg.$$

Def. 1.5.2: Set of recorders are called *a homogeneous space of recorders*, if all its elements equally receive all signals.

Def. 1.5.3: A real number c is *an information velocity about B to the recorder* $\mathbf{a}_1$ in a frame of reference $\left(\mathfrak{R}\mathbf{a}\widetilde{H}\right)$ if

$$c=\frac{\ell\left(\mathfrak{R}\mathbf{a}\widetilde{H}\right)\left(B,\mathbf{a}_1^{\bullet}B\right)}{\left[\mathbf{a}_1^{\bullet}B\mid\mathfrak{R}\mathbf{a}\widetilde{H}\right]-\left[B\mid\mathfrak{R}\mathbf{a}\widetilde{H}\right]}.$$

Th. 1.5.1: In all homogeneous spaces:

$$c=1.$$

That is in every homogenous space a propagation velocity of every information to every recorder for every frame reference equals to 1.

Th. 1.5.2: If $\mathfrak{R}$ is a homogeneous space, then

$$\left[\mathbf{a}_1^{\bullet}B\mid\mathfrak{R}\mathbf{a}\widetilde{H}\right]\geqslant\left[B\mid\mathfrak{R}\mathbf{a}\widetilde{H}\right].$$

Consequently, in any homogeneous space any recorder finds out that B "took place" not earlier than B "actually take place". "Time" is irreversible.

Th. 1.5.3: If $\mathbf{a}_1$ and $\mathbf{a}_2$ are elements of $\mathfrak{R}$,

$$\mathfrak{R}isISS\left(\mathbf{a},\widetilde{H}\right), \tag{7}$$

$$p:=\left[\mathbf{a}_1^{\bullet}B\mid\mathfrak{R}\mathbf{a}\widetilde{H}\right], \tag{8}$$

$$q:=\left[\mathbf{a}_2^{\bullet}\mathbf{a}_1^{\bullet}B\mid\mathfrak{R}\mathbf{a}\widetilde{H}\right], \tag{9}$$

$$z:=\ell\left(\mathfrak{R}\mathbf{a}\widetilde{H}\right)(\mathbf{a}_1,\mathbf{a}_2),$$

then

$$z=q-p.$$

According to Urysohn's theorem* [2]: any homogeneous space is homeomorphic to some set of points of real Hilbert space. If this homeomorphism is not Identical transformation, then $\mathfrak{R}$ will represent a non- Euclidean space. In this case in this "space-time" corresponding variant of General Relativity Theory can be constructed. Otherwise, $\mathfrak{R}$ is Euclidean space. In this case there exists *coordinates system* R^{μ} such that the following condition is satisfied: for all elements $\mathbf{a}_1$ and $\mathbf{a}_2$ of set $\mathfrak{R}$ there exist points $\mathbf{x}_1$ and $\mathbf{x}_2$ of system R^{μ} such that

$$\ell\left(\mathbf{a},\widetilde{H}\right)(\mathbf{a}_k,\mathbf{a}_s)=\left(\sum_{j=1}^{\mu}\left(x_{s,j}-x_{k,j}\right)^2\right)^{0.5}.$$

In this case R^{μ} is called *a coordinates system of frame of reference* $\left(\mathfrak{R}\mathbf{a}\widetilde{H}\right)$ and numbers $\left\langle x_{k,1},x_{k,2},\ldots,x_{k,\mu}\right\rangle$ are called *coordinates of recorder* $\mathbf{a}_k$ in R^{μ}.

A coordinates system of a frame of reference is specified accurate to transformations of shear, turn, and inversion.

Def. 1.5.4: Numbers $\left\langle x_1,x_2,\ldots,x_{\mu}\right\rangle$ are called *coordinates* of B in *a coordinate system* R^{μ} of *a frame of reference* $\left(\mathfrak{R}\mathbf{a}\widetilde{H}\right)$ if there exists a recorder $\mathbf{b}$ such that $\mathbf{b}\in\mathfrak{R}$, $\natural(\mathbf{a})(\mathbf{b},B)$ and these numbers are the coordinates in R^{μ} of this recorder.

Th. 1.5.4: In a coordinate system R^{μ} of a frame of reference $\left(\mathfrak{R}\mathbf{a}\widetilde{H}\right)$: if z is a distance length between B and C, coordinates of B are

$$(b_1,b_2,\ldots,b_n)$$

coordinates of C are

$$(c_1,c_2,\ldots,c_3)$$

then

$$z=\left(\sum_{j=1}^{\mu}\left(c_j-b_j\right)^2\right)^{0.5}.$$

Def. 1.5.5: Numbers $\left\langle x_1,x_2,\ldots,x_{\mu}\right\rangle$ are called *coordinates of the recor-der* $\mathbf{b}$ *in the coordinate system* R^{μ} *at the instant t of the frame of reference* $\left(\mathfrak{R}\mathbf{a}\widetilde{H}\right)$ if for every B the condition is satisfied: if

$$t=\left[\mathbf{b}^{\bullet}B\mid\mathfrak{R}\mathbf{a}\widetilde{H}\right]$$

then coordinates of $\ll\mathbf{b}^{\bullet}B\gg$ in coordinate system R^{μ} of frame of reference $\left(\mathfrak{R}\mathbf{a}\widetilde{H}\right)$ are the following:

$$\left\langle x_1,x_2,\ldots,x_{\mu}\right\rangle.$$

Let v be the real number such that $|v|<1$.

*Pavel Samuilovich Urysohn, a.k.a. Pavel Uryson (February 3, 1898, Odessa — August 17, 1924, Batz-sur-Mer) was a Jewish mathematician who is best known for his contributions in the theory of dimension, and for developing Urysohn's Metrization Theorem and Urysohn's Lemma, both of which are fundamental results in topology.

Th. 1.5.5: In a coordinates system R^{μ} of a frame of reference $\left(\mathfrak{R}\mathbf{a}\widetilde{H}\right)$: if in every instant t: coordinates of*:

$$\mathbf{b} : \left\langle x_{\mathbf{b},1} + v \cdot t, x_{\mathbf{b},2}, x_{\mathbf{b},3}, \ldots, x_{\mathbf{b},\mu} \right\rangle,$$
$$\mathbf{g}_0 : \left\langle x_{0,1} + v \cdot t, x_{0,2}, x_{0,3}, \ldots, x_{0,\mu} \right\rangle,$$
$$\mathbf{b}_0 : \left\langle x_{0,1} + v \cdot t, x_{0,2} + l, x_{0,3}, \ldots, x_{0,\mu} \right\rangle,$$

and

$$t_C = \left[\mathbf{b}^{\bullet} C \mid \mathfrak{R}\mathbf{a}\widetilde{H}\right],$$
$$t_D = \left[\mathbf{b}^{\bullet} D \mid \mathfrak{R}\mathbf{a}\widetilde{H}\right],$$
$$q_C = \left[\mathbf{b}^{\bullet} C \uparrow \mathbf{b}, \{\mathbf{g}_0, A, \mathbf{b}_0\}\right],$$
$$q_D = \left[\mathbf{b}^{\bullet} D \uparrow \mathbf{b}, \{\mathbf{g}_0, A, \mathbf{b}_0\}\right],$$

then

$$\lim_{l \to 0} 2 \cdot \frac{l}{\sqrt{(1 - v^2)}} \cdot \frac{q_D - q_C}{t_D - t_C} = 1.$$

Consequently, moving at speed v κ-clock are times slower than the one at rest.

Th. 1.5.6: Let: v ($|v| < 1$) and l be real numbers and k_i be natural ones.

Let in a coordinates system R^{μ} of a frame of reference $\left(\mathfrak{R}\mathbf{a}\widetilde{H}\right)$: in each instant t coordinates of

$$\mathbf{b} : \left\langle x_{b,1} + v \cdot t, x_{b,2}, x_{b,3}, \ldots, x_{b,\mu} \right\rangle,$$
$$\mathbf{g}_j : \left\langle y_{j,1} + v \cdot t, y_{j,2}, y_{j,3}, \ldots, y_{j,\mu} \right\rangle,$$
$$\mathbf{u}_j : \left\langle y_{j,1} + v \cdot t, y_{j,2} + l/\left(k_1 \cdot \ldots \cdot k_j\right), y_{j,3}, \ldots, y_{j,\mu} \right\rangle,$$

for all $\mathbf{b}_i$: if $\mathbf{b}_i \in \mathfrak{I}$, then coordinates of

$$\mathbf{b}_i : \left\langle x_{i,1} + v \cdot t, x_{i,2}, x_{i,3}, \ldots, x_{i,\mu} \right\rangle,$$
$$\widetilde{T} \text{ is } \left\langle \{\mathbf{g}_1, A, \mathbf{u}_1\}, \{\mathbf{g}_2, A, \mathbf{u}_2\}, \ldots, \left\{\mathbf{g}_j, A, \mathbf{u}_j\right\}, \ldots \right\rangle.$$

In that case: $\mathfrak{I}$ is $ISS\left(\mathbf{b}, \widetilde{T}\right)$.

Therefore, a inner stability survives on a uniform straight line motion.

Th. 1.5.7: Let:

1) in a coordinates system R^{μ} of a frame of reference $\left(\mathfrak{R}\mathbf{a}\widetilde{H}\right)$ in every instant t:

$$\mathbf{b} : \left\langle x_{\mathbf{b},1} + v \cdot t, x_{\mathbf{b},2}, x_{\mathbf{b},3}, \ldots, x_{\mathbf{b},\mu} \right\rangle,$$
$$\mathbf{g}_j : \left\langle y_{j,1} + v \cdot t, y_{j,2}, y_{j,3}, \ldots, y_{j,\mu} \right\rangle,$$
$$\mathbf{u}_j : \left\langle y_{j,1} + v \cdot t, y_{j,2} + l/\left(k_1 \cdot \ldots \cdot k_j\right), y_{j,3}, \ldots, y_{j,\mu} \right\rangle,$$

for every recorder $\mathbf{q}_i$: if $\mathbf{q}_i \in \mathfrak{I}$ then coordinates of

$$\mathbf{q}_i : \left\langle x_{i,1} + v \cdot t, x_{i,2}, x_{i,3}, \ldots, x_{i,\mu} \right\rangle,$$
$$\widetilde{T} \text{ is } \left\langle \{\mathbf{g}_1, A, \mathbf{u}_1\}, \{\mathbf{g}_2, A, \mathbf{u}_2\}, \ldots, \left\{\mathbf{g}_j, A, \mathbf{u}_j\right\}, \ldots \right\rangle,$$

$$C : \left\langle C_1, C_2, C_3, \ldots, C_{\mu} \right\rangle,$$
$$D : \left\langle D_1, D_2, D_3, \ldots, D_{\mu} \right\rangle,$$
$$t_C = \left[C \mid \mathfrak{R}\mathbf{a}\widetilde{H}\right],$$
$$t_D = \left[D \mid \mathfrak{R}\mathbf{a}\widetilde{H}\right];$$

2) in a coordinates system $R^{\mu\prime}$ of a reference frame $\left(\mathfrak{I}\mathbf{b}\widetilde{T}\right)$:

$$C : \left\langle C'_1, C'_2, C'_3, \ldots, C'_{\mu} \right\rangle,$$
$$D : \left\langle D'_1, D'_2, D'_3, \ldots, D'_{\mu} \right\rangle,$$
$$t'_C = \left[C \mid \mathfrak{I}\mathbf{b}\widetilde{T}\right],$$
$$t'_D = \left[D \mid \mathfrak{I}\mathbf{b}\widetilde{T}\right].$$

In that case:

$$t'_D - t'_C = \frac{(t_D - t_C) - v\,(D_1 - C_1)}{\sqrt{1 - v^2}},$$
$$D'_1 - C'_1 = \frac{(D_1 - C_1) - v\,(t_D - t_C)}{\sqrt{1 - v^2}}.$$

This is the Lorentz spatial-temporal transformation.

Conclusion

Thus, if you have some set of objects, dealing with information, then "time" and "space" are inevitable. And it doesn't matter whether this set is part our world or some other worlds, which don't have a space-time structure initially.

I call such "Time" the Informational Time.

Since, we get our time together with our information system all other notions of time (thermodynamical time, cosmological time, psychological time, quantum time etc.) should be defined by that Informational Time.

Submitted on August 18, 2014 / Accepted on August 20, 2014

References

1. Quznetsov G. Final Book on Fundamental Theoretical Physics. American Research Press, Rehoboth (NM), 2011, 15–48; viXra.org: 1111.0051.
2. Urysohn P. Zum Metrisationsproblem. *Math. Ann.*, 1925, v. 94, 309–315.

*Below v is a real positive number such that $|v| < 1$.

Indications for a Diurnal and Annual Variation in the Anisotropy of Diffusion Patterns — A Reanalysis of Data Presented by J. Dai (2014, Nat. Sci.)

Felix Scholkmann

Bellariarain 10, 8038 Zürich, Switzerland. E-mail: felix.scholkmann@gmail.com

Anisotropic diffusion patterns of a toluidine blue colloid solution in water were recently reported by J. Dai (*Nat. Sci.*, 2014, v. 6 (2), 54–58). According to Dai's observations the fluctuation of anisotropy showed a diurnal and annual periodicity. Since these observations were only qualitatively described in the original manuscript, the data was reassessed by performing a detailed statistical analysis. The analysis revealed that indeed (i) the diffusion patterns exhibit a non-random characteristic (i.e. the maximum diffusion trend is not uniformly distributed), and (ii) a diurnal as well as an annual oscillation could be extracted and modeled with a sinusoidal function. In conclusion, the present analysis supports Dai's findings about anisotropy in diffusion of colloids in water with a daily and annual periodicity. Possible explanations of the observed effect are discussed and suggestions for further experiments are given.

1 Introduction

Recently, J. Dai published an interesting observation [1]: the diffusion of a toluidine blue colloid solution in water measured over a 3-year time span showed anisotropic patterns, i.e. a preferred direction of diffusion (quantified by the maximum diffusion trend (MDT)) could be detected. Additionally, the MDT values showed non-random fluctuations with daily (diurnal) and yearly (annual) periods.

In the manuscript published by Dai the observed diurnal and annual variability was only qualitatively described and lacks a statistical analysis of the obtained data. This fact motivated the author of the present paper to reassess the data by performing a detailed statistical analysis. Thus, the aim of the present paper was to reanalyze the interesting experimental results reported by Dai using statistical methods.

2 Materials and methods

As reported by Dai [1] the experimental setup and the procedure was following: a circular plastic disc, covered in a container, was filled with deionized water, and 10 µl of a 0.5% Toluidine blue ($C_{15}H_{16}ClN_3S$) solution was dropped in the center of the disc filled with water. Under constant illumination and temperature, the developing diffusion pattern was then photographed at different times (t = 30 s, 630 s, 1230 s, 1830 s and 2430 s; i.e. every 10 minutes for 40 minutes after initially waiting 30 seconds). The MDT with respect to the local north-south direction of the geomagnetic field (0° = 360° = east, clockwise scaling) was determined according to the diffusion trend at t = 1830 s. According to Dai, the diffusion experiment was performed on 15 days between December 22, 2011 and March 23, 2013. On each day, the experiment was repeated each hour over the whole day (i.e. 24 experiments/day).

For the subsequent analysis, the raw data were extracted from Figure 3 of [1]. The analysis aimed to address two specific questions: (i) Do the measured MDT values follow a uniform distribution (indicating that the underlying process is purely random)? To evaluate this, the values for each day were tested using the Chi-square test to determine whether they obey a uniform distribution. The significance level was set to $\alpha = 0.05$. (ii) Is there a diurnal and annual oscillation present in the data? This was analyzed using two approaches. First, a sinusoidal function of the form $f(\mathrm{MDT}) = a_0 + a_1 \cos(\mathrm{MDT}\omega)$ (with the free parameters a_0, a_1 and ω) was fitted to the daily and the seasonally grouped data using the Trust-Region-Reflective Least Squares Algorithm. The grouping of the data according to the seasons was performed as in Dai (i.e. Table 1 of [1]). Second, it was tested whether the distributions of the MDT values differ for the four seasons. Therefore a nonparametric test (Wilcoxon rank-sum test) was employed. Due to the multiple comparison situations, a False Discovery Rate correction to the obtained p-values was applied. The data analysis was performed in Matlab (version 2008b, The MathWorks, Natick, Massachusetts).

3 Results

Figure 1(a) shows the raw (hourly) MDT data as obtained from Figure 3 of [1]. In Figure 2(b), the median values and the respective median absolute deviations of daily intervals are plotted. The data grouped according to the seasons are depicted in Figure 2(c), and Figure 2(d) shows the block average for the daily values.

The analysis about the randomness in the data revealed that neither the daily nor the seasonally grouped MDT values follow a uniform distribution ($p < 0.05$). The seasonally grouped data showed a significant trend: the MDT values in spring were higher compared to summer ($p < 0.0001$), autumn ($p < 0.0001$) and winter ($p = 0.0131$) whereas no statistically significant difference could be detected between the distribution of the MDT values for the combinations summer vs. autumn ($p = 0.7269$), summer vs. winter ($p = 0.8509$)

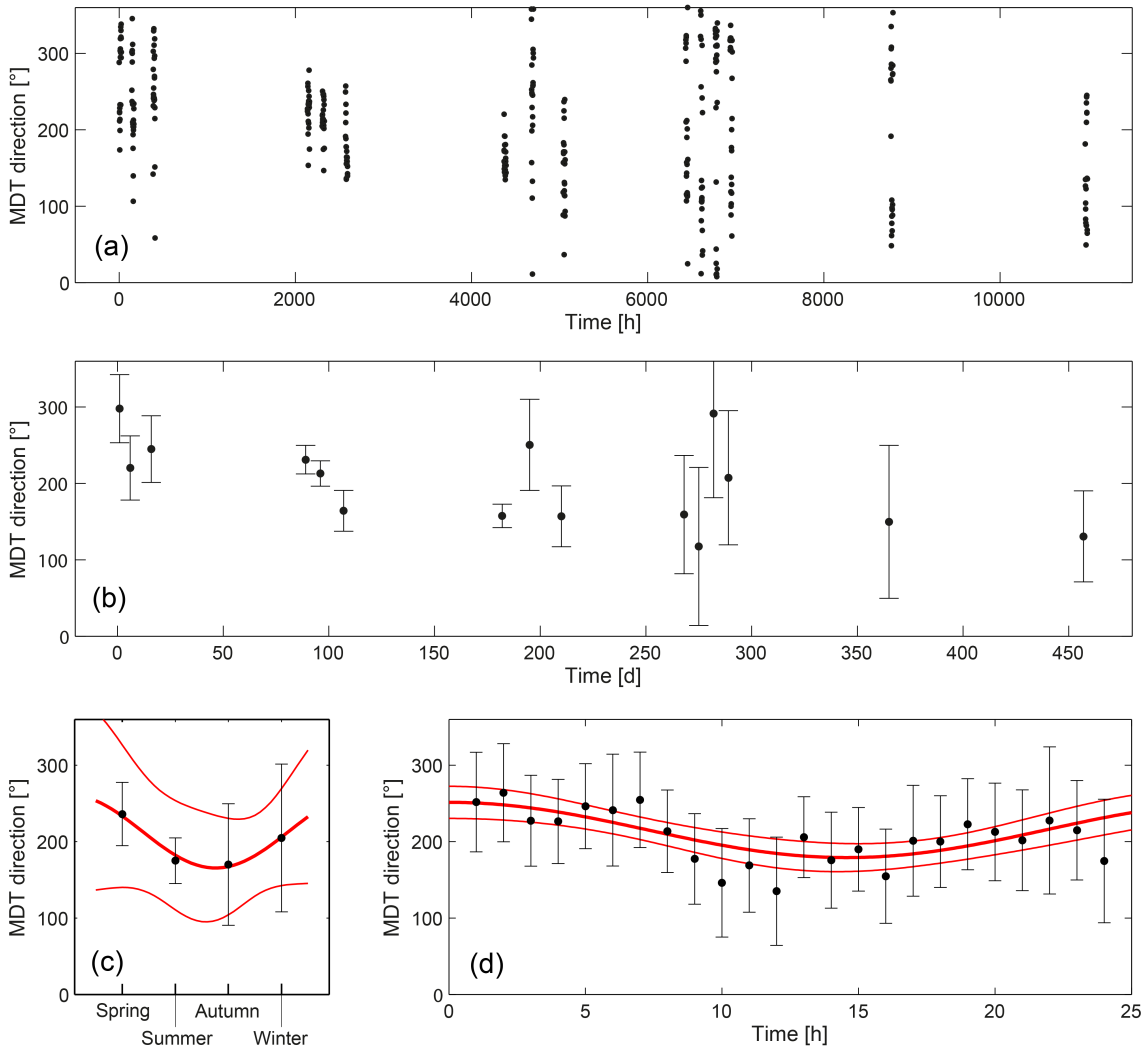

Fig. 1: (a) Raw data as given in Table 1 and Figure 1 of Dai [1]. (b) Daily averaged MDT values (median ± median absolute deviation). (c) Averages MDT values according to the seasons with fitted sinusoidal function (bold red line) and error bounds (95%, thin red lines). (d) Block average of daily MDT values with fitted sinusoidal function (bold red line) and error bounds (95%, thin red lines).

and autumn vs. winter ($p = 0.8902$). Fitting a sinusoidal function to the daily and seasonally grouped MDT data resulted in a good correlation quantified by the squared Pearson correlation coefficient (r^2) and root-mean-square error (RMSE): (i) seasonally grouped data: $r^2 = 0.9821$, RMSE = 50.25, and (ii) daily grouped data: $r^2 = 0.4885$, RMSE = 26.21. The fit with a linear function showed lower r^2 values (seasonally grouped data: $r^2 = 0.1735$, RMSE = 33.96, daily grouped data: $r^2 = 0.1579$, RMSE = 32.86).

4 Discussion

Based on the analysis performed the following two conclusion can be drawn:

(i) The measured MDT values obtained by Dai do not follow a random uniform distribution, i.e. there is a statistically significant ($p < 0.05$) trend in the direction of diffusion.

(ii) The MDT value fluctuations are not random either, i.e. a diurnal and annual oscillation explains the variability better than a linear fit.

Both conclusions are in agreement with the conclusion drawn by Dai in the original paper [1]. In order to establish the causes behind these observations, three possibilities should be considered:

Systematic errors. Changes in environmental parameters (e.g. temperature, humidity, pressure and illumination), electrostatic effects and surface irregularities of the experimental setup could have an effect on diffusion processes observed. However, even though such effects could explain the first finding (i.e. non-randomness of the MDT data) the second find-

ing (i.e. diurnal and seasonal periods in the MDT data) is hard to explain since such systemic influences must then create gradients in the diffusion process with diurnal and annual variability. In a temperature-controlled room with constant illumination and with a setup operating on a flat surface (as was the case according to Dai [1]) the formation of such periodic changes of spatial gradients is quite unlikely.

Classical geophysical and astrophysical effects. Particles of a medium in a rotating system experience a deviation of the isotropic distribution due to the centrifugal and Coriolis force [2]. Whereas the centrifugal force causes a radially outward drift of the particles, the Coriolis force induces a force perpendicular to the particle's direction of motion. Considering the earth's rotation and it's revolution around the sun, a net force can be calculated that represents a "helical force field over the earth" [3]. As discussed by He et al. [3–6] this force has a diurnal and annual variability. Another possible factor contributing to the anisotropic diffusion may be the anisotropy in arrival direction of cosmic rays. The anisotropy of cosmic rays is well documented [7–11], but it is difficult to explain how cosmic rays would cause the changes in MDT since the transported momentum of cosmic rays is very small (e.g. for a muon with a mass of $1883531475 \times 10^{-28}$ kg and travelling with light speed, a momentum in the order of 10^{-11} Ns results).

Other effects. A third option in explaining the experimental results of Dai is to consider them caused by (i) the "anisotropy of space" (as experimentally investigated over decades by Shnoll et al. [12–17]), interaction with (ii) the (quantum) vacuum (which, according to experimental findings of Graham and Lahoz, can be regarded as "something in motion" [18]), (iii) a "cosmological vector potential" [19], or (iv) a fundamental medium [20–31], also regarded as a "complex tension field" [32]. In this context, a relation of the observed anisotropic diffusion to the Saganc effect [33–36] should be considered too. Dai himself considers the observed effect caused by a global astrophysical force or entity (termed "universal field") [1, 37]. In addition, the anisotropic diffusion effect could be related to the signal (with an annual oscillation) detected by the DAMA/LIBRA/NaI experiments designed to detect dark matter [38–40], or the observation of direction-dependent temporal fluctuations in radiation from radon in air at confined conditions [41–43]. Finally, the effect could be related to the observation of an annual fluctuation in radioactive decay which was reported by several groups so far (e.g. [44–47]).

The most similar experiment to the present one was conducted by Kaminsky & Shnoll [12] who analyzed the dynamical behavior of fluctuations of the velocity of Brownian motion. Therefore, the motion fluctuations of two aqueous suspensions of 450-nm polystyrene microspheres were measured by dynamic light scattering. By analyzing the dynamical characteristics of the fluctuations with the histogram analysis method developed by the research group of Shnoll, it was discovered that the "shapes of the histograms in the independent Brownian generators vary synchronously". In a further analysis it could be shown that the direction of the experimental setup with respect to the cardinal directions has an influence on the results: the shape of the histograms were most similar when the recorded time series were not shifted to each other (in case of the alignment to the north-south direction), or shifted with $\Delta t = 11.6$ ms (in case of the alignment to the west-east direction). This clearly indicates that there is an anisotropy of the observed effect. One could speculate that the source of this anisotropy and the source of the anisotropy of diffusion as described in the present paper are similar, or even identical.

5 Conclusion

In conclusion, the re-analysis of the data obtained by Dai [1] revealed that measured MDT values (i) do not follow a random uniform distribution, and (ii) exhibit two fluctuations with a daily and annual period, respectively. For further research, the diffusion experiments need to be repeated and the experimental setup optimized. Examples of optimization include improved shielding the experimental setups against environmental influences and the simultaneous measurement of environmental parameters (e.g. temperature, humidity, pressure, illumination, acceleration of the setup in all three directions of space, fluctuations of the geomagnetic field, etc.). Performing the same experiment simultaneously at different geographical positions could also put forward new indications about the origin of the effect. Also repeating the experiments with different kinds of shielding could offer new insights.

Acknowledgement

I thank Prof. Jiapei Dai (Wuhan Institute for Neuroscience and Neuroengineering, South-Central University of Nationalities, Wuhan, China) for discussions and manuscript reviews, and Rachel Scholkmann for proofreading of the manuscript.

Submitted on August 23, 2014 / Accepted on September 1, 2014

References

1. Dai J. Macroscopic anisotropic Brownian motion is related to the directional movement of a "Universe field". *Natural Science*, 2014, v. 6 (2), 54–58.
2. Welander P. Note on the effect of rotation on diffusion processes. *Tellus*, 1965, v. 18 (1), 63–66.
3. He Y. J., Qi F. & Qi S. C. Effect of chiral helical force field on molecular helical enantiomers and possible origin of biomolecular homochirality. *Medical Hypotheses*, 1998, v. 51 (2), 125–128.
4. He Y. J., Qi F., & Qi S. C. Effect of earth's orbital chirality on elementary particles and unification of chiral asymmetries in life on different levels. *Medical Hypotheses*, 2000, v. 54 (5), 783–785.
5. He Y. J., Qi F., & Qi S. C. Periodicity of Earth's orbital chirality and possible mechanism of biological rhythms. *Medical Hypotheses*, 2000, v. 55 (3), 253–256.

6. He Y. J., Qi F., & Qi S. C. Earth's orbital chirality and driving force of biomolecular evolution. *Medical Hypotheses*, 2001, v. 56 (4), 493–496.
7. Amenomori M., Ayabe S., Bi X. J., Chen D., Cui S. W., Danzengluobu, et al. Anisotropy and corotation of galactic cosmic rays. *Science*, 2006, v. 314 (5798), 439–443.
8. Guillian G., Hosaka J., Ishihara K., Kameda J., Koshio Y., Minamino A., et al. Observation of the anisotropy of 10 TeV primary cosmic ray nuclei flux with the Super-Kamiokande-I detector. *Physical Review D*, 2007, v. 75, 062003.
9. Hayashida N., Nagano M., Nishikawa D., Ohoka H., Sakaki N., Sasaki M., et al. The anisotropy of cosmic ray arrival directions around 10^{18} eV. *Astroparticle Physics*, 1999, v. 10 (4), 303–311.
10. Monstein C., & Wesley J. P. Solar system velocity from muon flux anisotropy. *Apeiron*, 1996, v. 3 (2), 33–37.
11. Schwadron N. A., Adams F. C., Christian E. R., Desiati P., Frisch P., Funsten H. O., et al. (2014). Global anisotropies in TeV cosmic rays related to the sun's local galactic environment from IBEX. *Science*, 2014, v. 343 (6174), 988–990.
12. Kaminsky A. V., & Shnoll S. E. Cosmophysical factors in the fluctuation amplitude spectrum of brownian motion. *Progress in Physics*, 2010, v. 3, 25–30.
13. Rubinstein I. A., Kaminskiy A. V., Tolokonnikova A. A., Kolombet V. A., & Shnoll S. E. Basic phenomena of "macroscopic fluctuations" are repeated on light beams generated by lasers or light-emitting diodes. *Biophysics*, 2014, v. 59 (3), 492–502.
14. Shnoll S. E. Changes in the fine structure of stochastic distributions as a consequence of space-time fluctuations. *Progress in Physics*, 2006, v. 2 (2), 39–45.
15. Shnoll S. E. Cosmophysical factors in stochastic processes. American Research Press, Rehoboth (New Mexico, USA), 2012.
16. Shnoll S. E. Fractality, "coastline of the universe", movement of the Earth, and "macroscopic fluctuations". *Biophysics*, 2013, v. 58 (2), 265–282.
17. Shnoll S. E. On the cosmophysical origin of random processes. *Progress in Physics*, 2014, v. 10 (4), 207–208.
18. Graham G. M., & Lahoz D. G. Observation of static electromagnetic angular momentum in vacuo. *Nature*, 1980, v. 285, 154–155.
19. Baurov Yu A. Global Anisotropy of Physical Space. Nova Science Publishers, New York (USA), 2004.
20. Cahill R. T. Discovery of dynamical 3-space: Theory, experiments and observations – A review. *American Journal of Space Science*, 2013, v. 1 (2), 77–93.
21. Carvalho M. & Oliveira A. L. A new version of the Dirac's æther and its cosmological applications. *Foundations of Physics Letters*, 2003, v. 16 (3), 255–263.
22. Consoli M., Pluchino A., Rapisarda A., & Tudisco S. The vacuum as a form of turbulent fluid: Motivations, experiments, implications. *Physica A: Statistical Mechanics and its Applications*, 2014, v. 394, 61–73.
23. Davies P. Out of the ether: the changing face of the vacuum. *New Scientist*, 2011, v. 212 (2839), 50–52.
24. Davies P. C. W. Quantum vacuum friction. *Journal of Optics B: Quantum and Semiclassical Optics*, 2005, v. 7 (3), S40–S46.
25. Lee T. D. Is the physical vacuum a medium? *Transactions of the New York Academy of Sciences*, 1980, v. 40 (1), 111–123.
26. Michelson A. A. The relative motion of the earth and the luminiferous ether. *American Journal of Science*, 1881, v. 22, 120–129.
27. Michelson A. A. & Morley E. On the relative motion of the earth and the luminiferous ether. *American Journal of Science*, 1887, v. 34 (203), 333–345.
28. Miller D. C. The ether-drift experiment and the determination of the absolute motion of the earth. *Reviews of Modern Physics*, 1933, v. 5 (3), 203–242.
29. Rothall D. P., & Cahill, R. T. Dynamical 3-Space: Observing gravitational wave fluctuations and the Shnoll effect using a Zener diode quantum detector. *Progress in Physics*, 2014, v. 10 (1), 16–18.
30. Shaw D. W. Flowing aether: A concept. *Physics Essays*, 2013, v. 26 (4), 523–530.
31. Zlosnik T. G., Ferreira P. G. & Starkman G. D. Modifying gravity with the aether: An alternative to dark matter. *Physical Review D*, 2007, v. 75, 044017.
32. Roychoudhuri C. Next frontier in physics – Space as a complex tension field. *Journal of Modern Physics*, 2012, v. 3 (10), 1357–1368.
33. Bouyer P. The centenary of Sagnac effect and its applications: From electromagnetic to matter waves. *Gyroscopy and Navigation*, 2014, v. 5 (1), 20–26.
34. Gift S. J. G. Light transmission and the Sagnac effect on the rotating earth. *Applied Physics Research*, 2013, v. 5 (5), 93–106.
35. Malykin G. B. Sagnac effect and Ritz ballistic hypothesis (Review). *Optics and Spectroscopy*, 2010, v. 109v (6), 951–965.
36. Velikoseltsev A., Schreiber U., Klügel T., Voigt S., & Graham R. Sagnac interferometry for the determination of rotations in geodesy and seismology. *Gyroscopy and Navigation*, 2010, v. 1 (4), 291–296.
37. Dai J. "Universe collapse model" and its roles in the unification of four fundamental forces and the origin and the evolution of the universe. *Natural Science*, 2012, v. 4 (4), 199–203.
38. Bernabei R., Belli P., Capella F., Caracciolo V., Castellano S., Cerulli R., et al. The annual modulation signature for dark matter: DAMA/LIBRA-phase1 results and perspectives. *Advances in High Energy Physics*, 2014, 605659.
39. Bernabei R., Belli P., Capella F., Cerulli R., Dai C. J., d'Angelo A., et al. First results from DAMA/LIBRA and the combined results with DAMA/NaI. *The European Physical Journal C*, 2008, v. 56 (3), 333–355.
40. Ling F.-S., Sikivie P., & Wick S. Diurnal and annual modulation of cold dark matter signals. *Physical Review D*, 2004, v. 79, 123503.
41. Steinitz G., Kotlarsky P., & Piatibratova O. Anomalous non-isotropic temporal variation of gamma-radiation from radon (progeny) within air in confined conditions. *Geophysical Journal International*, 2013, v. 193, 1110–1118.
42. Steinitz G., Piatibratova, O., & Gazit-Yaari N. Influence of a component of solar irradiance on radon signals at 1 km depth, Gran Sasso, Italy. *Proceedings of the Royal Society A*, 2013, v. 469 (2159), 20130411.
43. Steinitz G., Piatibratova O., & Kotlarsky P. Sub-daily periodic radon signals in a confined radon system. *Journal of Environmental Radioactivity*, 2014, v. 134, 128–135.
44. Sturrock P. A., Fischbach E., Javorsek II D, Lee R. H., Nistor J. & Scargle, J.D. Comparative study of beta-decay data for eight nuclides measured at the Physikalisch-Technische Bundesanstalt. *Astroparticle Physics*, 2014, v. 59, 47–58.
45. O'Keefe D., Morreale B. L., Lee R. H., Buncher J. B., Jenkins J. H., Fischbach E., Gruenwald T, Javorsek II D & Sturrock P.A. Spectral content of 22Na/44Ti decay data: implications for a solar influence. *Astrophysics and Space Science*, 2013, v. 344 (2), 297–303.
46. Jenkins J. H., Fischbach E, Buncher J. B., Gruenwald J. T., Krause D. E., Mattes J.J. Evidence of correlations between nuclear decay rates and Earth–Sun distance. *Astrophysics and Space Science*, 2009, v. 32 (1), 42–46.
47. Parkhomov A. G. Deviations from beta radioactivity exponential drop. *Journal of Modern Physics*, 2011, v. 2 (11), 1310–1317.

Solar Flare Five-Day Predictions from Quantum Detectors of Dynamical Space Fractal Flow Turbulence: Gravitational Wave Diminution and Earth Climate Cooling

Reginald T. Cahill

School of Chemical and Physical Sciences, Flinders University, Adelaide 5001, Australia. Email: reg.cahill@flinders.edu.au

Space speed fluctuations, which have a 1/f spectrum, are shown to be the cause of solar flares. The direction and magnitude of the space flow has been detected from numerous different experimental techniques, and is close to the normal to the plane of the ecliptic. Zener diode data shows that the fluctuations in the space speed closely match the Sun Solar Cycle 23 flare count, and reveal that major solar flares follow major space speed fluctuations by some 6 days. This implies that a warning period of some 5 days in predicting major solar flares is possible using such detectors. This has significant consequences in being able to protect various spacecraft and Earth located electrical systems from the subsequent arrival of ejected plasma from a solar flare. These space speed fluctuations are the actual gravitational waves, and have a significant magnitude. This discovery is a significant application of the dynamical space phenomenon and theory. We also show that space flow turbulence impacts on the Earth's climate, as such turbulence can input energy into systems, which is the basis of the Zener Diode Quantum Detector. Large scale space fluctuations impact on both the sun and the Earth, and as well explain temperature correlations with solar activity, but that the Earth temperatures are not caused by such solar activity. This implies that the Earth climate debate has been missing a key physical process. Observed diminishing gravitational waves imply a cooling epoch for the Earth for the next 30 years.

1 Introduction

We report evidence that space flow turbulence causes solar flares, and that very simple Zener Diode Quantum Detectors, ZDQD, may be easily used to measure and characterise this turbulence. As well the major space flow turbulence precedes the solar flare eruptions by some 6 days, making it possible to have an early warning system in operation so as to limit damage to spacecraft electronics, power system networks, and other electronic infrastructure systems, when the resulting plasma reaches Earth. We demonstrate these developments by two methods: 1st by showing that the current fluctuations from ZDQD over the last Solar Cycle 23 track very accurately the Solar Flare count rate, see Fig. 1. Those correlations do not establish any causal relation. However in Fig. 6 we establish that significant space speed fluctuations cause the solar flares, as the flares are delayed by some 6 days. The solar flare data is of the Halloween Space Weather Storm of 2003, while the ZDQD data is from a GCP detector*.

*The GCP network is a worldwide collection of Zener Diode detectors that report space fluctuations every 1 sec. However it was not set up for that purpose, and was incorrectly based on the belief that quantum fluctuations are truly random and intrinsic to each quantum system, see http://noosphere.princeton.edu/. The GCP network was then being used to suggest that correlations in the network data were not caused by any physical process, but by collective human "consciousness". This has been shown to be false, as the correlated fluctuations have been shown to be caused by flowing space turbulence [1–3].

2 Dynamical space

The dynamics and detection of space is a phenomenon that physics missed from its beginning, with space modelled as a geometric entity without structure or time dependence. That has changed recently with the determination of the speed and direction of the solar system through the dynamical space, and the characterisation of the flow turbulence: gravitational waves. Detections used various techniques have all produced the same speed and direction Cahill [1–6]. The detected dynamical space was missing from all conventional theories in physics: Gravity, Electromagnetism, Atomic, Nuclear, Climate,... The detection of the dynamical space has led to a major new and extensively tested theory of reality, and goes under the general name of Process Physics [7]. Here we cite only those aspects relevant to Solar Flares and Climate Change.

The Schrödinger equation extension to include the dynamical space is [8]

$$i\hbar\frac{\partial\psi(\mathbf{r},t)}{\partial t} = -\frac{\hbar^2}{2m}\nabla^2\psi(\mathbf{r},t) + V(\mathbf{r},t)\psi(\mathbf{r},t) + -i\hbar\left(\mathbf{v}(\mathbf{r},t)\cdot\nabla + \frac{\mathbf{1}}{\mathbf{2}}\nabla\cdot\mathbf{v}(\mathbf{r},\mathbf{t})\right)\psi(\mathbf{r},t). \quad (1)$$

Here $\mathbf{v}(\mathbf{r},t)$ is the velocity field describing the dynamical space at a classical field level, and the coordinates $\mathbf{r}$ give the relative location of $\psi(\mathbf{r},t)$ and $\mathbf{v}(\mathbf{r},t)$, relative to a Euclidean embedding space, and also used by an observer to

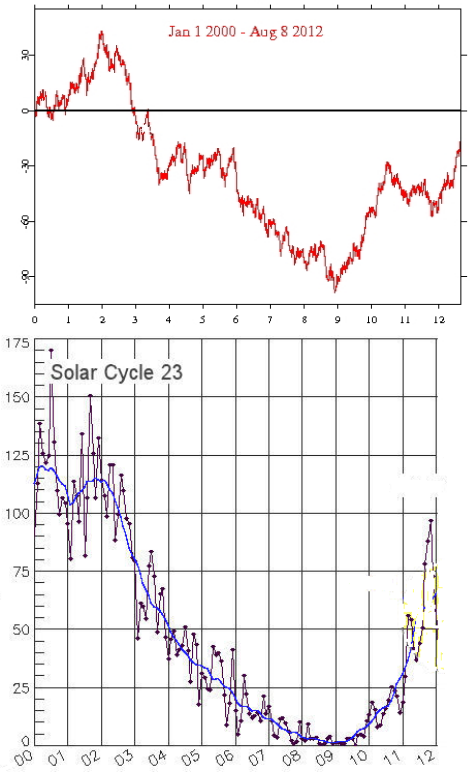

Fig. 1: Top: Measure of Zener diode GCP network current fluctuations over Solar Cycle 23, beginning with zero on January 1, 2000, adapted from R. Nelson, *Long Term Cumulative Deviation of Network Variance:* http://noosphere.princeton.edu/longterm.html. Bottom: Sunspot numbers for the same time period, adapted from T. Phillips, http://science.nasa.gov/media/medialibrary/2013/03/01/shortfall.jpg. We see the close correlation between these two phenomena. A causal relationship between space speed fluctuations and sunspots is demonstrated in Fig. 6: space flow fluctuations/turbulence precede by some 6 days the solar flares, implying that it is the space flow turbulence that causes the solar flares. This data shows the weakening of the solar cycle as being caused by weakening of the space flow turbulence. The data in Fig. 8 shows sea temperature history tracking solar flares, but not caused by the solar flares. There is a fundamental difference between correlations and cause and effect dynamics.

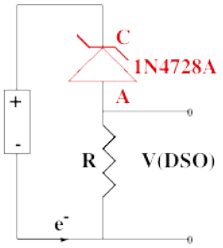

Fig. 2: Circuit of Zener Diode Gravitational Wave Detector, showing 1.5V AA battery, two 1N4728A Zener diodes operating in reverse bias mode, and having a Zener voltage of 3.3V, and resistor R= 10KΩ. Voltage V across resistor is measured and used to determine the space driven fluctuating tunnelling current through the Zener diodes. Current fluctuations from two collocated detectors are shown to be the same, but when spatially separated there is a time delay effect, so the current fluctuations are caused by space speed fluctuations [2, 3]. Using diodes in parallel increases S/N. The data used herein is from a GCP detector that has a XOR gate that partially degrades the data.

locate structures. At sufficiently small distance scales that embedding and the velocity description is conjectured to be not possible, as then the dynamical space requires an indeterminate dimension embedding space, being possibly a quantum foam [7]. This minimal generalisation of the original Schrödinger equation arises from the replacement $\partial/\partial t \rightarrow \partial/\partial t + \mathbf{v}.\nabla$, which ensures that the quantum system properties are determined by the dynamical space, and not by the embedding coordinate system. The same replacement is also to be implemented in the original Maxwell equations, yielding that the speed of light is constant only wrt the local dynamical space, as observed, and which results in lensing from stars and black holes. The extra $\nabla\cdot\mathbf{v}$ term in (1) is required to make the hamiltonian in (1) hermitian. Essentially the existence of the dynamical space in all theories has been missing. The dynamical theory of space itself is briefly reviewed below. The dynamical space velocity has been detected with numerous techniques, dating back to the 1st detection, the Michelson-Morley experiment of 1887, which was misunderstood, and which lead to physics developing flawed theories of the various phenomena noted above. A particularly good technique used the NASA Doppler shifts from spacecraft Earth-flybys, [6], to determine the anisotropy of the speed of EM waves, as indicated in Fig. 4. All successful detection techniques have observed significant fluctuations in speed and direction: these are the actually "gravitational waves", because they are associated with gravitational and other effects*

A significant effect follows from (1), namely the emergence of gravity as a quantum effect: a wave packet analysis shows that the acceleration of a wave packet, due to the space terms alone (when $V(\mathbf{r}, t) = 0$), given by $\mathbf{g} = d^2<\mathbf{r}>/dt^2$, [8], gives

$$g(\mathbf{r}, t) = \frac{\partial \mathbf{v}}{\partial t} + (\mathbf{v}\cdot\nabla)\mathbf{v}. \qquad (2)$$

That derivation showed that the acceleration is independent of the mass m: whence we have the 1st derivation of the Weak Equivalence Principle, discovered experimentally by Galileo. As noted below the dynamical theory for $\mathbf{v}(\mathbf{r}, t)$ has explained numerous gravitational phenomena.

*Note that vacuum-mode Michelson interferometers, such as LIGO, cannot detect these wave effects. Only dielectric-mode versions have detected such waves, although there is a variety of other successful techniques [1, 4]. In particular we report here the role of these waves in solar flare excitations and Earth climate science.

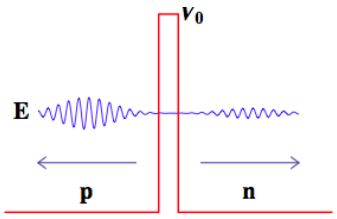

Fig. 3: Reflected (LHS) and transmitted (RHS) wave packets after interaction with barrier at a reverse-biased *pn* junction, as in Fig. 2. Energy E of wave packet is less than potential barrier height V_0. The wave function transmission varies with the speed $\mathbf{v}$ of the passing space as that varies $E \to E + \hbar\mathbf{k}\cdot\mathbf{v}$ according to (1) and so we may measure $\mathbf{v}$.

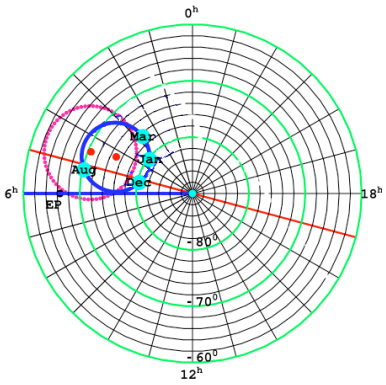

Fig. 4: South celestial pole region. The dot (red) at RA=4.3^h, Dec=75°S, and with speed 486km/s, is the direction of motion of the solar system through space determined from NASA spacecraft Earth-flyby Doppler shifts [6], as revealed by the EM radiation speed anisotropy. The thick (blue) circle centred on this direction is the observed velocity direction for different months of the year, caused by Earth orbital motion and sun 3-space inflow. The corresponding results from the 1925/26 Miller gas-mode interferometer are shown by 2nd dot (red) and its aberration circle (red dots). For December 8, 1992, the speed is 491km/s from direction RA=5.2^h, Dec=80°S, see Table 2 of [6]. EP is the pole direction of the plane of the ecliptic, and so the space flow is close to being perpendicular to the plane of the ecliptic.

3 Dynamical 3-space

The experimental data reveals the existence of a dynamical space. It is a simple matter to arrive at the dynamical theory of space, and the emergence of gravity as a quantum matter effect, as noted above. The key insight is to note that the emergent quantum-theoretic matter acceleration in (2), $\partial\mathbf{v}/\partial t + (\mathbf{v}\cdot\nabla)\mathbf{v}$, is also, and independently, the constituent Euler acceleration $\mathbf{a}(\mathbf{r}, t)$ of the space flow velocity field,

$$\mathbf{a}(\mathbf{r}, t) = \lim_{\Delta t\to 0} \frac{\mathbf{v}(\mathbf{r} + \mathbf{v}(\mathbf{r}, t)\Delta t, t + \Delta t) - \mathbf{v}(\mathbf{r}, t)}{\Delta t}$$

$$= \frac{\partial\mathbf{v}}{\partial t} + (\mathbf{v}\cdot\nabla)\mathbf{v} \qquad (3)$$

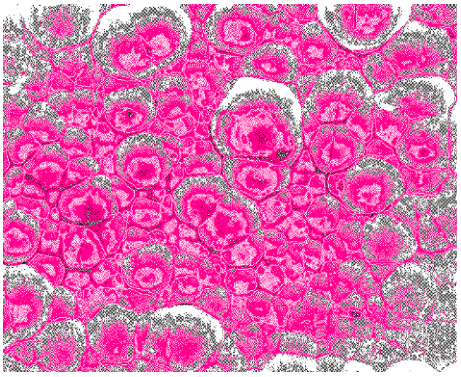

Fig. 5: Representation of the fractal wave data revealing the fractal textured structure of the 3-space, with cells of space having slightly different velocities and continually changing, and moving wrt the Earth with a speed of ~500 km/s, and in the directions indicated in Fig. 4, namely almost perpendicular to the plane of the ecliptic. This "red space" is suggestive of the 1/f spectrum of the detected fluctuations, see [5]. These space flow fluctuations inject energy into both the sun and the Earth. For solar flare effects low pass filtering of the data is necessary to isolate cells that overlap the Earth and sun, as in Fig .6.

which describes the acceleration of a constituent element of space by tracking its change in velocity. This means that space has a structure that permits its velocity to be defined and detected, which experimentally has been done. This then suggests, from (2) and (3), that the simplest dynamical equation for $\mathbf{v}(\mathbf{r}, t)$ is

$$\nabla\cdot\left(\frac{\partial\mathbf{v}}{\partial t} + (\mathbf{v}\cdot\nabla)\mathbf{v}\right) = -4\pi G\rho(\mathbf{r}, t);\quad \nabla\times\mathbf{v} = \mathbf{0} \qquad (4)$$

because it then gives $\nabla.\mathbf{g} = -4\pi G\rho(\mathbf{r}, t)$, $\nabla\times\mathbf{g} = \mathbf{0}$, which is Newton's inverse square law of gravity in differential form. Hence the fundamental insight is that Newton's gravitational acceleration field $\mathbf{g}(\mathbf{r}, t)$ for matter is really the acceleration field $\mathbf{a}(\mathbf{r}, t)$ of the structured dynamical space*, and that quantum matter acquires that acceleration because it is fundamentally a wave effect, and the wave is refracted by the accelerations of space.

While the above leads to the simplest 3-space dynamical equation this derivation is not complete yet. One can add additional terms with the same order in speed spatial derivatives, and which cannot be *a priori* neglected. There are two such terms, as in

$$\nabla\cdot\left(\frac{\partial\mathbf{v}}{\partial t} + (\mathbf{v}\cdot\nabla)\mathbf{v}\right) + \frac{5\alpha}{4}\left((trD)^2 - tr(D^2)\right) + ... = -4\pi G\rho \qquad (5)$$

where $D_{ij} = \partial v_i/\partial x_j$. However to preserve the inverse square law external to a sphere of matter the two terms must have

*With vorticity $\nabla\times\mathbf{v} \neq \mathbf{0}$ and relativistic effects, the acceleration of matter becomes different from the acceleration of space [7].

coefficients α and $-\alpha$, as shown. Here α is a dimensionless space self-interaction coupling constant, which experimental data reveals to be, approximately, the fine structure constant, $\alpha = e^2/\hbar c$, [11]. The ellipsis denotes higher order derivative terms with dimensioned coupling constants, which come into play when the flow speed changes rapidly wrt distance. The observed dynamics of stars and gas clouds near the centre of the Milky Way galaxy has revealed the need for such a term [9], and we find that the space dynamics then requires an extra term:

$$\nabla\cdot\left(\frac{\partial \mathbf{v}}{\partial t} + (\mathbf{v}\cdot\nabla)\mathbf{v}\right) + \frac{5\alpha}{4}\left((trD)^2 - tr(D^2)\right) +$$

$$+\delta^2\nabla^2\left((trD)^2 - tr(D^2)\right) + ... = -4\pi G\rho \qquad (6)$$

where δ has the dimensions of length, and appears to be a very small Planck-like length [9]. This then gives us the dynamical theory of 3-space. It can be thought of as arising via a derivative expansion from a deeper theory, such as a quantum foam theory, [7]. Note that the equation does not involve c, is non-linear and time-dependent, and involves non-local direct interactions. Its success implies that the universe is more connected than previously thought. Even in the absence of matter there can be time-dependent flows of space.

Note that the dynamical space equation, apart from the short distance effect - the δ term, there is no scale factor, and hence a scale free structure to space is to be expected, namely a fractal space. That dynamical equation has back hole and cosmic filament solutions [9, 11], which are non-singular because of the effect of the δ term. At large distance scales it appears that a homogeneous space is dynamically unstable and undergoes dynamical breakdown of symmetry to form a spatial network of black holes and filaments, [11], to which matter is attracted and coalesces into gas clouds, stars and galaxies.

The dynamical space equation (6) explains phenomena such as Earth bore-hole gravity anomalies, from which the value of α was extracted, flat rotation curves for spiral galaxies, galactic black holes and cosmic filaments, the universe growing/expanding at almost a constant rate, weak and strong gravitational lensing of light,... [4,9–11]. A significant aspect of the space dynamics is that space is not conserved: it is continually growing, giving the observed universe expansion, and is dissipated by matter. As well it has no energy density measure. Nevertheless it can generate energy into matter.

4 Detecting dynamical space speed and turbulence with diodes

The Zener diode in reverse bias mode can easily and reliably measure the space speed fluctuations, Fig. 2, and two such detectors can measure the speed and direction of the space flow and waves, Cahill [1–4]. Consider plane waves with energy $E = \hbar\omega$. Then (1) with $v = 0$ and $V = 0$ gives $\psi = e^{-\omega t + i\mathbf{k}\cdot\mathbf{r}}$. When $v \neq 0$, but locally uniform wrt to the diode, the energy becomes $E \to E + \hbar\mathbf{k}\cdot\mathbf{v}$. This energy shift can be easily detected by the diode as the electron transmission current increases with increased energy*. By using spatially separated diodes the speed and direction has been measured [1–4], and agrees with other detection techniques.

Although this Zener diode effect was only discovered in 2013, [3], Zener diode detectors have been available commercially for much longer, and are known as Random Event Generators, (REG). That terminology was based on the flawed assumption that the quantum tunnelling fluctuations were random wrt an average. However the data in [3] 1st showed that this is not the case. That experimental result contradicts the standard interpretation of "randomness" in quantum processes, which dates back to the Born interpretation in 1926. To the contrary the recent experiments show that the fluctuations are not random, but are directly determined by the fluctuations in the passing dynamical space.

5 Gravitational waves and solar flares

Fig. 1 shows the strong correlation between gravitational wave turbulence, as detected by the Earth-based ZDQD network, and the count rate of solar flares. At very low frequencies we can determine correlations based upon large "cells" of space, Fig. 5, passing almost perpendicular to the plane of the ecliptic. One key discovery herein is that the large space flow turbulences are the cause of significant solar flares, as shown in Fig. 6, top plot. That shows that the pattern of solar flares during the Halloween Space Weather Storms of 2003 closely match the pattern of 6-day-delayed space turbulence. Hence by using low-pass filtered data from Earth based ZDQD it is possible to predict with some 5 day warning the occurrence of major solar flares. This effect reveals the the space turbulence generates energetic activity in the sun, which eventually reaches the surface. However Fig. 6, bottom plot, suggests that the same mechanism is not relevant to Coronal Mass Ejections, although the data reported herein is limited to only one case.

6 Space flow turbulence and earth weather

There have been many studies noting correlations between solar cycles and changes in the Earth Weather, see [13] for review and references. The most notable being the Maunder minimum 1645-1715, during which there was no sunspot activity, and which coincided with the "little ice age". However correlations do not provide causal relations. The assumption has always been that increased sunspot activity results in increased solar irradiance which subsequently causes increased Earth temperatures, although no convincing mechanism has

*The Zener diode currents reported in [1–4] were incorrectly determined. The Digital Storage Oscilloscope (DSO)was operated with 50Ω input impedance, which meant the voltage was developed across that resistance and not the 10kΩ cited, and shown in Fig. 2. This means that the actual tunnelling currents were 200 times larger. This had no effect on the conclusions.

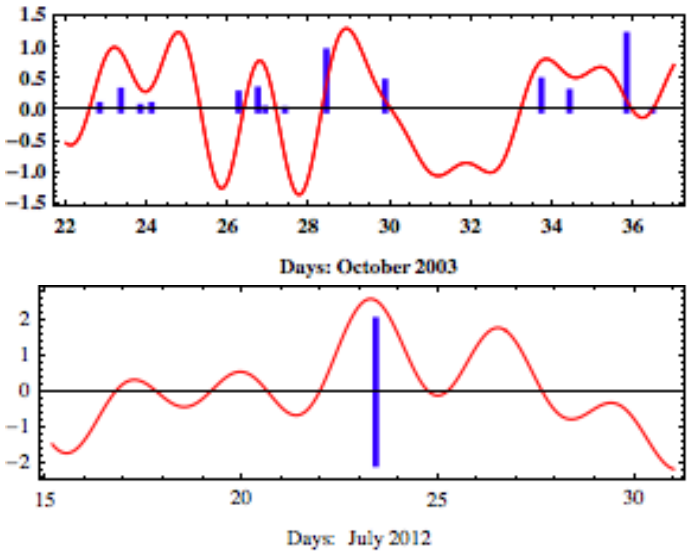

Fig. 6: Top: Vertical blue lines indicate start times of major solar flares beginning October 22, 2003. The height of the lines is indicative of the magnitude of the solar flare, and is on a logarithmic scale. These solar flares are known as the Halloween Space Weather Storms of 2003, [12]. The curve is data from a single ZDQD, located in Switzerland, low-pass filtered to include only periods longer than 2 days, and advanced in time by 6 days, and plotted relative to the average. For a space speed of 500 km/s this corresponds to a cell size ~0.5 of the Sun-Earth distance. This advance followed from matching the two data sets. The low-pass filter ensures that we see space fluctuations corresponding to cell sizes that can overlap the Earth and the sun, as the space flow is close to being perpendicular to the plane of the ecliptic, as shown by the analysis of the NASA Earth-flyby spacecraft Doppler shifts in Fig. 4, [6]. The strong correlation between the two data sets show that solar flares follow increases in the space velocity, by some 6 days: the solar flares are caused by the space fluctuations: these fluctuations are a galactic phenomenon. Bottom: Vertical blue line indicates start of massive Coronal Mass Ejection (CME) on July 23, 2012, and plotted with ZDQD low-pass data, but without time shift. The main speed fluctuation peak coincides with the CME, on July 23. This suggests that CME may not be caused by space fluctuations, and that the coincident peak may be gravitational waves produced by the extremely large mass ejection, although there is a smaller peak in the ZDQD data some 6 days earlier.

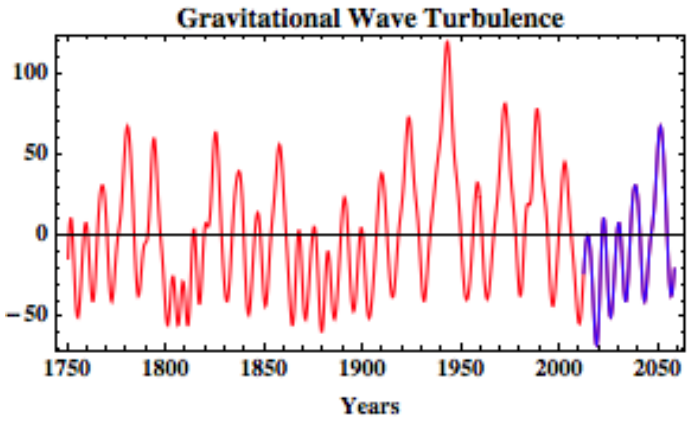

Fig. 7: Plot of Gravitational Wave Turbulence vs years 1749 to present (red plot), based upon Solar Flare counts as a proxy, as shown in Fig. 1. Data adapted from from D. Archibald, Solar Update March 2012 (http://www.warwickhughes.com/blog/?p=2753), [15]. The Solar Flare data has been low-pass filtered using Fast Fourier Transfoms. It is argued herein that the 11 year cycle and longer cycles are caused by galactic space flow turbulence, which can now be easily measured using ZDQD. Beyond 2014 we have used the Fourier amplitudes to extrapolate to 2050 (blue plot), which assumes an ongoing 1/f spectrum. This extrapolation suggests we are facing an epoch of low space flow turbulence, and hence reduced Earth temperatures. The modern warm period extended from 1900s to end of solar cycle 23 (the last cycle in red).

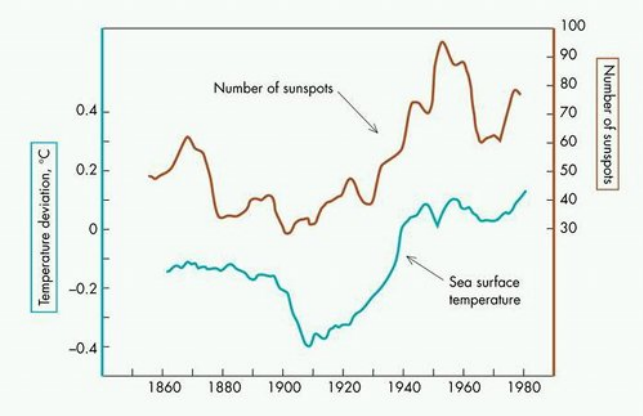

Fig. 8: Shows strong correlations between solar sunspot numbers and Earth sea surface temperature deviations. This, however, does not imply a causal relation between these two phenomena, as was also noted in Fig. 1. It is conjectured herein that the cause is the galactic space flow turbulence, which pumps energy into both the sun and the Earth.

been accepted. However the variation in irradiation is too small to cause the observed Earth temperature fluctuations. See Fig. 8 for correlations between sea temperature and solar flare counts. However the data herein offers a different mechanism, namely that the Earth's climate is affected by changes in the space flow turbulence, which is very evident in Fig. 1, with the causal relation established in Fig. 6. Such space flow fluctuations change the energy of matter, according to $\hbar\mathbf{v}\cdot\mathbf{k}$, as discussed above. These energy changes are the basis of the detection of the space flow turbulence by the ZDQD technique. So this suggests another possible factor affecting the Earth's climate, namely an energy generation that arises from space flow turbulence directly interacting with the Earth. The heating mechanism is that atoms/molecules having a momentary wave vector $\mathbf{k}$ have their energy raised if $\mathbf{k}\cdot\mathbf{v} > 0$. These then scatter with lower energy atoms/molecules and so dissipate the temporary energy lift to the gas in general. The GCP ZDQD data, going back some 18 years, thus provides an incredible data set that could be used to test this conjecture. Another indication of heat production internal to the Earth is that the geoneutrino flux from the decay of uranium-238 and thorium-232 can explain only about 50% of the heat production of the Earth of some 44.2±1.0 TW [14]. So there would appear to be another source of ongoing energy production within the Earth, and this could arise from space-flow turbulence effects.

Beginning Solar Cycle 24 is the weakest in more than 50 years. Fig. 7 shows the low frequency gravitational wave turbulence measure using the solar flare count as a proxy, which follows from the data in Fig. 1, and so permitting an analysis of such turbulence back to 1750. However by using Fourier transforms to extract the frequency spectrum and phases we may use that data to extrapolate into the future, which is shown in blue in Fig. 7, from mid 2014 to 2050. The prediction is that there will be a reduced energy generation in the Earth system over the next 30 years, as the galactic space turbulence will enter an epoch of reduced turbulence, as in 1860-1910, and resulting in the cooling of the Earth's atmosphere.

7 Conclusions

The discovery of the Zener Diode quantum detector effect has rendered the detection of 3-space flow turbulence, gravitational waves*, to be trivial and robust. The speed and direction of the flow from such detectors has confirmed the results from earlier experiments, beginning with Michelson and Morley in 1887 using a gas-mode interferometer. Other experimental techniques have used RF speeds in coaxial cables, dual RF coaxial cables and optical fibers, RF speeds in dual coaxial cables, to mention only some: see [1, 4] for recent reviews. The major implication is that space exists, because it is detectable, has significant fractal flow turbulence, and is a complex dynamical system, contrary to the claims since 1905 that space does not exist. The turbulence effects are significant, typically some 20% of the average flow velocity at present. The dynamical theory has become well established by testing against various experimental and observational phenomena [6, 9–11]. Here we have reported evidence that solar flares are caused by major gravitational wave fluctuations. Using Zener Diode gravitational wave detectors and low pass filtering the data now offers the opportunity to predict with some 5 days warning of a major solar flare. As these detectors are so simple they could be included on all future space probes, as a larger scanning region would considerably increase reliability of the new warning system. The data used here comes from the GCP project, which has had Zener diode detectors operating for some 18 years, but was based upon an incorrect assumption that the current fluctuations in the reverse-biased pn junction were random quantum fluctuation, as asserted in the usual interpretation of the quantum theory. However recent experiments [2, 3], and without the XOR gate used in GCP detectors, it was shown that the diode current fluctuations are completely determined by fluctuations in the passing space. Nevertheless the GCP data base represents an enormously significant record of 3-space turbulence, which will permit various studies to be undertaken. A second major discovery is that the long established correlations between Earth temperature fluctuations and solar flare counts is explained by both phenomena being a result of gravitational waves, and not by the very small changes in sun irradiance that accompanies solar flares. This has led to the prediction that there is a diminution epoch of gravitational waves that is already detectable in Figs. 1 and 6, that will

*The detected gravitational waves are not those of GR. Such waves have never been detected.

result in a cooling of the Earth's atmosphere, as was experienced in earlier Earth epochs when the gravitational waves underwent a period of diminished activity. Dropping temperatures would normally decrease cereal food production, but that may be compensated for by extra growth following form the increased CO_2 levels. We note that the statistical arguments in [16] are invalidated by the discovery of the space flow turbulence effect reported herein: Climate Science has been missing a key physical process until now.

Acknowledgements

This report is from the Flinders University Gravitational Wave Detector Project. Thanks to GCP and its director Dr Roger Nelson for the public availability of extensive and valuable data from the GCP ZenerDiode international network: http://noosphere.princeton.edu/extract.html

Submitted on September 6, 2014 / Accepted on September 11, 2014

References

1. Cahill R.T. Review of Gravitational Wave Detections: Dynamical Space, *Physics International*, 2014, v. 5(1), 49–86.
2. Cahill R.T. Gravitational Wave Experiments with Zener Diode Quantum Detectors: Fractal Dynamical Space and Universe Expansion with Inflation Epoch. *Progress in Physics*, 2014, v. 10(3), 131–138.
3. Cahill R.T. Nanotechnology Quantum Detectors for Gravitational Waves: Adelaide to London Correlations Observed. *Progress in Physics*, 2013, v. 4, 57–62.
4. Cahill R.T. Discovery of Dynamical 3-Space: Theory, Experiments and Observations - A Review. *American Journal of Space Science*, 2013, v. 1(2), 77–93.
5. Cahill R.T. Characterisation of Low Frequency Gravitational Waves from Dual RF Coaxial-Cable Detector: Fractal Textured Dynamical 3-Space. *Progress in Physics*, 2012, v. 3, 3–10.
6. Cahill R.T. Combining NASA/JPL One-Way Optical-Fiber Light-Speed Data with Spacecraft Earth-Flyby Doppler-Shift Data to Characterise 3-Space Flow. *Progress in Physics*, 2009, v. 4, 50–64.
7. Cahill R.T. Process Physics: From Information Theory to Quantum Space and Matter. *Nova Science Pub., New York*, 2005.
8. Cahill R.T. Dynamical Fractal 3-Space and the Generalised Schrödinger Equation: Equivalence Principle and Vorticity Effects, *Progress in Physics*, 2006, v. 1, 27–34.
9. Cahill R.T. and Kerrigan D. Dynamical Space: Supermassive Black Holes and Cosmic Filaments. *Progress in Physics*, 2011, v. 4, 79–82.
10. Cahill R.T. and Rothall D. Discovery of Uniformly Expanding Universe. *Progress in Physics*, 2012, v. 1, 63–68.
11. Rothall D.P. and Cahill R.T. Dynamical 3-Space: Black Holes in an Expanding Universe, *Progress in Physics*, 2013, v. 4, 25–31.
12. Weaver M. (ed) *et al.* Halloween Space Weather Storms of 2003, NOAA Technical Memorandum OAR SEC-88, 2004.
13. Phillips T. Solar Variability and Terrestrial Climate, http://science.nasa.gov/science-news/science-at-nasa/2013/08jan_sunclimate/
14. KamLAND Collaboration, Partial Radiogenic Heat Model for Earth Revealed by Geoneutrino Measurements. *Nature Geoscience*, 2011, v. 4, 647–651.
15. Archibald D. The Past and Future of Climate, 2010, http://www.davidarchibald.info/papers/Past-and-Future-of-Climate.pdf
16. Kokic P., Crimp S., Howden M. A Probabilistic Analysis of Human Influence on Recent Record Global Mean Temperature Changes, *Climate Risk Management*, 2014, v. 3, 1–12.

Proton-Neutron Bonding in the Deuteron Atom and its Relation to the Strong Force as Viewed from the Planck Vacuum Theory

William C. Daywitt

National Institute for Standards and Technology (retired), Boulder, Colorado. Email: wcdaywitt@me.com

This paper argues that the two-particle proton-neutron bond results from the proton-proton/Planck-vacuum coupling force associated with the two particles. The neutron is assumed to be a proton with a weakly attached electron whose sole function is to eliminate the Coulomb repulsion between the two protons. Results lead to a simple model of the deuteron atom and a definition for the strong force.

1 Introduction

The proton core (e_*, m_p) located at the radius $r = 0$ exerts the two-term coupling force [1]

$$F(r) = -\left(\frac{e_*^2}{r^2} - \frac{m_p c^2}{r}\right) = -\frac{e_*^2}{r^2}\left(1 - \frac{r}{r_p}\right) \qquad (1)$$

on the omnipresent Planck vacuum (PV) state, where r_p $(= e_*^2/m_p c^2)$ is the Compton radius at which the force vanishes. The radius r extends from the core to any point within the PV continuum. The massless bare charge is e_* and m_p is the proton rest mass. Since the Planck particles within the PV suffer a primordial zero-point agitation that is the source of the zero-point electromagnetic fields, the radius r in (1) is an average over the small instantaneous random motion $(r(t) - r$ at $r \approx 0)$ of the proton's bare charge (e_*) [2, 3]. In part, the response of the PV to the force (1) is to create the proton mass m_p from the zero-point-field driven proton charge (e_*).

Figure 1 is a plot of the normalized coupling force

$$\frac{F(r)}{e_*^2/r_p^2} = \frac{F(r)}{m_p c^2/r_p} = -\frac{r_p^2}{r^2} + \frac{r_p}{r} \qquad (2)$$

where the abscissa is in units of r_p (equation (5) is used in the calculation). The two fiducial points, $r = r_p$ and $r = 2r_p$, are the radii at which the force vanishes and attains its maximum respectively. The Compton radius r_p has been discussed in a number of earlier papers (see `www.planckvacuum.com`). It is seen in what follows that the separation between the proton and neutron cores in the deuteron is related to the maximum at $2r_p$.

The coupling potential from (1) is

$$V(r) = -\int F(r)dr + V_0 \qquad (3)$$

where $V(r_p) = 0$ yields the normalized potential

$$\frac{V(r)}{m_p c^2} = -\frac{r_p}{r} + 1 + \ln\frac{r_p}{r}\,. \qquad (4)$$

The corresponding mass and Compton radius of the proton are tied to the PV state via the Compton relations

$$r_p m_p c^2 = r_* m_* c^2 = e_*^2 \qquad (= c\hbar) \qquad (5)$$

which are a manifestation of the fact that the proton possesses a Compton radius r_p, where r_* and m_* are the Compton radius and mass of the Planck particles making up the negative energy PV.

For $r \ll r_p$, (1) reduces to

$$F(r) = -\frac{e_*^2}{r^2} = \frac{(e_*)(-e_*)}{r^2} \qquad (6)$$

where (e_*) belongs to the proton and $(-e_*)$ belongs to the separate Planck particles of the PV.

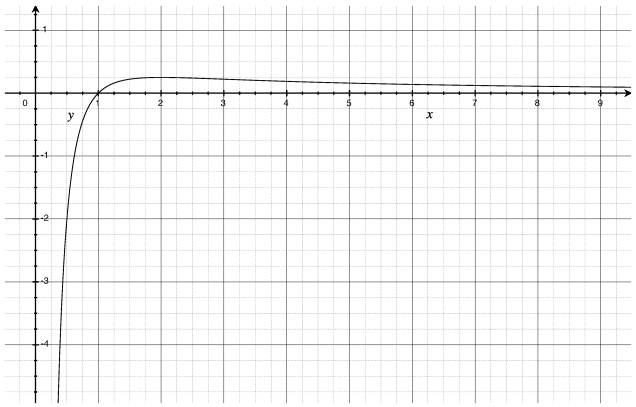

Fig. 1: The graph plots $F(r)/(e_*^2/r_p^2)$, with $r_p = 1$. The maximum of the curve is at $2r_p = 2$.

The neutron is assumed to be a proton with a negative charge weakly attached to make the neutron charge-neutral. Theoretically, it is tempting to assume that this added negative charge is the massless bare charge $(-e_*)$. However, the zero-point fields permeate both free space and any particle in that space [3]; and if that particle is the bare charge, that bare charge rapidly becomes an electron or a proton, depending upon whether the charge is negative or positive respectively. Thus the added negative charge in the neutron is assumed in the PV theory to be an electron.

2 Proton-proton bond

The PV is a degenerate state [5], which implies that the force in (1) does not distort the vacuum structure, except possibly

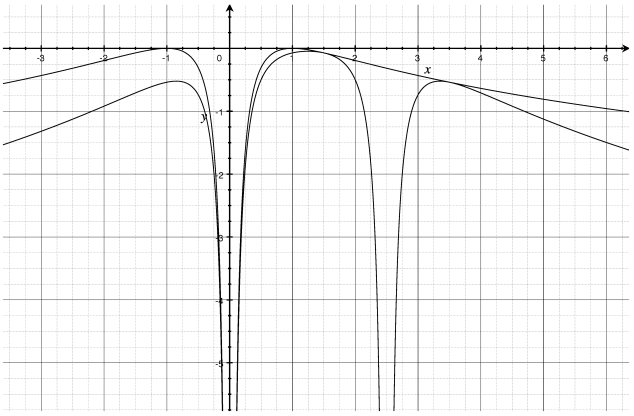

Fig. 2: The graph plots $V(t)/m_pc^2$ (the upper curve) and $V_t(r)/m_pc^2$ (the three-humped curve) with $x_0 = 2.5r_p$ and $r_p = 1$. The two intersect points are at $r = x_0 \pm r_p = 2.5 \pm 1$.

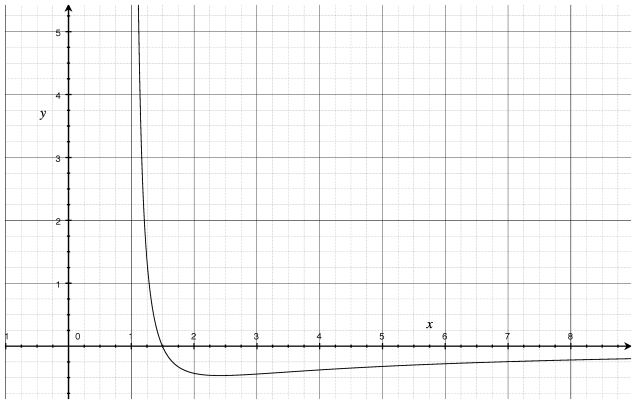

Fig. 3: The graph plots $W(x_0)$ with $r_p = 1$. The minimum of the curve is at $x_0 \approx 2.4r_p = 2.4$.

deep within the proton core. Thus the total coupling force felt by the PV due to two protons (the free proton and the proton in the neutron) is the sum of two forces similar to (1). If the two protons are separated by distance equal to x_0, with one of the protons at the origin, the total normalized proton-proton/PV coupling potential is simply (with $\mathbf{r} = (x, 0, 0)$)

$$\frac{V_t(r)}{m_pc^2} = -\frac{r_p}{r} + 1 + \ln\frac{r_p}{r} - \frac{r_p}{|r-x_0|} + 1 + \ln\frac{r_p}{|r-x_0|}$$

$$= -r_p\left(\frac{r+|r-x_0|}{r|r-x_0|}\right) + 2 + \ln\left(\frac{r_p^2}{r|r-x_0|}\right) \qquad (7)$$

which is plotted in Figure 2 with x_0 set to $2.5r_p$, where the abscissa is in units of the proton Compton radius r_p. The upper curve is the potential for a single proton at the coordinate origin. The three-hump two-proton curve intersects the single-proton curve at the two points (8) where the second potential in the first equation of (7) vanishes. The potential difference between the intersect points provides a means for determining the equilibrium separation $\overline{x_0}$ (the assumed separation between the proton and neutron cores in the deuterium atom). The two intersect radii in Figure 2 follow easily from

$$V_t(r) = V(r) \qquad \Longrightarrow \qquad r = x_0 \pm r_p \qquad (8)$$

and appear on either side of x_0.

To determine the equilibrium $\overline{x}_0$, it is convenient to define

$$W(x_0) \equiv \frac{V_t(x_0+r_p) - V_t(x_0-r_p)}{m_pc^2} \qquad (9)$$

$$= \frac{V(x_0+r_p) - V(x_0-r_p)}{m_pc^2} \qquad (10)$$

in terms of the separation distance x_0, which is plotted in Figure 3 with r_p set to one. The equilibrium $\overline{x_0}$ is then obtained from

$$\frac{dW(x_0)}{dx_0} = \frac{2r_p(x_0^2 - r_p^2) - 4r_p^2x_0}{(x_0^2 - r_p^2)^2} = 0 \qquad (11)$$

whose solution is

$$x_0 = (1 \pm 2^{1/2})r_p \qquad (12)$$

yielding

$$\overline{x_0} = (1 + 2^{1/2})r_p \approx 2.4r_p \qquad (13)$$

for the deuteron proton-neutron core separation. A very rough experimental estimate (Appendix A) for the separation is $3.0r_p$.

3 Strong force

The vanishingly small magnitude ($< r_p/39000$) of the proton-core radius [4] suggests that it may be related to the so called strong force F_s. So identifying the Coulomb force from (6) as the strong force leads to the ratio

$$\frac{F_s(r)}{F_g(r)} = \frac{(e_*)(-e_*)/r^2}{-m_p^2G/r^2} = \frac{m_*^2}{m_p^2} = \frac{r_p^2}{r_*^2} \sim 10^{38} \qquad (14)$$

of that force to the gravitational force F_g between two proton masses separated by a distance r ($G = e_*^2/m_*^2$ from [1, 5], and (5) are used in the calculation).

To reiterate, the positive charge in (14) is the bare charge of the proton and the negative charge corresponds to the bare charges of the separate Planck particles in the PV. So (14) is a composite ratio involving the proton-PV coupling force for $r \ll r_p$ and the free-space gravitational force.

4 Summary and comments

The PV theory assumes that the proton-neutron bond results from the proton-proton/PV coupling force associated with the proton and the proton-part of the neutron. It explains the proton-neutron bond as a minimum in the proton/PV coupling

potentials as characterized by equations (8)–(13) and Figure 3, with a minimum at $2.4r_p$ that is directly related to the maximum force at $2r_p$ in Figure 1. This characterization assumes that the bonding takes place suddenly when $x_0 = \overline{x_0}$ as the proton and neutron approach each other. That is, the two nucleons do not possess some type of strong *mutual* attraction for $x_0 \neq \overline{x_0}$. In summary, then, the proton-neutron bond in the PV theory is a new type of bonding that intimately involves the invisible, negative-energy vacuum state and its interaction with the proton core (e_*, m_p).

The strong force, $(e_*)(-e_*)/r^2$, is seen to be a force existing between the positive proton charge and the separate negative charges of the PV. It is not a force acting between two free space particles.

Appendix A: deuteron size

This is a rough heuristic estimate of the separation distance between the proton and neutron cores within the deuteron. It starts with the standard formula for the radius of the stable nucleus with a mass number A [6, p.551]

$$R(A) = 1.2\,A^{1/3}\,[\text{fm}] = 5.71 r_p A^{1/3} \qquad \text{(A1)}$$

in units of femtometers or the proton Compton radius r_p (= 0.21 fm). The radii of the proton and neutron are defined by $A = 1$, and the deuteron by $A = 2$. Inserting these parameters into (A1) leads to the radii $R_1 = 5.71r_p$ and $R_2 = 7.19r_p$ for the nucleons and deuteron respectively.

Taking the cores at the origin of the two spheres defined by R_1 and R_2, it is easy to see that the separation between the nucleon cores in the deuteron is

$$2(R_2 - R_1) = 2(7.19r_p - 5.71r_p) \approx 3.0r_p\,. \qquad \text{(A2)}$$

Submitted on September 7, 2014 / Accepted on September 13, 2014

References

1. Daywitt W.C. The Electron and Proton Planck-Vacuum Forces and the Dirac Equation. *Progress in Physics*, 2014, v. 2, 114–115.
2. Daywitt W.C. Why the Proton is Smaller and Heavier than the Electron. *Progress in Physics*, 2014, v. 10, 175–177.
3. Daywitt W.C. The Source of the Quantum Vacuum. *Progress in Physics*, 2009, v. 1, 27–32. In the first line of the last paragraph in Appendix A of this paper "$p = \hbar/r_L$" should read "$m\gamma c = \hbar/r_L$".
4. Daywitt W.C. The Dirac Proton and its Structure. To be published in the International Journal of Advanced Research in Physical Science (IJARPS). See also `www.planckvacuum.com`.
5. Daywitt W.C. The Planck Vacuum. *Progress in Physics*, 2009, v. 1, 20–26.
6. Leighton R.B. *Principles of Modern Physics*. McGraw-Hill Book Co., New York, Toranto, London, 1959.

Properties of Nuclear Superdeformed Rotational Bands in A ∼ 190 Mass Region

A. M. Khalaf[1] and M. D. Okasha[2]

[1]Physics Department, Faculty of Science, Al-Azhar University, Cairo, Egypt. E-mail: ali_khalaf43@hotmail.com
[2]Physics Department, Faculty of Science (Girls College), Al-Azhar University, Cairo, Egypt. E-mail: mady200315@yahoo.com

Two-parameters formula based on the conventional collective rotational model is applied to describe superdeformed rotational bands (SDRB's) in nuclei in the $A \sim 190$ mass region, namely the five SDRB's ^{192}Hg(SD1), ^{194}Hg(SD1), ^{194}Hg(SD2), ^{194}Pb(SD1) and ^{194}Pb(SD2). The bandhead spins of the observed levels have been extracted by first and second-hand estimation corresponding to pure rotator and our proposed formula respectively by plotting the E-Gamma Over Spin (EGOS) versus spin. A computer simulated search program is used to extract the model parameters in order to obtain a minimum root mean square (rms) deviation between the calculated and the experimental transition energies The values of spins resulting from second estimation method are excellent consistent with spin assignment of other models. The calculated transition energies, level spins, rotational frequencies, kinematic and dynamic moments of inertia are systematically examined. The difference in γ- ray transition energies ΔE_γ between transitions in the two isotones ^{192}Hg(SD1) and ^{194}Pb(SD1) were small and constant up to rotational frequency $\hbar\omega \sim 0.25$ MeV. Therefore, these two bands have been considered as identical bands. The $\Delta I = 2$ energy staggering observed in ^{194}Hg(SD1) and ^{194}Hg(SD2) of our selected SDRB's are also described from a smooth reference representing the finite difference approximation to the fourth order derivative of the transition energies at a given spin.

1 Introduction

Superdeformed (SD) nuclei were observed in a wide range of nuclear chart, and a wealth of experimental data on the resulting superdeformed rotational bands (SDRR's) was accumulated in recent years [1, 2]. These bands consists of long cascades of regularly spaced quadruple γ-ray transitions, which reveal a high degree of collectivity in a strongly deformed prolate nucleus. Lifetime measurements lead to very large values for the quadrupole moments of $Q_0 \sim 15 - 20$ eb which indeed correspond to an elongated ellipsoid with an axis ratio close to 2:1.

The superdeformation at high angular momentum remains one of the most interesting and challenging topics of nuclear structure. At present, although a general understanding of the properties of such SD nuclei has been achieved, there are still many open un expected problems. One of the outstanding experimental problems in the study of SD nuclei concerns their decay to the ground state. After a rapid decay out occurs over 2-4 states, and transitions linking the SD band to known levels in the first well are unobserved. As a result, the excitation energy, spin and parity of the levels in the first well are unobserved. As a result several theoretical approaches to predict the spins of SD bands were suggested [3–14].

To date, SD spectroscopy has given us much information concerning the behavior of moment of inertia in SD nuclei. For example it was shown [15] that for SD nuclei near $A \sim 150$, the variation in the dynamical moment of inertia $J^{(2)}$ with rotational frequency $\hbar\omega$ is dependant on the proton and neutron occupation of high-N intruder orbitals. For most SD bands in even-even and odd-A nuclei in the $A \sim 190$, $J^{(2)}$ exhibits a smooth gradual increase with increasing $\hbar\omega$ [16], which is due to the gradual alignment of quasinucleons occupying high -N intruder orbitals (originating from the $i_{13/2}$ proton and $j_{15/2}$ neutron subshells)in the presence of the pair correlations, while in the odd-odd nuclei, quite a good part of the moments of inertia for SD bands keep constant.

An unexpected discovery was the existence of identical bands (IB's) [17–21]. IB's are two bands in different nuclei, which have essentially identical transition energies within 2 keV, and thus essentially identical dynamical moment of inertia.

It was found that some SDRB's in different mass regions show an unexpected $\Delta I = 2$ staggering effects in the γ-ray energies [22–25]. The effect is best seen in long rotational sequences, where the expected regular behavior of the energy levels with respect to spin or to rotational frequency, is perturbed. The result is that the rotational sequences is split into two parts with states separated by $\Delta I = 4$ (bifurcation) shifting up in energy and the intermediate states shifting down in energy. The curve found by smoothly interpolating the band energy of the spin sequence $I, I + 4, I + 8, ...$, is some what displaced from the corresponding curve of the sequence $I+2, I+6, I+10, ...$ The magnitude of the displacement in the gamma transition energy is found to be in the range of some hundred eV to a few keV. The $\Delta I = 2$ staggering effect has attracted considerable interest in the nuclear structure community. A few theoretical proposal for the possible explanation of this $\Delta I = 2$ staggering have already been made [26–31].

Calculations using the cranked Nilsson-Strutinsky

method [32], and the Hartee-Fock method [33] suggest that nuclei with $N = 112$ and $Z = 80$ or 82 should be particularly stable, due to the existence of SD gaps in the single particle spectrum. As a result ^{192}Hg and ^{194}Pb are considered as doubly magic SD nuclei. Excited SD bands in these two nuclei are therefore expected to exist a somewhat higher excitation energies, and consequently to be populated with lower intensity than excited SD bands in other nuclei in this region.

In this paper, we shall present a theoretical study for Hg and Pb nuclei, our results are in framework of collective rotational formula including two parameters, obtained by adopted best fit method. We need first and second estimation to predict the spins for the studied SDRB's, and the best fitted parameters have been used to evaluate the E2 transition γ-ray energies, rotational frequencies, kinematic and dynamic moments of inertia. The appearance of identical bands (IB's) and the occurrance of a $\Delta I = 2$ staggering effect have been examined.

2 Parametrization of SDRB's by Two-Parameter Collective Rotational Formula

For the description of normally deformed (ND) bands, some useful expressions were presented. Bohr and Mottelson [34] pointed out that, under the adiabatic approximation, the rotational energy of an axially symmetric even-even nucleus may be expanded as (for $k = 0$, where k is the projection of the angular momentum I onto the symmetric axis) a power series in terms of of I^2=I(I+1):

$$E(I) = A[I(I+1)] + B[I(I+1)]^2 \tag{1}$$

with common constants A and B. We will adopt the energy of the SD state with spin I by equation (1).

For SD bands, gamma-ray transition energies are unfortunately, the only spectroscopic information universally available. The gamma-ray transition energy between levels differing by two units of angular momentum $\Delta I = 2$ are:

$$\begin{aligned} E_\gamma(I) &= E(I) - E(I-2) \\ &= (I-1/2)\left[4A + 8B(I^2 - I + 1)\right]. \end{aligned} \tag{2}$$

3 Spin Assignment of SDRB's in A ∼ 190 Mass Region

In the method used, the energies of the SD nuclear rotational bands are firstly expressed by pure rotator as a first estimation of bandhead spin

$$E(I) = AI(I+1). \tag{3}$$

Thus

$$E_\gamma(I) = 4A(I - 1/2). \tag{4}$$

If I_0 represent the bandhead spin, then

$$\frac{E_\gamma(I_0+4)}{E_\gamma(I_0+2)} = \frac{4I_0+14}{4I_0+6}. \tag{5}$$

Therefore,

$$I_0 = \frac{1}{4}\left[\frac{8E_\gamma(I_0+2)}{E_\gamma(I_0+4) - E_\gamma(I_0+2)} - 6\right]. \tag{6}$$

The ratio $E_\gamma(I)$ over spin I (E-Gamma Over Spin(EGOS)) is given by

$$EGOS = \frac{E_\gamma(I)}{I - 1/2} = 4A \tag{7}$$

when EGOS plotted against spin, it gives horizontal line.

For second estimation of bandhead spin, our proposed formula equation (1) is used, thus EGOS becomes

$$EGOS = 4A + 8B(I^2 - I + 1) \tag{8}$$

which decrease hyperbolically.

4 Rotational Frequency and Moments of Inertia

In the framework of nuclear collective rotational model with $k = 0$, the rotational frequency $\hbar\omega$ for the expression (1) is given by

$$\begin{aligned} \hbar\omega(I) &= \frac{dE(I)}{d\sqrt{I(I+1)}} \\ &= 2A\left[I(I+1)\right]^{\frac{1}{2}} + 4B\left[I(I+1)\right]^{\frac{3}{2}}. \end{aligned} \tag{9}$$

The kinematic $J^{(1)}$ and dynamic $J^{(2)}$ moments of inertia for the expression(1) are:

$$\begin{aligned} \frac{J^{(1)}}{\hbar^2} &= \frac{1}{\sqrt{I(I+1)}}\left[\frac{dE(I)}{d\sqrt{I(I+1)}}\right]^{-1} \\ &= J_0 - \frac{B}{A^2}[I(I+1)] \\ &+ \frac{2B^2}{A^3}[I(I+1)]^2 - 4\frac{B^3}{A^4}[I(I+1)]^3 \end{aligned} \tag{10}$$

$$\begin{aligned} \frac{J^{(2)}}{\hbar^2} &= \left[\frac{d^2E(I)}{d[I(I+1)]^2}\right]^{-1} \\ &= J_0 - 3\frac{B}{A^2}[I(I+1)] \\ &+ 18\frac{B^2}{A^3}[I(I+1)^2] - 108\frac{B^3}{A^4}[I(I+1)]^3 \end{aligned} \tag{11}$$

where J_0 is refereed to as the bandhead moment of inertia

$$J_0 = \frac{1}{2A}. \tag{12}$$

The two moments of inertia are obviously dependent.

One has

$$J^{(2)} = J^{(1)} + \omega\frac{dJ^{(1)}}{d\omega}. \tag{13}$$

Table 1: Bandhead spin for ^{194}Hg(SD1) derived from EGOS for first estimation A=5.2902 keV, $I_0 = 10.5$

I	E_γ	EGOS^{cal}(keV/$\hbar$)			EGOS^{exp}(keV/$\hbar$)		
$\hbar$	(keV)	I_0-2	I_0	I_0+2	I_0-2	I_0	I_0+2
12.5	253.929	25.392	21.16	18.137	25.393	21.160	18.137
14.5	296.2512	24.687	21.16	18.515	24.665	21.142	18.499
16.5	338.572	24.183	21.16	18.809	24.084	21.073	18.732
18.5	380.894	23.805	21.16	19.044	23.586	20.966	18.869
20.5	423.216	23.512	21.16	19.237	23.144	20.830	18.936
22.5	465.537	23.376	21.16	19.397	22.738	20.670	18.948
24.5	507.859	23.084	21.16	19.533	22.357	20.494	18.917
26.5	550.180	22.924	21.16	19.649	21.995	20.303	18.852
28.5	592.502	22.788	21.16	19.750	21.650	20.104	18.764
30.5	634.824	22.672	21.16	19.838	21.316	19.895	18.652
32.5	677.145	22.571	21.16	19.916	20.997	19.685	18.527
34.5	719.467	22.483	21.16	19.985	20.689	19.472	18.390
36.5	761.788	22.405	21.16	20.047	20.394	19.261	18.247
38.5	804.110	22.336	21.16	20.102	20.108	19.050	18.097
40.5	846.432	22.274	21.16	20.153	19.840	18.848	17.950
42.5	888.753	22.218	21.16	20.198	19.591	18.658	17.810
44.5	931.075	22.168	21.16	20.240	19.360	18.480	17.676
46.5	973.396	22.122	21.16	20.279	19.148	18.316	17.553

The dynamical moment of inertia varies often in a very sensitive way with rotational frequency $\hbar\omega$. In particular for rigid rotor, we shall obtain:

$$J^{(2)} = J^{(1)} = J_{rigid}. \tag{14}$$

Experimentally, for SDRB's, the gamma-ray transition energies are the only spectroscopic information universally available. Therefore, to compare the structure of the SD bands, information about their gamma-ray transition energies are commonly translated into values of rotational frequency $\hbar\omega$ and moments of inertia:

$$\hbar\omega = \frac{1}{4}[E_\gamma(I) + E_\gamma(I+2)] \qquad \text{(MeV)} \tag{15}$$

$$J^{(1)}(I-1) = \frac{2I-1}{E_\gamma(I)} \qquad (\hbar^2\text{MeV}^{-1}) \tag{16}$$

$$J^{(2)}(I) = \frac{4}{\Delta E_\gamma(I)} \qquad (\hbar^2\text{MeV}^{-1}) \tag{17}$$

where $\Delta E_\gamma(I)$=$E_\gamma(I+2)$-$E_\gamma(I)$ is the difference between two consecutive transition energies. Therefore, the dynamical moment of inertia $J^{(2)}$ which is linked to the second derivatives of energy, does not depend on the knowledge of the spin I but only on the measured transition energies. Theoretically, the $J^{(2)}$ moment of inertia reflects the curvature of the single-particle orbitals, while experimentally it is simply extracted from the measured γ-ray energies. In terms of A and B, yield directly:

$$J^{(1)} = \frac{1}{2[A + 2B(I^2 - 2I + 1)]}, \tag{18}$$

$$J^{(2)} = \frac{1}{2[A + B(6I^2 + 6I + 5)]}. \tag{19}$$

5 Identical Bands in SDRB's

Since the experimental discovery of SD bands in rapidly rotating nuclei, many unexpected features of these highly excited configurations were observed. One of the most striking feature is the existence of identical bands (IB's) or twin bands, that is identical transition energies E_γ in bands belonging to neighboring nuclei with different mass numbers. To determine whether a pair of bands is identical or not, one must calculate the difference between their gamma-transition energies of the two bands 1 and 2, ΔE_γ=$E_\gamma(1)$-$E_\gamma(2)$.

6 ΔI = 2 Staggering Effect in Transition Energies

To explore more clearly the $\Delta I = 2$ staggering, for each band the deviation of transition energies from a smooth reference is determined by calculating the finite difference approximation to the fourth derivative of the γ-ray energies at a given spin d^4E_γ/dI^4. This smooth reference is given by

$$\begin{aligned}\Delta^4 E_\gamma(I) &= \tfrac{1}{16}[E_\gamma(I-4) \\ &\quad -4E_\gamma(I-2) + 6E_\gamma(I) \\ &\quad -4E_\gamma(I+2) + E_\gamma(I+4)].\end{aligned} \tag{20}$$

This formula includes five consecutive transition energies and is denoted by five-point formula. For equation (1), we can easily notice that in this case $\Delta^4 E_\gamma(I)$ vanishes.

Table 2: The same as in Table (1) but for second estimation $A = 5.5904$ keV and B= -3.395×10^{-4} keV, $I_0 = 10$

I	E_γ	EGOS^{cal}(keV/$\hbar$)			EGOS^{exp}(keV/$\hbar$)		
$\hbar$	(keV)	I_0-2	I_0	I_0+2	I_0-2	I_0	I_0+2
12	253.102	26.642	22.008	18.748	26.729	22.080	18.809
14	295.399	25.686	21.881	19.058	25.738	21.925	19.096
16	336.884	24.954	21.734	19.250	24.976	21.753	19.267
18	377.513	24.355	21.572	19.359	24.347	21.565	19.353
20	417.181	23.838	21.393	19.403	23.805	21.364	19.376
22	455.830	23.375	21.201	19.397	23.321	21.151	19.351
24	493.408	22.949	20.996	19.349	22.877	20.930	19.288
26	529.873	22.547	20.779	19.268	22.462	20.701	19.195
28	565.185	22.164	20.552	19.158	22.075	20.469	19.082
30	599.324	21.793	20.316	19.026	21.704	20.232	18.948
32	632.266	21.432	20.071	18.873	21.353	19.997	18.803
34	664.012	21.079	19.821	18.704	21.018	19.763	18.649
36	694.573	20.733	19.565	18.521	20.698	19.532	18.490
38	723.943	20.392	19.305	18.327	20.391	19.304	18.326
40	752.145	20.057	19.041	18.123	20.104	19.086	18.166
42	779.183	19.726	18.775	17.912	19.839	18.883	18.015
44	805.102	19.400	18.508	17.694	19.593	18.692	17.870
46	829.924	19.078	18.240	17.472	19.368	18.517	17.737

7 Results and Discussion

The SDRB's ^{192}Hg(SD1), ^{194}Hg(SD1), ^{194}Hg(SD2), ^{194}Pb(SD1) and ^{196}Pb(SD1) in $A \sim 190$ mass region are considered. For each nucleus the optimized two parameters A,B of the model in question are fitted to reproduce the observed experimental γ-ray transition energies $E_\gamma^{exp}(I)$. The procedure is repeated for several trial values A,B by using a computer simulation search programm. The best parameters lead to minimize the root mean square (rms) deviation

$$\chi = \left[\frac{1}{N}\sum_{i=1}^{N}\left[\frac{E_\gamma^{exp}(I_i) - E_\gamma^{cal}(I_i)}{E_\gamma^{exp}(I_i)}\right]^2\right]^{\frac{1}{2}} \qquad (21)$$

where N is the total number of experimental points considered in fitting procedure. The experimental data are taken from reference [1,2]. The bandhead spins of the observed levels have been extracted by applying the first and second-hand estimations corresponding to pure rotator and our proposed formula respectively by plotting EGOS versus spin.

The EGOS is a horizontal line for the exact I_0 and will shift to parabola when $I_0 \pm 2$ is assigned to I_0 for pure rotator (first estimation) and three parabola curves for our proposed model (second estimation). As an example, this procedure illustrated in Figure (1) for ^{194}Hg(SD1) for bandheads $I_0 + 2$, I_0, $I_0 - 2$. The closed circles represents the experimental values while the solid curves the calculated ones. The numerical values are presented in Tables (1,2).

The resulting best parameters A,B of the model and the values of the lowest bandhead spins I_0 and the bandhead moment of inertia J_0 for our selected SDRB's are listed in Table (3).

In framework of the applied theoretical model, the dynamic $J^{(2)}$ and kinematic $J^{(1)}$ moments of inertia corresponding to the calculated spins have been extracted. The comparison between the experimental γ-ray transition energies and our calculations using the values of the model parameters given in Table(1) for the SD bands of our selected nuclei is illustrated in Figure(2).

Figure (3) illustrates the calculated kinematic $J^{(1)}$ (open circle) and dynamic $J^{(2)}$ (closed circle) moments of inertia as a function of rotational frequency $\hbar\omega$. Both the moments of inertia $J^{(1)}$ and $J^{(2)}$ exhibits a smooth increase with increasing rotational frequency, the $J^{(2)}$ is significantly larger than $J^{(1)}$ over a large rotational frequency range.

Investigating the tables and figures, we know that the γ-ray transition energies, the kinematic $J^{(1)}$ and dynamic $J^{(2)}$ moments of inertia of the SD states can be quantitatively described excellently with our two-parameters collective rotational formula. The $J^{(2)}$ values for both ^{192}Hg(SD1) and ^{194}Pb(SD1) are very close over the entire frequency range $\hbar\omega < 0.25$ MeV. However, at higher frequencies the differences in transition energies are no longer constant.

Moreover, the SD band of ^{194}Pb(SD1) is populated at lower spin values $I_0 = 6\hbar$ than that of ^{192}Hg(SD1), $I_0 = 10\hbar$. The difference in γ-ray energies ΔE_γ between transitions in ^{192}Hg(SD1) and ^{194}Pb(SD1) are plotted in Figure (4). Up to $\hbar\omega \sim 0.25$ MeV, the ΔE_γ values are small and constant. Therefore, these two bands have been considered as identical bands (IB), however at higher frequency the difference in transition energies are no longer constant. also the difference

Table 3: The adapted model parameters A,B obtained by fitting procedure, the suggested bandhead spins I_0 and the bandhead moments of inertia J_0. The SDRB's are identified by the lowest observed E_γ.

SDRB	A(keV)	$B(10^{-4}\text{keV})$	$I_0(\hbar)$	$J_0(\hbar^2\text{MeV}^{-1})$	E_γ(keV)
^{192}Hg(SD1)	5.6470	-3.5087	8	88.5425	214.4
^{194}Hg(SD1)	5.5904	-3.3951	10	89.4390	253.93
^{194}Hg(SD2)	5.3154	-2.2537	8	94.0662	200.79
^{194}Pb(SD1)	5.6637	-1.5590	4	88.2815	124.9
^{196}Pb(SD1)	5.7282	-3.1319	6	87.2874	171.5

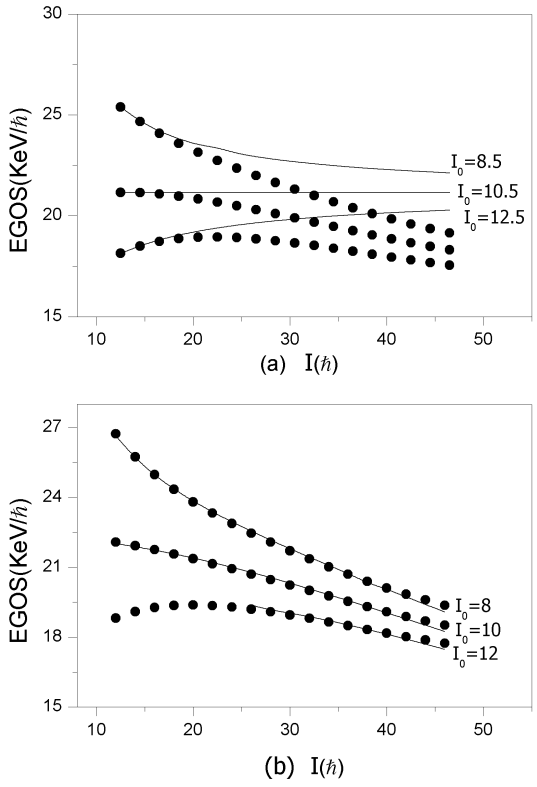

Fig. 1: EGOS versus spin to determine the band head spin for ^{194}Hg(SD-1) (a) for first estimation (b) for second estimation.

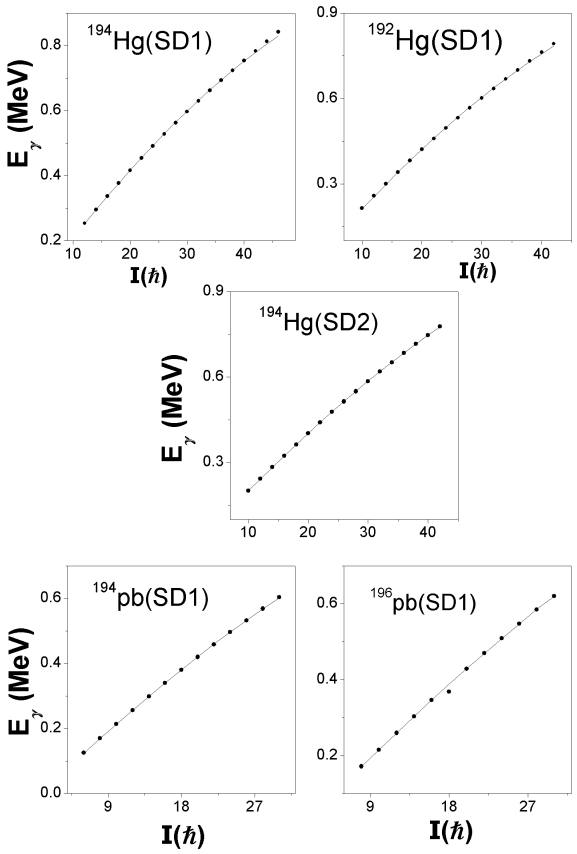

Fig. 2: Theoretical (solid curve) and experimental (closed circles) gamma-ray transition energies E_γ of the SD bands observed in even-even Hg and Pb nuclei. The theoretical values are calculated with the corresponding parameters taken from Table (3).

ΔE_γ between ^{194}Hg(SD1) and ^{192}Hg(SD1) is approximately 4 keV at low frequency (see Figure (4)) are too longer to consider these two bands as identical ones.

Another result of the present work is the observation of a $\Delta I = 2$ staggering effects in the transition energies for ^{194}Hg(SD1) and ^{194}Hg(SD2). For each band, the deviation of the γ-ray transition energies from a smooth reference representing the finite difference approximation to the fourth derivative of the γ-ray transition energies in a $\Delta I = 2$ band is calculated. Figure (5) show the resulting values of $\Delta^4 E_\gamma(I)$ against rotational frequency $\hbar\omega$ for the two SD bands. A significant staggering has been observed for ^{194}Hg(SD2) in frequency range $\hbar\omega \sim 0.3$ MeV.

8 Conclusion

We studied in a simple version of two parameters collective model the five SDRB's ^{192}Hg(SD1), ^{194}Hg(SD1,SD2), ^{194}Pb(SD1) and ^{196}Pb(SD1) in the mass region 190. Transition energies, rotational frequencies, dynamic and kinematic

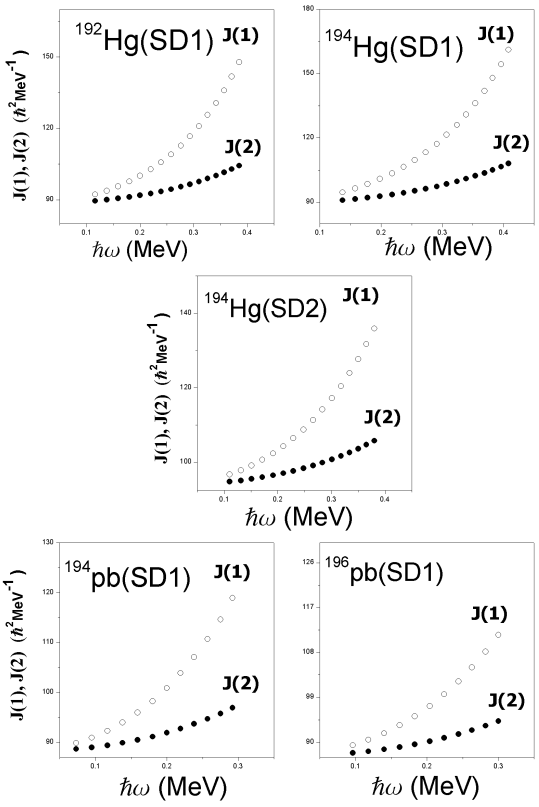

Fig. 3: The calculated results of kinematic $J^{(1)}$ (open circles) and dynematic $J^{(2)}$ (closed circles) moments of inertia plotted as a function of the rotational frequency $\hbar\omega$ for the studied SDRB's.

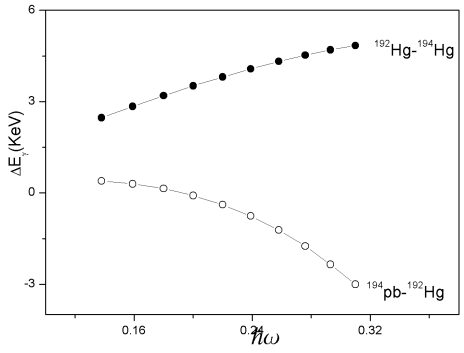

Fig. 4: Differences in the calculated γ-ray transition energies between ^{192}Hg(SD-1)-^{194}Pb(SD-1) and between ^{192}Hg(SD-1)-^{194}Hg(SD-1).

moments of inertia have been calculated. An excellent agreement with the experimental data justifies the application of

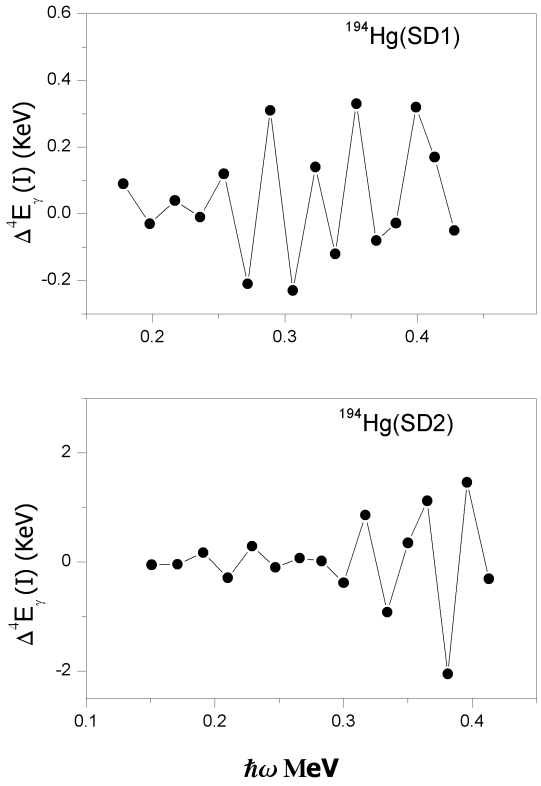

Fig. 5: The $\Delta = 2$ staggering obtained by the five points formula $\Delta^4 E_\gamma(I)$ as a function of rotational frequency $\hbar\omega$ for ^{194}Hg(SD-1, SD-2).

this version of the model. For the first-hand estimation of the bandhead spin I_0 of each SD band we have used the simple rigid rotator to extrapolated the experimentally transition energies, and from the ratio between two consecutive transition energies $\frac{E_\gamma(I_0+4)}{E_\gamma(I_0+2)}$, the spin value of the bandhead has been calculated. For second hand estimation of I_0, the EGOS versus spin for our model are plotted, the plot gives three parabola curves for I_0 and $I_0 \pm 2$. The existence of identical bands in the isotones ^{192}Hg(SD1) and ^{194}Pb(SD1) are investigated. The $\Delta I = 2$ staggering has been examined in the notation of Cedercwall [23]. The staggering plot has been extracted and investigated.

Submitted on August 21, 2014 / Accepted on August 29, 2014

References

1. Singh B., Zymwina R. and Firestone R.B. Table of Superdeformed Nuclear Bands and Fission Isomers: Third Edition. *Nuclear Data Sheets*, 2002, v. 97, 41–295.
2. National Nuclear Data Center NNDC, Brookhaven National Laboratory [Cited on July 2012] http://www.nndc.bnl.gov/chart/
3. Becker J.A. et al. Level spin and moments of inertia in superdeformed nuclei near A = 194. *Nuclear Physics*, 1990, v. A520, C187–C194.

4. Draper J.E. et al. Spins in superdeformed bands in the mass 190 region. *Physical Review*, 1990, v. C42, R1791.
5. Zeng J.Y. et al. Criteria of the Spin Assignment of Rotational Band. *Communications in Theoretical Physics*, 1995, v. 24, 425.
6. Hegazi A.M., Ghoniem M.H. and Khalaf A.M. Theoretical Spin Assignment for Superdeformed Rotational Bands in Mercury and Lead Nuclei. *Egyptian Journal of Physics*, 1999, v. 30, 293–303.
7. Khalaf A.M. et al. Bandhead Spin Determination and Moment of Inertia of Superdeformed Nuclei in Mass Region 60-90 Using Variable Moment of Inertia Model. *Egyptian Journal of Physics*, 2002, v. 41, 151–165.
8. Saber E. Spin Propostion of Rotational Bands in Superdeformed Nuclei by Using Experimental Gamma-Transition Energies. M.Sc. Thesis, Al-Azhar University, Egypt, 2005.
9. Gaballah N. Properties of Dynamical Moments of Inertia in Superdeformed Nuclei. M.Sc. Thesis, Al-Azhar University, Egypt, 2008.
10. Taha M.M. Behavior of Interacting Boson Model In Framework of Group Theory. Ph.D. Thesis, Al-Azhar University, Egypt, 2010.
11. Sayed M.S. Properties of Superdeformed Nuclei and High Spin States. M.Sc. Thesis, Cairo University, Egypt, 2004.
12. Inakurr T. et al. Static and Dynamic Non-Axial Octupole Deformations Suggested by SKYRME-HF and Selfconsistent RPA Calculations. *International Journal of Modern Physics*, 2004, v. E13, 157–167.
13. Muntain I. and Sabiczcwski A. Superdeformed ground state of superheavy nuclei. *Physics Letters*, 2004, v. B586, 254–257.
14. He X.T. et al. The intruder orbitals in superdeformed bands and alignment additivity of odd-odd nuclei in the A∼190 region. *Nuclear Physics*, 2005, v. A760, 263–273.
15. W. Nazarewicz W., Wgss R. and Jhonson A. Structure of superdeformed bands in the A ∼ 150 mass region. *Nuclear Physics*, 2005, v. A503, 285–330.
16. Janssens R.V.F. and Khoo T.L. Superdeformed Nuclei. *Annual Review of Nuclear and Particle Science*, 1991, v. 41, 321–355.
17. Byrski T. et al. Observation of identical superdeformed bands in N=86 nuclei. *Physical Review Letters*, 1990, v. 64, 1650–1657.
18. Girod M. et al. Microscopic descriptions of collective SD bands in the A=190 mass region with the Gogny force. *Zeitschrift für Physik A, Hadrons and Nuclei*, 1997, v. A358, 177–178.
19. He X.T. et al. The $i_{13/2}$ proton intruder orbital and the identical superdeformed bands in 193, 194, 195Tl. *European Physical Journal*, 2005, v. A23, 217–222.
20. Chen Y.J. et al. Theoretical simulation for identical bands. *European Physical Journal*, 2005, v. A24, 185–191.
21. Khalaf A.M., Taha M.M. and Kotb M. Identical Bands and $\Delta I = 2$ Staggering in superdeformed Nuclei in A ∼ 150 Mass Region using Three Parameters Rotational Model. *Progress in Physics*, 2012, v. 4, 39–43.
22. Flibotte S. et al. $\Delta I = 4$ bifurcation in a superdeformed band: Evidence for a C4 symmetry. *Physical Review Letters*, 1993, v. 71, 4299–4305.
23. Cederwall B. et al. New features of superdeformed bands in Hg194. *Physical Review Letters*, 1994, v. 72, 3150–3155.
24. Flibotte S. et al. Multiparticle excitations and identical bands in the superdeformed Gd-149 nucleus. *Nuclear Physics* , 1995, v. A584, 373–396.
25. Haslip D.S. et al. $\Delta I = 4$ Bifurcation in Identical Superdeformed Bands. *Physical Review Letters*, 1997, v. 78, 3447–3461.
26. Hamamoto I. and Mottelson B. Superdeformed rotational bands in the presence of Y44 deformation. *Physics Letters*, 1994, v. B333, 294–298.
27. Pavlichenkov L.M. and Flibotte S. C4 symmetry and bifurcation in superdeformed bands. *Physical Review*, 1995, v. C51, R460.
28. Macchiovelli A.O. et al. C4 symmetry effects in nuclear rotational motion. *Physical Review*, 1995, v. C51, R1.
29. Lian-Ao Wu and Hiroshi Toki. Evidence on delta I = 4 bifurcation in ground bands of even-even nuclei and the theoretical explanation with the interacting boson model. *Physical Review Letters* ,1997, v. 79, 2006–2009.
30. Khalaf A.M. and Sirag M.M. Analysis of $\Delta I = 2$ Staggering in Nuclear Superdeformed Rotational Bands. *Egyptian Journal of Physics*, 2006, v. 35, 359–375.
31. Saber E. Theoretical Study of Staggering Phenomena in Energies of High Spin Nuclear Rotational Bands. Ph. D. Thesis, Al-Azhar University, Egypt, 2009.
32. Satula W. et al. Structure of superdeformed states in Au and Ra nuclei. *Nuclear Physics*, 1991, v. A529, 289–314.
33. Krieger S.J. et al. Super-deformation and shape isomerism: Mapping the isthmus. *Nuclear Physics*, 1992, v. A542, 43–52.
34. Bohr A. and Mettelson B.R. Nuclear Structure, vol. 2, W.A. Benjamin, 1975.

First and Second Least Action Principles: de Broglie Frequency and Neutron Decay

Paulo Roberto Silva

Departmento de Física (Retired Associate Professor), ICEx, Universidade Federal de Minas Gerais, Belo Horizonte, MG, Brazil.
E-mail: prsilvafis@gmail.com

We propose two kinds of least action principles. The first one is defined in a periodic time, and when applied to creation and annihilation of particle pairs, leads to the formula for the de Broglie frequency. The second one is defined in a double-time's metric, namely the longitudinal and transverse (related to the discreteness of the space) times. If applied to a problem dealing with the fluctuations of the metric, this second principle permit us to infer a coherence time. We interpret this as the neutron decay time, where we take the fluctuation in the kinetic energy as being the difference between the mass-energy of the neutron minus the sum of the mass-energies of the proton and electron. The neutron decay time evaluated in this way, does not make any explicit reference to the weak interactions.

1 Introduction

The least action (or Hamilton's) principle [1, 2] states that the variation of the action A gives null result, namely

$$\delta A = \delta \int L dt = 0. \tag{1}$$

In equation (1) L is the Lagrangian function, which depends on the coordinates and velocities and sometimes also on the time. Performing the variation of the action A we consider the various paths, all of them starting in the initial time t_1 and ending in the final time t_2.

2 The de Broglie Frequency

In this section we are giving somewhat more general character to the Lagrangian L, as being associated to some kind of field which is able to create or to destroy virtual particles pairs from the vacuum. Let us take the difference between the initial and final times, as being a time interval of period T,

$$t_2 - t_1 = T. \tag{2}$$

Now we write

$$\delta A = \delta \oint L dt = \oint \delta L \, dt = 0. \tag{3}$$

In equation (3) we used the closed-line-integral symbol, but here it means that the difference in time is a periodic time interval. Pursuing further we get

$$\oint \delta L \, dt = \int_0^{T/2} \delta L \, dt + \int_{T/2}^{T} \delta L \, dt = 0. \tag{4}$$

Indeed the creation and annihilation of particles pairs is a stochastic process, but we are going to consider a "regularized" form of it and we write

$$\int_0^{T/2} \delta L \, dt = -h, \text{ and } \int_{T/2}^{T} \delta \mathrm{L} \, \mathrm{dt} = +\mathrm{h}. \tag{5}$$

According to equation (5), in the first half period a quantum of action is destroyed, and in the second half one a quantum of action is created. The sum of the two contributions gives null result, recovering the classical case of the least action principle.

Now we take the first integral of (5) as being the process of creation of a virtual particle-antiparticle pair. We have

$$\int_0^{T/2} \delta L \, dt = < \delta L > \int_0^{T/2} dt \tag{6}$$

In equation (6) $< \delta L >$ corresponds to a time average of the quantity δL. Next we interpret it as the energy decreasing of the vacuum as a means to create a particle-antiparticle pair. Therefore we have

$$< \delta L >_{|\text{first half period}} = -2mc^2. \tag{7}$$

From equations (6) and (7), we get

$$2mc^2 \frac{T}{2} = h, \tag{8}$$

leading to

$$mc^2 = h\nu. \tag{9}$$

Observe that equation (9) is the relation for the de Broglie's frequency, where $\nu \equiv 1/T$.

3 The second action and the time of coherence

Inspired in the spirit of the string theory [3], we define a second action $A^{(2)}$, where the integration of the Lagrangian function will be also done along a "transverse time" t', besides the integration which is usually performed along the "longitudinal time" t. We write

$$A^{(2)} = \int \int L \, dt dt'. \tag{10}$$

Now let us consider, as in reference [4], a fluctuating contribution for the Lagrangian such that

$$\delta L = \frac{1}{2m} p_i \chi_{ij} p_j, \tag{11}$$

where χ_{ij} is a tensor connecting the fluctuating momenta of a particle of mass m. By taking the variation of the second action, equation (10), we have

$$\delta A^{(2)} =< \delta L > \int\int dt dt' = 0. \tag{12}$$

We observe that in this case, the average quantity $< \delta L >$ is equal to zero, due to the fluctuating nature of δL, namely

$$< \delta L >= \frac{1}{2m} < p_i \chi_{ij} p_j >= 0. \tag{13}$$

In equation (12) we have extracted from the double integral, the "first momentum" or the time-average of the function δL.

By analogy with the previous section where we have obtained the frequency of de Broglie, let us evaluate the second momentum (the variance) of δL. We write

$$\int\int (\delta L)^2 dt dt' =< (\delta L)^2 > \int_0^{\tau/2} dt \int_0^{\lambda/c} dt' = h^2, \tag{14}$$

where τ is the coherence time and λ is the Planck length. Meanwhile we have

$$< (\delta L)^2 >= \frac{p^4}{4m^2}. \tag{15}$$

From equation (14) and (15) we have

$$\frac{p^4}{4m^2} \frac{\tau\lambda}{2c} = h^2, \tag{16}$$

and solving equation (16)for the coherence time we get

$$\tau = \frac{8m^2 ch^2}{p^4 \lambda}. \tag{17}$$

4 Neutron decay and the discreteness of the space-time

In the previous section, the quantum fluctuations on the metric [4] were related to the discreteness of the space-time. Then a transverse time λ/c was considered, by taking a string of width equal to the Planck length λ. On the other hand, in the neutron-decay's reaction, we have the available maximum kinetic energy K given by

$$K = (m_n - M_p - m_e)c^2 = \frac{p^2}{2m}. \tag{18}$$

From equations (17) and (18) we get

$$\tau = \frac{2ch^2}{K^2 \lambda}. \tag{19}$$

Numerical evaluation of equation (19) gives for the coherence time τ, the magnitude

$$\tau = 1.04 \times 10^3 s. \tag{20}$$

This value for the coherence time must be compared with the calculated and measured times of the neutron decay, both of approximately 900 s (please see references [5] and [6]). This result suggests that the neutron decay, besides being a process governed by the weak interactions, can also be related to the fluctuations of the metric and to the discreteness of the space-time.

5 Concluding remarks

Besides to be essentially a quantum object, due to its size and its mass-energy content, neutron also is a composed particle with its three constituent quarks of two down and one upper flavor. Proton also is a composed particle, but some conservation laws seem to forbid its decay. We can imagine that in the decay process of the neutron, there is an intermediate step where we have a fluctuation between the wave function describing the integer neutron and the total wave function describing the reaction's products. It seems that the fluctuating kinetic energy introduced in section 4, nicely accounts for this feature of the neutron decay. Jointly with the here introduced concept of second action, which also considers the discreteness of the space-time, we were able to estimate the neutron decay time without explicit reference to the weak interactions [5–7]. Finally a paper entitled "Improved Determination of the Neutron Lifetime", was recently published in the Physical Review Letters [8] (please see the discussions and the references cited therein.)

Submitted on September 26, 2014 / Accepted on September 29, 2014

References

1. Tolman R.C. The Principles of Statistical Mechanics, Oxford University Press, 1967, p. 16.
2. Landau L. and Lifchitz E. Mécanique, Editions Mir, Moscow, 1966.
3. McMahon, String Theory Demystified, McGrawHill, 2009.
4. Chaves A.S. et al, Annals of Physics (NY), 1994, v. 231, 174.
5. Silva P.R. Weak Interactions Made Simple, viXra: 1210.0014v1.
6. Particle Data Group, *Physics Letters*, 1008, v. 204B, 1.
7. Griffiths D.J. Introduction to Elementary Particles, Wiley, New York, 1987.
8. A.T. Yue et al. *Physical Review Letters*, 2013, v. 111, 222501.

Wave-Particle Duality in the Elastodynamics of the Spacetime Continuum (STCED)

Pierre A. Millette

E-mail: PierreAMillette@alumni.uottawa.ca, Ottawa, Canada

We examine the nature of the wave-particle duality in the Elastodynamics of the Spacetime Continuum (STCED), due to the propagation of deformations in the STC by longitudinal dilatation and transverse distortion wave displacements. We first consider the special case of Electromagnetism which consists of transverse waves only, and use the photon wavefunction to demonstrate that $|\Psi|^2$ represents a physical energy density, not a probability density. However, normalization by the system energy allows use of the probabilistic formulation of quantum theory. In the STCED longitudinal and transverse wave equations, the transverse wave is the source of the interference pattern in double slit experiments, influencing the location of the longitudinal wave, as observed experimentally. We note the similarity of STCED wave-particle duality and Louis de Broglie's "double solution".

1 Introduction

As shown previously, in the Elastodynamics of the Spacetime Continuum (*STCED*) [1–6], energy propagates in the STC (spacetime continuum) as wave-like deformations which can be decomposed into *dilatations* and *distortions*.

Dilatations include an invariant change in volume of the spacetime continuum which is the source of the associated rest-mass energy density of the deformation. The rest-mass energy density of this longitudinal mode is given by [1, see Eq.(32)]

$$\rho c^2 = 4\bar{\kappa}_0 \varepsilon \tag{1}$$

where ρ is the dilatation rest-mass density, c is the speed of light, $\bar{\kappa}_0$ is the bulk modulus of the *STC* (the resistance of the spacetime continuum to *dilatations*), and ε is the volume dilatation. On the other hand, *distortions* correspond to a change of shape (shearing stress) of the spacetime continuum without a change in volume and are thus massless.

Thus deformations propagate in the spacetime continuum by longitudinal (*dilatation*) and transverse (*distortion*) wave displacements. This provides a natural explanation for wave-particle duality, with the transverse mode corresponding to the wave aspects of the deformations and the longitudinal mode corresponding to the particle aspects of the deformations.

2 Wave-particle duality in Electromagnetism

In Electromagnetism, as shown in [1, see (121)], the volume dilatation is $\varepsilon = 0$. Hence, the photon is massless and there is no longitudinal mode of propagation. Electromagnetic waves are massless transverse distortion waves.

The photons correspond to an energy flow along the direction of propagation in 3-space resulting from the Poynting vector. This longitudinal electromagnetic energy flux is massless as it is due to distortion, not dilatation, of the spacetime continuum. However, because this energy flux is along the direction of propagation, it gives rise to the particle aspect of the electromagnetic field, the photon. We should note however that the modern understanding of photons is that they are massless excitations of the quantized electromagnetic field, not particles *per se*. Thus in this case, the kinetic energy in the longitudinal direction is carried by the distortion part of the deformation, while the dilatation part, which carries the rest-mass energy, is not present as the mass is 0.

This situation provides us with an opportunity to investigate the transverse mode of propagation, independently of the longitudinal mode. In general, the transverse propagation of electromagnetic waves is given by sinusoidal waves ψ and the intensity of the waves, corresponding to the energy density, is given by $|\psi|^2$. This is equivalent to the modulus squared of the wavefunction used in Quantum Mechanics as a probability density. A full analysis requires that we investigate further the Quantum Mechanics of the photon, and in particular, the photon wavefunction.

2.1 Photon wavefunction

The photon wavefunction is a first quantization description of the electromagnetic field [7,8]. Historically, this development was not done, as second quantization of the electromagnetic field was first developed. As a result, photon wave mechanics is not fully accepted in the scientific community, mainly because of the differences between particle and photon dynamics. As opposed to a particle, the photon has zero rest-mass and propagates at the speed of light. In addition, the position operator cannot be defined for a photon, only the momentum operator (photon localization problem).

Bialynicki-Birula [8–12], Sipe [13], and more recently Mohr [14], Raymer and Smith [15–17] and others have derived and promoted the use of the photon wavefunction. Bialynicki-Birula defines the photon wavefunction as "a complex vector-function of space coordinates r and time t that adequately describes the quantum state of a single photon" [8].

He sees three advantages to introducing a photon wavefunction [11]: it provides 1) a unified description of both massive and massless particles both in first quantization and second quantization; 2) an easier description of photon dynamics without having to resort to second quantization; 3) new methods of describing photons.

As pointed out in [7] and references therein, the photon wave equation is now used to study the propagation of photons in media, the quantum properties of electromagnetic waves in structured media, and the scattering of electromagnetic waves in both isotropic and anisotropic inhomogeneous media. Raymer and Smith [16, 17] have extended the use of the photon wavefunction to the analysis of multi-photon states and coherence theory. To the above list, in this paper, we add an additional benefit of the photon wavefunction: the clarification of the physical interpretation of the quantum mechanical wavefunction.

The photon wavefunction is derived from the description of the electromagnetic field based on the complex form of the Maxwell equations first used by Riemann, Silberstein and Bateman [8] (the Riemann–Silberstein vector). As summarized by Bialynicki-Birula [12], "[t]he Riemann–Silberstein vector on the one hand contains full information about the state of the classical electromagnetic field and on the other hand it may serve as the photon wave function in the quantum theory". The Maxwell equations are then written as [8]

$$\begin{aligned} i\,\partial_t \mathbf{F}(\mathbf{r},t) &= c\,\nabla\times\mathbf{F}(\mathbf{r},t) \\ \nabla\cdot\mathbf{F}(\mathbf{r},t) &= 0 \end{aligned} \tag{2}$$

where

$$\mathbf{F}(\mathbf{r},t) = \left(\frac{\mathbf{D}(\mathbf{r},t)}{\sqrt{2\epsilon_0}} + i\,\frac{\mathbf{B}(\mathbf{r},t)}{\sqrt{2\mu_0}}\right) \tag{3}$$

and where $\mathbf{D}(\mathbf{r},t)$ and $\mathbf{B}(\mathbf{r},t)$ have their usual significance.

Then the dynamical quantities like the energy density and the Poynting vector are given by [8]

$$\begin{aligned} E &= \int \mathbf{F}^*\cdot\mathbf{F}\;\mathrm{d}^3r \\ \mathbf{S} &= \frac{1}{2ic}\int \mathbf{F}^*\times\mathbf{F}\;\mathrm{d}^3r \end{aligned} \tag{4}$$

where $\mathbf{F}^*$ denotes the complex conjugate. The sign selected in (3) reflects positive helicity (projection of the spin on the direction of momentum) corresponding to left-handed circular polarization. Photons of negative helicity corresponding to right-handed circular polarization are represented by changing the sign from i to $-i$ in (3). Hence (3) can be written as

$$\mathbf{F}_{\pm}(\mathbf{r},t) = \left(\frac{\mathbf{D}(\mathbf{r},t)}{\sqrt{2\epsilon_0}} \pm i\,\frac{\mathbf{B}(\mathbf{r},t)}{\sqrt{2\mu_0}}\right) \tag{5}$$

to represent both photon polarization states.

A photon of arbitrary polarization is thus represented by a combination of left- and right-handed circular polarization states. The photon wavefunction is then given by the six-component vector

$$\Psi(\mathbf{r},t) = \begin{pmatrix} \mathbf{F}_+(\mathbf{r},t) \\ \mathbf{F}_-(\mathbf{r},t) \end{pmatrix}. \tag{6}$$

The corresponding photon wave equation is discussed in [11].

2.2 Physical interpretation of the photon wavefunction

From (6) and (5), we calculate the modulus squared of the photon wavefunction to obtain [7]

$$|\Psi(\mathbf{r},t)|^2 = \left(\frac{\epsilon_0|\mathbf{E}|^2}{2} + \frac{|\mathbf{B}|^2}{2\mu_0}\right). \tag{7}$$

The modulus squared of the photon wavefunction $\Psi(\mathbf{r},t)$ gives the electromagnetic energy density at a given position and time. This is the physical interpretation of the quantum mechanical $|\Psi(\mathbf{r},t)|^2$ for electromagnetic transverse waves in the absence of longitudinal waves.

Bialynicki-Birula proposes to convert $|\Psi(\mathbf{r},t)|^2$ to a probability density as required by the accepted quantum mechanical probabilistic interpretation [11]. This he achieves by dividing the modulus squared of the photon wavefunction by the expectation value of the energy $<E>$ [11, see his equation (44)]. In this way, it is made to describe in probabilistic terms the energy distribution in space associated with a photon.

Thus the probabilistic formulation of quantum theory is preserved, while the physical interpretation of $|\Psi|^2$ is shown to correspond to an energy density. Raymer and Smith [17] state that "[a] strong argument in favour of the energy-density wave function form of PWM [Photon Wave Mechanics] is that it bears strong connections to other, well-established theories—both quantum and classical—such as photodetection theory, classical and quantum optical coherence theory, and the biphoton amplitude, which is used in most discussions of spontaneous parametric down conversion".

Hence, we have to conclude that the appropriate physical interpretation of $|\Psi|^2$ is that it represents a physical energy density, not a probability density. However, the energy density can be converted to a probability density once it is normalized with the system energy (as done by Bialynicki-Birula for the photon wavefunction). In this way, *STCED* does not replace the probabilistic formulation of quantum theory, it just helps to understand the physics of quantum theory. The two formulations are equivalent, which explains the success of the probabilistic formulation of quantum theory. In actual practice, the quantum mechanical probability formulation can be used as is, as it gives the same results as the physical energy density formulation of *STCED*. However, the physical intensity waves of *STCED* help us understand the physics of the quantum mechanical wavefunction and the physics of wave-particle duality.

It is important to note that the energy density physical interpretation of $|\Psi|^2$ applies just as much to systems as to single particles, as for the probability density interpretation.

3 Wave-particle duality in STCED

In *STCED*, the displacement u^ν of a deformation from its undeformed state can be decomposed into a longitudinal (dilatation) component $u^\nu_\parallel$ and a transverse (distortion) component $u^\nu_\perp$. The volume dilatation ε is given by the relation [1, see (44)]

$$\varepsilon = {u_\parallel}^\mu{}_{;\mu}. \tag{8}$$

The longitudinal displacement wave equation and the transverse displacement wave equation of a deformation are given respectively by [1, see (196)]

$$\begin{aligned} \nabla^2 u^\nu_\parallel &= -\frac{\bar\mu_0 + \bar\lambda_0}{\bar\mu_0}\varepsilon^{;\nu} \\ \nabla^2 u^\nu_\perp &+ \frac{\bar k_0}{\bar\mu_0}\,\varepsilon(x^\mu)\; u^\nu_\perp = 0 \end{aligned} \tag{9}$$

where ∇^2 is the 4-D operator, $\bar\lambda_0$ and $\bar\mu_0$ are the Lamé elastic constants of the spacetime continuum and $\bar k_0$ is the elastic force constant of the spacetime continuum. The constant $\bar\mu_0$ is the shear modulus (the resistance of the continuum to *distortions*) and $\bar\lambda_0$ is expressed in terms of $\bar\kappa_0$, the bulk modulus (as in (1) in Section 1) according to

$$\bar\lambda_0 = \bar\kappa_0 - \bar\mu_0/2 \tag{10}$$

in a four-dimensional continuum. The wave equation for $u^\nu_\parallel$ describes the propagation of longitudinal displacements, while the wave equation for $u^\nu_\perp$ describes the propagation of transverse displacements in the spacetime continuum. The *STCED* deformation wave displacements solution is similar to Louis de Broglie's "double solution" [18, 19].

3.1 Wave propagation in STCED

The electromagnetic case, as seen in Section 2, provides a physical interpretation of the wavefunction for transverse wave displacements. This interpretation should apply in general to any wavefunction Ψ. In *STCED*, in the general case, every deformation can be decomposed into a combination of a transverse mode corresponding to the wave aspect of the deformation, and a longitudinal mode corresponding to the particle aspect of the deformation [2]. Thus the physical interpretation of Section 2.2 applies to the general *STCED* transverse wave displacements, not only to the electromagnetic ones.

Hence, $|\Psi|^2$ represents the physical intensity (energy density) of the transverse (*distortion*) wave, rather than the probability density of quantum theory. It corresponds to the transverse field energy of the deformation. It is not the same as the particle, which corresponds to the longitudinal (*dilatation*) wave displacement and is localized within the deformation via the massive volume dilatation, as discussed in the next Section 3.2. However, $|\Psi|^2$ can be normalized with the system energy and converted into a probability density, thus allowing the use of the existing probabilistic formulation of quantum theory. Additionally, the physical intensity waves of *STCED* help us understand the physics of wave-particle duality and resolve the paradoxes of quantum theory.

3.2 Particle propagation in STCED

Particles propagate in the spacetime continuum as longitudinal wave displacements. Mass is proportional to the volume dilatation ε of the longitudinal mode of the deformation as per (1). This longitudinal mode displacement satisfies a wave equation for ε, different from the transverse mode displacement wave equation for Ψ. This longitudinal dilatation wave equation for ε is given by [1, see (204)]

$$\nabla^2\varepsilon = -\frac{\bar k_0}{2\bar\mu_0 + \bar\lambda_0}\, u^\nu_\perp \varepsilon_{;\nu}\,. \tag{11}$$

It is important to note that the inhomogeneous term on the R.H.S. includes a dot product coupling between the transverse displacement $u^\nu_\perp$ and the gradient of the volume dilatation $\varepsilon_{;\nu}$ for the solution of the longitudinal dilatation wave equation for ε. This explains the behavior of electrons in the double slit interference experiment.

The transverse distortion wave equation for $\omega^{\mu\nu}$ [1, see (210)]

$$\nabla^2\omega^{\mu\nu} + \frac{\bar k_0}{\bar\mu_0}\,\varepsilon(x^\mu)\;\omega^{\mu\nu} = \frac{1}{2}\frac{\bar k_0}{\bar\mu_0}\left(\varepsilon^{;\mu}u^\nu_\perp - \varepsilon^{;\nu}u^\mu_\perp\right) \tag{12}$$

shows a R.H.S. cross product coupling between the transverse displacement $u^\nu_\perp$ and the gradient of the volume dilatation $\varepsilon^{;\mu}$ for the solution of the transverse distortion wave equation for $\omega^{\mu\nu}$. The transverse distortion wave $\omega^{\mu\nu}$ corresponds to a multi-component wavefunction Ψ.

A deformation propagating in the spacetime continuum consists of a combination of a transverse and a longitudinal wave. The transverse wave is the source of the interference pattern in double slit experiments, which impacts the location of the associated longitudinal wave of the individual particle in generating the interference pattern. The longitudinal dilatation wave behaves as a particle and goes through one of the slits, even as it follows the interference pattern dictated by the transverse distortion wave, as observed experimentally [20, see in particular Figure 4] and as seen in the coupling between $\varepsilon_{;\nu}$ and $u^\nu_\perp$ in (11) and (12) above.

These results are in agreement with the results of the Jánossy-Naray, Clauser, and Dagenais and Mandel experiments on the self-interference of photons and the neutron interferometry experiments performed by Bonse and Rauch [21, see pp. 73-81]. The transverse distortion wave generates the interference pattern, while the longitudinal wave's dilatation (particle) follows a specific action, with its final location guided by the transverse wave's interference pattern.

The longitudinal wave is similar to the de Broglie "singularity-wave function" [18]. However, in *STCED* the particle is not a singularity of the wave, but is instead characterized by its mass which arises from the volume dilatation propagating as part of the longitudinal wave. There is no need for the collapse of the wavefunction Ψ, as the particle resides in the longitudinal wave, not the transverse one. A measurement of a particle's position is a measurement of the longitudinal wave, not the transverse wave.

4 Discussion and conclusion

In this paper, we have examined the nature of the wave-particle duality that comes out of the Elastodynamics of the Spacetime Continuum (*STCED*). We have noted that deformations propagate in the spacetime continuum by longitudinal (*dilatation*) and transverse (*distortion*) wave displacements, which provides a natural explanation for wave-particle duality, with the transverse mode corresponding to the wave aspects of the deformations and the longitudinal mode corresponding to the particle aspects of the deformations.

We have considered the special case of Electromagnetism, which is characterized by a transverse mode (the electromagnetic radiation), but no longitudinal mode (as the photon is massless), to help in the clarification of the physical interpretation of the quantum mechanical wavefunction. To that purpose, we have considered the photon wavefunction, and have demonstrated that the physical interpretation of $|\Psi|^2$ represents an energy density, not a probability density. However, it can be normalized with the system energy to be converted to a probability density and allow the use of the probabilistic formulation of quantum theory. We have also noted that the energy density physical interpretation of $|\Psi|^2$ applies just as much to systems as to single particles.

We have then looked at the general *STCED* case, where every deformation can be decomposed into a combination of a transverse mode corresponding to the wave aspect of the deformation, and a longitudinal mode corresponding to the particle aspect of the deformation, and concluded that the physical interpretation of the photon wavefunction applies to the general *STCED* transverse wave displacements, not only to the electromagnetic ones.

We have reviewed the *STCED* longitudinal dilatation wave equation for ε corresponding to the mass component (particle) and the transverse distortion wave equation for $\omega^{\mu\nu}$ corresponding to a multi-component wavefunction Ψ. We have noted the coupling on the R.H.S. of both equations between $\varepsilon^{,\mu}$ and $u^{\nu}_{\perp}$, showing that even though the transverse wave is the source of the interference pattern in double slit experiments as for the photon wavefunction, and the longitudinal dilatation wave behaves as a particle, the latter follows the interference pattern dictated by the transverse distortion wave as observed experimentally.

We have also noted the similarity of *STCED* wave-particle duality to Louis de Broglie's "double solution" and "singularity-wave function", even though in *STCED* the particle is not a singularity of the wave, but is instead characterized by its mass which arises from the volume dilatation propagating as part of the longitudinal wave.

Submitted on September 15, 2014 / Accepted on October 6, 2014

References

1. Millette P. A. Elastodynamics of the Spacetime Continuum. *The Abraham Zelmanov Journal*, 2012, v. 5, 221–277.
2. Millette P. A. On the Decomposition of the Spacetime Metric Tensor and of Tensor Fields in Strained Spacetime. *Progress in Physics*, 2012, v. 4, 5–8.
3. Millette P. A. The Elastodynamics of the Spacetime Continuum as a Framework for Strained Spacetime. *Progress in Physics*, 2013, v. 1, 55–59.
4. Millette P. A. Derivation of Electromagnetism from the Elastodynamics of the Spacetime Continuum. *Progress in Physics*, 2013, v. 2, 12–15.
5. Millette P. A. Strain Energy Density in the Elastodynamics of the Spacetime Continuum and the Electromagnetic Field. *Progress in Physics*, 2013, v. 2, 82–86.
6. Millette P. A. Dilatation–Distortion Decomposition of the Ricci Tensor. *Progress in Physics*, 2013, v. 4, 32–33.
7. Chandrasekar N. Quantum Mechanics of Photons. *Adv. Studies Theor. Phys.*, 2012, v. 6 (8), 391–397.
8. Byalinicki-Birula I. Photon Wave Function. In Wolf E., ed. Progress in Optics XXXVI. Elsevier, Amsterdam, 1996, 245–294. arXiv: quant-ph/0508202v1.
9. Byalinicki-Birula I. On the Wave Function of the Photon. *Acta Physica Polonica A*, 1994, v. 86, 97–116.
10. Byalinicki-Birula I. *Acta Physica Polonica A*, 1995, v. 34, 885.
11. Byalinicki-Birula I. The Photon Wave Function. In Eberly J. H., Mandel L., Wolf E., eds. Coherence and Quantum Optics VII. Plenum, New York, 1996, 313–294.
12. Byalinicki-Birula I. Photon as a Quantum Particle. *Acta Physica Polonica B*, 2006, v. 37 (3), 935–946.
13. Sipe J. E. Photon Wave Functions. *Phys. Rev. A*, 1995, v. 52, 1875–1883.
14. Mohr P. J. Solutions of the Maxwell Equations and Photon Wave Functions. *Annals of Physics*, 2010, v. 325, 607–663.
15. Raymer M. G., Smith B. J. The Maxwell Wave Function of the Photon. *Proc. SPIE*, 2005, v. 5866, 293. arXiv: quant-ph/0604169.
16. Smith B. J., Raymer M. G. Two-Photon Wave Mechanics. *Phys. Rev. A* 2006, v. 74 062104. arXiv: quant-ph/0605149v3.
17. Smith B. J., Raymer M. G. Photon Wave Functions, Wave-Packet Quantization of Light, and Coherence Theory. *New Journal of Physics*, 2007, v. 9, 414. arXiv: 0708.0831.
18. de Broglie L. Non-Linear Wave Mechanics. Elsevier Publishing, Amsterdam, 1960.
19. de Broglie L. Les incertitudes d'Heisenberg et l'interprétation probabiliste de la Mécanique Ondulatoire. Gauthier-Villars, Paris, 1982. Available in English: Heisenberg's Uncertainties and the Probabilistic Interpretation of Wave Mechanics. Kluwer Academic Publishers, Dordrecht, 1990.
20. Hasselbach F. Recent Contributions of Electron Interferometry to Wave-Particle Duality. In Selleri F., ed. Wave-Particle Duality. Plenum, New York, 1992, 109–125.
21. Selleri F. Quantum Paradoxes and Physical Reality. Kluwer Academic Publishers, Dordrecht, 1990.

Gödel's Universe Revisited

Patrick Marquet

11 rue des Chapelles, 94350 Villiers/Marne, Paris, France
E-mail: patrick.marquet6@wanadoo.fr

This paper investigates the Gödel's exact solution of the Einstein equations which describes a stationary homogeneous cosmological Universe inducing closed timelike curves CTCs). This model is generally dismissed because it exhibits a rotational symmetry and it requires a non zero cosmological constant in contradiction with the current astronomical observations. If the cosmological term is assumed to be slightly variable, we show that this metric can be compatible with the Hubble expansion, which makes the Gödel model a viable representation of our Universe.

Introduction

In his original paper [1], Kurt Gödel has derived an exact solution to Einstein's field equations in which the matter takes the form of a pressure-free perfect fluid (dust solution). This $\mathfrak{R}^4$ manifold is homogeneous but non-isotropic and it exhibits a specific rotational symmetry which allows for the existence of *closed time like curves* since the light cone opens up and tips over as the Gödel radial coordinate increases. In addition, it implies a *non zero cosmological term* and a constant scalar curvature, therefore it doesnot admit a *Hubble* expansion *in the whole*, which tends to contradict all current observations.

We suggest here to stick to the Gödel model which we consider as the *true* Universe, and we state that the Hubble expansion can yet be maintained in a particular location with specific coordinates transformations, where the Gödel rotation is *unobservable*.

In this distinguished location, our derivations lead to an *open Universe* without cosmological term and as a result, no future singularity will ever appear in this *local* World.

Our model however, is bound to a main restriction: for physical reasons, it provides a solution which holds only for the existence of the cosmic scale factor, *within* the Gödel metric.

This improved Gödel Universe which we present here, has nevertheless the advantage of agreeably coping with the observational facts.

Some notations

Space-time indices: 0, 1, 2, 3.
Newton's gravitation constant: G.
The velocity of light is $c = 1$.
Space-time signature: -2.

1 Homogeneous space-times

1.1 Roberston-Walker space

Our actual observed Universe is spatially *homogeneous*: if we can see these observations identically in different directions, the model is said *isotropic*. The Robertson-Walker metric is an exact spherically symmetric solution. This property would imply that the Universe admits a six-parameter group of isometries whose surfaces of transitivity are space-like three-surfaces of constant curvatures. (An action of a group is transitive on the manifold $\mathfrak{M}$, if it can map any point of $\mathfrak{M}$ into any other point of $\mathfrak{M}$.) The spatial metric is expressed by

$$dl^2 = \frac{dr^2}{1 + r^2/F^2} + r^2\left(\sin^2\theta\, d\varphi^2 + d\theta^2\right). \qquad (1.1)$$

In the full RW model $F(t)$ is called the *cosmic scale factor* which varies with the (cosmic) proper time t of the whole space.

For an *open* (*infinite*) Universe, with *negative* curvature

$$K(t) = \frac{k}{F^2}, \qquad \text{where } k = -1. \qquad (1.2)$$

and the three-spaces are *diffeomorphic* to $\mathfrak{R}_3$.

The standard formulation is given by

$$(ds^2)_{\mathrm{RW}} = F^2\left(d\eta^2 - d\chi^2 - \sinh^2\chi\left(\sin^2\theta\, d\varphi^2 + d\theta^2\right)\right) \qquad (1.3)$$

with the usual parametrizations

$$dt = F\, d\eta \quad \text{and} \quad r = F\sinh\chi\,. \qquad (1.4)$$

In the RW Universe, the matter with mean density ρ is non interacting (dust) and the energy-momentum tensor is that of a *pressure free perfect fluid*:

$$T_{ab} = \rho\, u_a\, u_b\,. \qquad (1.5)$$

From the corresponding field equations we arrive at the temporal coordinate [2]

$$\eta = \pm\int \frac{dF}{F\sqrt{\left[\frac{8\pi G}{3}\rho F^2 + 1\right]}}, \qquad (1.6)$$

$$F = F_0\left(\cosh\eta - 1\right), \qquad (1.7)$$

with

$$F_0 = \frac{4\pi G\rho F^3}{3}, \qquad (1.8)$$

Where the $\pm$ sign depends on the light emitted either from the coordinates origin or reaching this origin.

1.2 The Gödel metric

The Gödel line element is generically given by

$$(ds^2)_{\mathrm{G}} = B^2\left[\, dx_0^2 - dx_1^2 + \frac{e^{2x_1}}{2}\, dx_2^2 - dx_3^2 + \right. \\ \left. + 2\, e^{2x_1}\,(dx_0 + dx_2)\right], \qquad (1.9)$$

where $B > 0$ is a constant in the original formulation.

This space-time has a five dimensional group of isometries which is transitive. It admits a five dimensional *Lie algebra of Killing vector fields* generated by a time translation ∂_{x_0}, two spatial translations ∂_{x_1}, ∂_{x_2} plus two further Killing vector fields:

$$\partial_{x_3} - x_2\partial_{x_3} \quad \text{and} \quad 2\, e^{x_1}\partial_{x_0} + x_2\,\partial_{x_3} + \left[\, e^{2x_1} - \frac{x_2^2}{2}\,\partial_{x_2}\right].$$

In all current papers, the Gödel metric is always described as the direct sum of the metric

$$(ds^2)_{\mathrm{G}_1} = B^2\left[\, dx_0^2 - dx_1^2 + dx_2^2\,\frac{e^{2x_1}}{2} + \right. \\ \left. + 2\, e^{x_1}\,(dx_0 + dx_2)\right] \qquad (1.10)$$

on the manifold $\mathfrak{M}_1 = \mathfrak{R}_3$ and

$$(ds^2)_{\mathrm{G}_2} = B^2(-dx_3^2) \qquad (1.11)$$

on the manifold $\mathfrak{M}_2 = \mathfrak{R}_1$.

This means that in the usual treatments, in order to analyze the properties of the Gödel solution it is always sufficient to consider only $\mathfrak{M}_1$. The coordinate dx_3 is deemed irrelevant and is thus simply suppressed in the classical representation, which in our opinion reveals a certain lack of completeness. In what follows, we consider the complete solution, where we assign a specific meaning to dx_3.

Let us remark that the Gödel space is homogeneous but not isotropic.

1.3 Classical features of Gödel's metric

Computing the connection coefficients $\Gamma_{ab}^{\ c}$ from the g_{ab} given in (1.9) eventually yield

$$R_{00} = 1, \quad R_{22} = e^{2x_1}, \quad R_{02} = R_{20} = e^{x_1}. \qquad (1.12)$$

All other R_{ab} vanish.

Hence:

$$R = \frac{1}{B^2}\,. \qquad (1.13)$$

The unit vector (world velocity) following the x_0-lines is shown to have the following contravariant components

$$\frac{1}{B},\ 0,\ 0,\ 0$$

and the covariant components

$$B,\ 0,\ B\,e^{x_1},\ 0$$

so we obtain

$$R_{ab} = \frac{1}{B^2}\, u_a\, u_b\,. \qquad (1.14)$$

Since the curvature scalar is a constant, the Gödel field equations read

$$(G_{ab})_{\mathrm{G}} = R_{ab} - \frac{1}{2}\, g_{ab} R = 8\pi G\rho\, u_a\, u_b + \Lambda\, g_{ab}\,, \qquad (1.15)$$

where Λ is the cosmological term which is here inferred as $-4\pi G\rho$, i.e.:

$$\frac{1}{B^2} = 8\pi G\rho\,, \qquad (1.16)$$

$$\Lambda = -\frac{R}{2} = -\frac{1}{2B^2}\,. \qquad (1.17)$$

We next define new coordinates (t, w, ϕ) on $\mathfrak{M}_1$ by

$$E^{x_1} = \cosh 2w + \cos\phi\, \sinh 2w\,, \qquad (1.18)$$

$$x_2\, e^{x_1} = \sqrt{2}\, \sin\phi\, \sinh 2w\,, \qquad (1.19)$$

$$\tan\frac{1}{2}\left(\phi + \frac{x_0 - 2t}{\sqrt{2}}\right) = e^{-2w} \tan\frac{\phi}{2}\,. \qquad (1.20)$$

This leads to the new line element

$$(ds^2)_{\mathrm{G}} = 4B^2\left(\left(dt^2 - dw^2 - dy^2 + \sinh^4 w - \sinh^2 w\right) d\phi^2 + \right. \\ \left. + 2\,\sqrt{2}\, \sinh^2 w\, d\phi\, dt\right) \qquad (1.21)$$

which exhibits the rotational symmetry of the solution about the axis $w = 0$, since we clearly see that the g_{ab} do not depend on θ. Gödel inferred that matter everywhere rotates with the angular velocity $2\sqrt{4\pi G\rho}$.

Let us consider the *reduced* Gödel metric

$$(ds^2)_{\mathrm{G}_1} = 4B^2\Big(\left(dt^2 - dw^2 + \sinh^4 w - \sinh^2 w\right) d\phi^2 + \\ + 2\,\sqrt{2}\, \sinh^2 w\, d\phi\, dt\Big).$$

All light rays emitted from an event on the symmetry axis reconverge at a later event on this axis, with the null geodesics forming a circular *cusp* [3].

If a curve c is defined by $\sinh^4 w = 1$, that is

$$c = \ln(1 + \sqrt{2}), \qquad (1.22)$$

hence, any circle $w > \ln(1+\sqrt{2})$ in the plane $t = 0$, is a *closed timelike curve*.

2 The modified Gödel metric

2.1 Conformal transformation

Now we will assume that the Λ-term is slightly varying with the time t, so B is also variable through the dust density. See (1.16) for detail.

By setting

$$y = r\cosh w, \tag{2.1}$$

where r is another radial parameter, we choose:

$$B = \frac{1}{2}\left(1 - \frac{L_0}{2\sqrt{t^2-y^2}}\right)^2 \tag{2.2}$$

where L_0 is a constant whose meaning will become apparent in the next sub-section. B is now identified with a conformal factor.

Note: one of the *Kretschmann scalar* is no longer an invariant

$$R_{abcd}R^{abcd} = \frac{6}{B^4} \tag{2.3}$$

which reflects the fact that the Gödel space-time may be not fully homogeneous.

Anticipating on our postulate, we will state that the variation of B is only localized in a certain region of the Gödel model. The Λ-term remains constant throughout the complete metric as initially derived, thus preserving its homogeneity.

2.2 The postulate

Our fundamental assumption will now consist of considering our *observed* Universe as being *local*. By local we mean that the rotation ϕ is *unobservable* since we assume that our world is situated at

$$w = 0.$$

Our (local) Universe is now becoming isotropic.

In this case, the Gödel metric reduces to a standard *conformal solution* where the light cone is centered about the t-axis:

$$(ds^2)_{\mathrm{G}} = \left[1 - \frac{L_0}{2\sqrt{t^2-r^2}}\right]^4 \left(dt^2 - dr^2\right). \tag{2.4}$$

We now make the following transformations

$$L_0 = F_0 \tag{2.5}$$

with F_0 defined in (1.8)

$$r = \frac{F_0}{2}e^{\eta}\sinh\chi\,, \qquad t = \frac{F_0}{2}e^{\eta}\cosh\chi\,, \tag{2.6}$$

$$\frac{F_0}{2}e^{\eta} = \sqrt{t^2-r^2}\,, \tag{2.7}$$

$$\tanh\chi = \frac{r}{t}\,, \tag{2.8}$$

and we retrieve the *Roberston-Walker* metric for an *open* Universe with the sole radial coordinate r:

$$(ds^2)_{\mathrm{RW}} = F^2(\eta)\left[d\eta^2 - d\chi^2\right]. \tag{2.9}$$

Remark: The Weyl tensor of the Gödel solution

$$C^{ab}{}_{cd} = R^{ab}{}_{cd} + \frac{R}{3}\delta^a{}_{[c}\delta_{d]}{}^b + 2\delta^{[a}{}_{[c}R_{d]}{}^{b]} \tag{2.10}$$

which has Petrov type D, vanishes for (2.9). Indeed, the equivalent metric (2.4) implies that $C^{ab}{}_{cd} = 0$ for this conformally flat space-time.

Our observed Universe would then be devoid of the Weyl curvature which explains why it is purely described in terms of the Ricci tensor alone. In this view, Einstein was perhaps an even more exceptional visionary mind than is yet currently admitted.

2.3 Hubble expansion

In our local world, the null geodesics are obviously given by $(ds^2)_{\mathrm{RW}} = 0$, that is

$$d\eta = \pm\, d\chi \tag{2.11}$$

and integrating

$$\chi = \pm\eta + const. \tag{2.12}$$

Let us place ourselves at $t(\eta)$, where we observe a light ray emitted at χ where its frequency is ν_0. In virtue of (2.12), the emission time will be $t(\eta-\chi)$, and we observe an apparent frequency given by:

$$\nu = \frac{\nu_0 F(\eta-\chi)}{F(\eta)}\,. \tag{2.13}$$

As $F(\eta)$ increases monotonically, we have $\nu < \nu_0$ which is the expression of a red shifted light. Most observed red shifts are rather small, so that $F(\eta-\chi)$ can be expanded as a Taylor series about $t(\eta-\chi) = t(\eta)$ and we finally get, limiting to the first two terms

$$F(\eta-\chi) = F(\eta) + \left[t(\eta-\chi) - t(\eta)\right]F'(\eta) \tag{2.14}$$

$$= F(\eta)\left\{1 + H_0\left[t(\eta-\chi) - t(\eta)\right]\right\} \tag{2.15}$$

where F' denotes differentiation with respect to η

$$H_0 = \frac{F'(\eta)}{F(\eta)} \tag{2.16}$$

is the present numerical value of *Hubble constant*.

The Gödel solution has a non-zero cosmological term, but **not** the local RW metric.

This agrees with the fact that our open local Universe has a singularity in the past and no singularity in the future [4], in accordance with astronomical observations.

Concluding remarks

Closed timelike curves turn out to exist in many other exact solutions to Einstein's field equations.

It would seem that the first model exhibiting this property was pioneered by C. Lanczos in 1924 [5], and later rediscovered under another form by W. J. Van Stockum in 1937 [6].

However, unlike the Gödel solution, the dust particles of these Universes are rotating about a geometrically distinguished axis.

Even worse, the matter density is shown to increase with radius w, a feature which seriously contradicts all current observations.

In this sense, the Gödel metric appears as a more plausible model characterizing a broaden Universe which is compatible with our astronomical data, provided one is prepared to accept the fact that our observed world is purely local.

Submitted on September 7, 2014 / Accepted on October 1, 2014

References

1. Gödel K. An example of a new type of cosmological solutions of Einstein's field equations of gravitation. *Reviews of Modern Physics*, 1949, v. 21, no. 3, 447–450.
2. Landau L. and Lifshitz E. The Classical Theory of Fields. Addison-Wesley, Reading (Massachusetts), 1962, p. 402 (French translation).
3. Hawking S. W. The Large Scale Structure of Space-Time. Cambridge University Press, Cambridge, 1987.
4. Fang Li Zhi and Ruffini R. Basic Concepts in Relativistic Astrophysics. World Scientific (Singapore), 1983.
5. Lanczos C. Über eine Stationäre Kosmologie im Sinne der Einsteinischer Gravitationstheorie. *Zeitschrift für Physik*, 1924, Bd. 21, 73.
6. Van Stockum W. J. The gravitational field of a distribution of particles rotating around an axis of symmetry. *Proc. Roy. Soc. Edinburgh*, 1937, v. A57, 135.

Progress in Physics is an American scientific journal on advanced studies in physics, registered with the Library of Congress (DC, USA): ISSN 1555-5534 (print version) and ISSN 1555-5615 (online version). The journal is peer reviewed and listed in the abstracting and indexing coverage of: Mathematical Reviews of the AMS (USA), DOAJ of Lund University (Sweden), Zentralblatt MATH (Germany), Scientific Commons of the University of St.Gallen (Switzerland), Open-J-Gate (India), Referential Journal of VINITI (Russia), etc. Progress in Physics is an open-access journal published and distributed in accordance with the Budapest Open Initiative: this means that the electronic copies of both full-size version of the journal and the individual papers published therein will always be acessed for reading, download, and copying for any user free of charge. The journal is issued quarterly (four volumes per year).

Electronic version of this journal: http://www.ptep-online.com

Postal address:
Department of Mathematics and Science,
University of New Mexico, 705 Gurley Avenue, Gallup, NM 87301, USA

Printed in the United States of America